

Radar-Camera Fusion for Object Detection and Semantic Segmentation in Autonomous Driving: A Comprehensive Review

Shanliang Yao¹, Runwei Guan¹, Xiaoyu Huang¹, Zhuoxiao Li¹, Xiangyu Sha¹,
 Yong Yue², Eng Gee Lim², Senior Member, IEEE, Hyungjoon Seo¹, Ka Lok Man², Xiaohui Zhu^{2,†}, Yutao Yue^{3,†}

Abstract—Driven by deep learning techniques, perception technology in autonomous driving has developed rapidly in recent years. To achieve accurate and robust perception capabilities, autonomous vehicles are often equipped with multiple sensors, making sensor fusion a crucial part of the perception system. Among these fused sensors, radars and cameras enable a complementary and cost-effective perception of the surrounding environment regardless of lighting and weather conditions. This review aims to provide a comprehensive guideline for radar-camera fusion, particularly concentrating on perception tasks related to object detection and semantic segmentation. Based on the principles of the radar and camera sensors, we delve into the data processing process and representations, followed by an in-depth analysis and summary of radar-camera fusion datasets. In the review of methodologies in radar-camera fusion, we address interrogative questions, including “why to fuse”, “what to fuse”, “where to fuse”, “when to fuse”, and “how to fuse”, subsequently discussing various challenges and potential research directions within this domain. To ease the retrieval and comparison of datasets and fusion methods, we also provide an interactive website: <https://XJTLU-VEC.github.io/Radar-Camera-Fusion>.

Index Terms—Autonomous driving, radar-camera fusion, object detection, semantic segmentation.

I. INTRODUCTION

AUTONOMOUS driving has excellent potential in mitigating traffic congestion and improving driving safety. Perception, akin to eyes in autonomous driving, constitutes the foundation for successive functions, such as motion prediction, path planning and maneuver control [1], [2]. To achieve optimal accuracy and robustness of the perception system, various sensors are integrated into autonomous vehicles, allowing for the utilization of their complementary and redundant characteristics [3], [4]. However, which sensors to choose and how to fuse the data between different sensors have emerged as challenging issues requiring further exploration.

Given the rich semantic information that can be perceived, cameras are widely utilized in autonomous driving for object

¹ Shanliang Yao, Runwei Guan, Xiaoyu Huang, Zhuoxiao Li, Xiangyu Sha and Hyungjoon Seo are with Faculty of Science and Engineering, University of Liverpool, Liverpool, UK. (email: {shanliang.yao, runwei.guan, x.huang42, zhuoxiao.li, sgxsha2, hyungjoon.seo}@liverpool.ac.uk).

² Yong Yue, Eng Gee Lim, Ka Lok Man and Xiaohui Zhu are with School of Advanced Technology, Xi'an Jiaotong-Liverpool University, Suzhou, China. {yong.yue, enggee.lim, ka.man, xiaohui.zhu}@xjtu.edu.cn).

³ Yutao Yue is with Institute of Deep Perception Technology, JITRI, Wuxi, China; XJTLU-JITRI Academy of Industrial Technology, Xi'an Jiaotong-Liverpool University, Suzhou, China; and Department of Mathematical Sciences, University of Liverpool, Liverpool, UK. (email: yueyutao@idpt.org).

† Corresponding author: xiaohui.zhu@xjtu.edu.cn, yueyutao@idpt.org

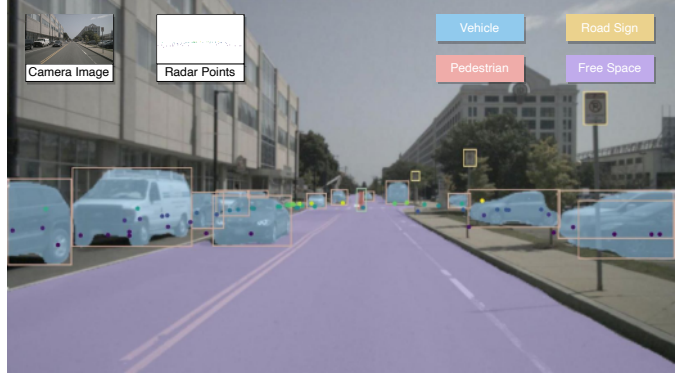


Fig. 1. Common scenario of object detection and semantic segmentation in autonomous driving. Boxes and masks represent the results of detection and segmentation, respectively. Dots indicate the location of each radar point, and the darker the dot, the closer the distance to the ego-vehicle. Image is generated from the nuScenes [5] dataset.

detection, segmentation and tracking. LiDARs calculate the distance to surrounding objects by measuring the time difference of the laser beam from emission to reception via the objects. The denser the laser beam emitted by a LiDAR sensor, the clearer an object's three-dimensional (3D) contour. These complementary features provided by cameras and LiDARs have made LiDAR-camera sensor fusion a hot topic in recent years, and achieved high accuracy in two-dimensional (2D) and 3D object detection [6]–[9], semantic segmentation [10], [11] and object tracking [12], [13]. Despite their strengths, both LiDARs and cameras suffer from the same defect of being sensitive to adverse weather conditions (e.g., rain, fog, snow) that can significantly diminish their field of view and object recognition capabilities. Additionally, neither LiDARs nor cameras can detect objects' velocities without using temporal information. In time-critical situations, relying solely on temporal information is not feasible, as estimating objects' velocities is crucial for collision avoidance. Moreover, the high cost of LiDAR products has brought certain difficulties in promoting their widespread adoption [14].

Compared to LiDARs and cameras, radars exhibit superior effectiveness under challenging lighting and weather conditions [15], [16]. Radars can also deliver accurate velocity estimation for all detected objects depending on the Doppler effect without requiring any temporal information [17]. With these characteristics, radars are widely used in Advanced

Driving Assistance Systems (ADAS) applications, including collision avoidance, Adaptive Cruise Control (ACC), Lane Change Assist (LCA) and Automatic Emergency Braking (AEB). For autonomous driving vehicles, radar-camera fusion makes it possible to not only perceive outlines, colors and textures of the surroundings, but also detect their velocities and ranges regardless of weather and lighting conditions, as depicted in Fig. 1.

Although radar sensors are popularly applied to vehicles, few studies focus on data fusion from radars and cameras. One reason for this is the limitations of radar output data, such as low resolution, sparse point clouds, uncertainty in elevation and clutter effects. Another reason is that up to now, the datasets containing both radar and camera data for autonomous driving applications are insufficient, making it challenging for researchers to conduct in-depth analysis. Additionally, applying or adapting existing LiDAR-based algorithms to radar point clouds yields poor results due to inherent differences of point clouds between the LiDAR sensor and radar sensor [17]. Radar point clouds are significantly sparser than their LiDAR counterparts, making it inefficient to extract objects' geometry information using LiDAR-based algorithms. Although Radar Cross Section (RCS) values in the radar sensor indicate the reflective intensity from the surface of an object, they are easily affected by numerous factors and cannot be used singularly to determine the classification of the target. In addition, though aggregating multiple radar frames enhances the density of the point clouds, it also causes a delay to the whole system. In summary, radar-camera fusion perception is significant in autonomous driving as well as challenging in implementation.

A. Related Surveys

Most sensor fusion surveys focus on LiDAR-camera [2], [18]–[20], or the broader field of multi-sensor fusion, including LiDAR, camera, radar and other sensors [3], [20]–[22]. Specifically, in multi-sensor fusion surveys, LiDARs and cameras are still the main research objectives. For example, Feng *et al.* [3] conducted a comprehensive survey on deep multi-modal object detection and semantic segmentation for autonomous driving. However, this survey mainly concentrates on fusion methods based on LiDARs and cameras, and briefly mentions some studies combining camera images and radar data.

To the best of our knowledge, [23] is the only survey that primarily focuses on radar-camera fusion for object detection in autonomous driving. However, it does not cover the radar-camera fusion dataset or the semantic segmentation task.

B. Contributions

With the limited focus on radar-camera fusion in existing surveys, it is challenging for researchers to gain an overview of this emerging research field. Our survey attempts to narrow this gap by providing a comprehensive review of radar-camera fusion in autonomous driving. The contributions of our review are summarized as follows:

- To the best of our knowledge, this is the first survey focusing on two fundamental perception problems for

radar-camera fusion, namely, object detection and semantic segmentation.

- We present an up-to-date (2019 - 2023) overview of radar-camera fusion datasets and algorithms, and conduct in-depth research on “why to fuse”, “what to fuse”, “where to fuse”, “when to fuse”, and “how to fuse”.
- We analyze the critical challenges and open questions in radar-camera fusion, and put forward potential research directions.
- We provide an interactive and updated website for better retrieving and comparing the fusion datasets and methods.

II. BACKGROUND

This section provides background information on radar-camera fusion in autonomous driving. We first introduce the components and working principles of the radar and camera sensors, followed by describing their advantages and disadvantages. By comparing the characteristics of the two sensors, we aim to demonstrate the importance of radar-camera fusion. Subsequently, as the perception module leverages data from specific sensors to understand the surroundings, we present basic concepts and highlight representative algorithms for two fundamental and crucial perception tasks: object detection and semantic segmentation.

A. Sensors

1) *Radar*: Radar is the abbreviation of Radio Detection And Ranging, which calculates the range and velocity of the target by transmitting radio waves and receiving the reflected waves from the target [24]. In autonomous driving applications, radar typically refers to the Millimeter-Wave (MMW) radar that works in the millimeter wave band with a wavelength of 1-10mm and frequency of 30-300GHz.

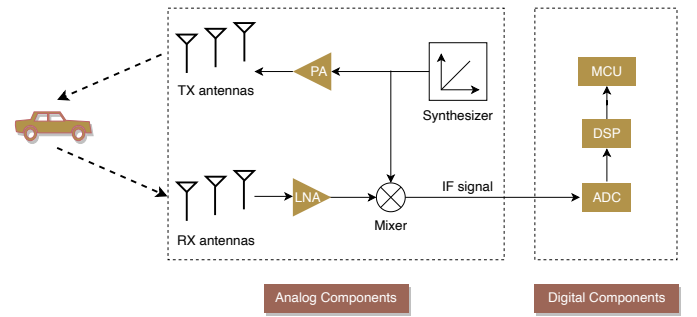


Fig. 2. Working principle of a radar sensor.

Fig. 2 demonstrates a basic radar system that comprises various analog components, like a synthesizer, a Power Amplifier (PA), transmitters (TX antennas), a Low Noise Amplifier (LNA), receivers (RX antennas) and a mixer, as well as digital components such as an Analog-to-Digital Converter (ADC), a Digital Signal Processor (DSP) and a MicroController Unit (MCU).

When the radar starts working, first, the synthesizer generates a linear frequency-modulated pulse called a “chirp”, which is amplified in power and transmitted by the TX

antenna. Second, the RX antenna captures the reflected chirp of the target that is amplified with low noise. Third, by combining the RX and TX signals, the mixer produces an Intermediate Frequency (IF) signal, which is then converted into digital values via the ADC. Generally, a radar system contains multiple TX and RX antennas, resulting in multiple IF signals. Information about the target object, such as range, Doppler velocity and azimuth angle, is contained in these IF signals, which can be separated by the DSP using embedding different signal processing algorithms [25]. Based on the extracted target information from the DSP and self-dynamic information, the MCU serves as a computer to evaluate system requirements and make informed decisions.

Based on the Time of Flight (TOF) principle, the radar sensor calculates the range from the object by the time difference between the transmitted and reflected signals. Based on the Doppler principle, when there is a relative movement between the emitted electromagnetic wave and the detected target, the frequency of the returned wave differs from that of the emitted wave. Thus, the target's relative velocity to the radar can be measured using this frequency difference. Leveraging the array signal processing method, the azimuth angle is calculated by the phase difference between the chirps reflected from the parallel RX antennas. Since RX antennas of traditional 3D radar sensors are only lined up in a 2D direction, targets are only detected in 2D horizontal coordinates without vertical height information. Recently, with advancements in radar technologies, 4D radar sensors have been developed with antennas arranged horizontally and vertically, enabling the measurement of elevation information.

In addition to the ability to measure range, Doppler velocity and azimuth angle, electromagnetic waves in the millimeter wave band have low atmospheric attenuation and better penetration of rain, smoke and dust [26]. These characteristics make the radar sensor work all day regardless of severe weather conditions. However, radar sensors still have certain limitations. They exhibit low angular resolution and cannot distinguish between closely located objects. Besides, the point clouds generated by radars are sparsely distributed, with only a few points on a pedestrian and a dozen points on a car. These points cannot adequately outline an object's contours, making it challenging to extract the geometric information [27], [28]. Furthermore, radars are weak in the perception of stationary obstacles. Moving targets can be distinguished from the surrounding scene in one dimension of range and velocity. However, radars are highly sensitive to metal, often resulting in strong reflections from stationary objects such as manhole covers on the ground. As a result, stationary objects are usually filtered in practice, resulting in a lack of detecting stationary obstacles.

2) *Camera*: The camera sensor usually consists of a lens, an image sensor, an Image Signal Processor (ISP) and an Input/Output (I/O) interface [29]. As illustrated in Fig. 3, the lens collects the light reflected from the target and converges it to the image sensor. Then, the image sensor converts light waves into electrical signals and converts electrical signals to digital values via an on-chip ADC. After that, the ISP performs post-processing (e.g., noise reduction) and converts

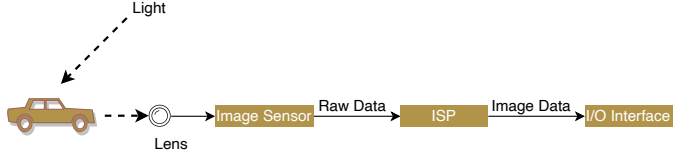


Fig. 3. Working principle of a camera sensor.

the digital values into a format of RGB data for images or videos. Finally, the image data is transferred and displayed via the I/O interface. In addition to RGB cameras, infrared lighting is also equipped with modern cameras, making them sense even at night. Moreover, gated cameras show robust perception capabilities in adverse weather, but lack color information [30], [31]. Gated imagers also rely on flood-light flash laser sources and time-synchronized cameras [32].

Cameras capture the rich appearance features of the objects, including colors, shapes and textures. After learning from neural networks, these features can be utilized to identify obstacles, including vehicles, pedestrians, bicycles and various traffic lights. However, cameras are passive sensors, indicating that the formation of an image requires incident light intake. When the light intake is adversely affected, such as insufficient light at night, extreme weather, water droplets or dust sticking to the lens, the imaging results will be unclear, and object detection performance may be significantly affected [33]. Besides, in autonomous driving, it is crucial to identify the distances of obstacles ahead. However, a target in three dimensions in the world coordinate system becomes a 2D target in the image coordinate system after being imaged by the camera sensor, resulting in a loss of distance information.

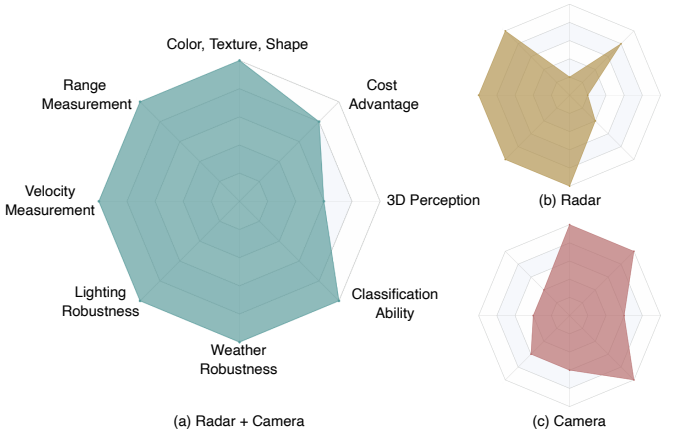


Fig. 4. Comparison of radar and camera characteristics. (a) Fusion characteristics of radar and camera. (b) Radar characteristics. (c) Camera characteristics.

3) *Comparison of Radar and Camera*: Through our extensive review, a clear and concise figure is designed to compare the characteristics of the two sensors, shown in Fig. 4. Specifically, the radar sensor is an active sensor and measures various information, including ranges, velocities and azimuth angles. Nowadays, radars equipped in driver-assistance systems can detect up to 300 meters, with a 140° horizontal field of view

and a less than 1° angular resolution [34], [35]. In addition, the radar sensor is able to adapt to darkness and extreme weather conditions, allowing it to work throughout the day. The camera sensor is a passive sensor that provides colors, textures and shapes of objects. With a resolution of up to 2K, the camera sensor performs much better in classification than the radar sensor. As far as system cost goes, both radars and cameras are relatively cost-effective and are mass-applied in vehicles.

To sum up, both the radar and camera have their strengths and weaknesses, and they cannot be substituted for each other. The most effective way to ensure adequate information acquisition is mutual integration. Based on their respective characteristics, complementary advantages can improve scenario understanding performance. In addition, when one of the sensors fails, the remaining one can continue working, thus increasing the reliability of the autonomous driving system. Hence, the fusion of radar and camera sensors is critical for perception accuracy and robustness in autonomous driving.

B. Perception Tasks

1) *Object Detection*: The object detection task involves identifying a particular object in a given image, locating its position and determining its category. Generally speaking, researchers use a rectangular or cubic bounding box to encompass the object. As there is no depth channel in 2D object detection, the rectangular bounding box is expressed as (x, y, h, w, c) , where (x, y) is the bounding box center, h and w are the height and width of the bounding box, and c is the class of the object. While the cubic bounding box for 3D object detection is described as $(x, y, z, h, w, l, \theta, c)$, where (x, y, z) represents the center of the 3D bounding box, h , w and l are the height, width and length of the bounding box, θ is the object's orientation, and c is its class.

In autonomous driving, object detection approaches have been widely used in detection vehicles [36], [37], pedestrians [38]–[40], traffic lights [41]–[44], and traffic signs [45]–[47]. According to different training steps, CNN-based object detection algorithms can be classified into two-stage and one-stage. Two-stage detection algorithms (e.g., R-CNN [48], SPPNet [49], Fast R-CNN [50], Faster R-CNN [51], FPN [52]) segregate the detection problem into two stages: the first step is to generate region proposals, and the second step is to refine the position and predict the classification of each object. Experimental results of these algorithms are high in precision and recall, but relatively slow in time. Without the region proposal generation phase, one-stage detection algorithms simultaneously predict the bounding boxes and the probability of classes within these boxes. Thus, one-stage detection algorithms are commonly faster than two-stage detection algorithms, but lower in accuracy. Some highly representative one-stage object detectors include the YOLO series [53]–[60], SSD [61] and RetinaNet [62].

Some detectors from two-stage or one-stage pre-define anchors with different sizes and aspect ratios, and then predict the offset to refine the anchors for the final bounding box. However, the results are closely related to the initial settings of the anchors, including their size, number and aspect ratio.

Thus, anchor-free object detection algorithms are proposed, allowing the network to learn the anchors' position and shape autonomously. Anchor-free object detectors are classified into two types. The first type is called dense prediction, where the position of the relative anchor is predicted densely, including YOLO [53], DenseBox [63], FCOS [64], FCOSv2 [65] and AutoAssign [66]. The other type focuses on detecting key points of targets, such as CornerNet [67], CenterNet [68], ExtremeNet [69], RepPoints [70] and Point-Set [71].

Exploiting the self-attention mechanism that enables the model to model the contextual features and their correlation, transformer-based methods have emerged as a recent breakthrough compared to CNN-based detectors. Some representative pure transformer detectors include DETR [72], Deformable DETR [73], RT-DETR [74], WB-DETR [75], Swin [76] and YOLOS [77]. Additionally, plenty of studies have endeavored to accelerate the conventional transformer block by the combination of convolution and self-attention, aggregating the advantages of both CNN and transformer, as exemplified by Conformer [78], EdgeVit [79], MobileViT [80], ViTAE [81] and Visformer [82].

2) *Semantic Segmentation*: Semantic segmentation involves clustering the basic components of input data into different semantically relevant regions. Essentially, it refers to assigning selected labels from a pre-defined set $Y = \{y_1, y_2, \dots, y_k\}$ to each pixel in an image dataset $D_c = \{d_1, d_2, \dots, d_m\}$ or each point in a radar dataset $D_r = \{d_1, d_2, \dots, d_n\}$.

The technique of semantic segmentation finds widespread application in the fields of free-space segmentation [83]–[88], lane segmentation [85], [86], [88]–[92] and obstacle segmentation [93]–[95] in autonomous driving. Fully Convolutional Network (FCN) [96] is a milestone in semantic segmentation as it enables end-to-end training of deep networks for this task. However, due to its failure to account for global contextual information, the obtained segmentation results tend to be coarse. Therefore, the encoder-decoder architecture has emerged to address this shortcoming, represented by SegNet [97], U-Net [98] and HRNet [99]. The encoder-decoder architecture typically uses an image classification network as its encoder, gradually reducing the spatial dimensions of the pooling layer. Meanwhile, the decoder gradually restores the details and spatial dimensions for segmentation purposes.

However, for encoder-decoder architectures, high-resolution representations are lost during the encoding process, reducing fine-grained information within the image. Dilated (or “atrous”) convolution structure is created to avoid decimating the input's resolution by adding a dilation rate to standard convolutions. This architecture enlarges the receptive field without increasing the parameters and avoids the loss of information caused by repeated pooling. Some notable examples of representative networks which apply dilated convolution structure include DeepLab series [100]–[103], ENet [104], PSPNet [105], DUC-HDC [106] and DenseASPP [107].

CNNs require multiple decoder stacks to map high-level features to the original spatial resolution. In contrast, transformer-based models can be graciously combined with a lightweight transformer decoder for segmentation mask prediction due to their global modeling capability and resolution invariance.

TABLE I
SUMMARY OF RADAR PARAMETER ESTIMATION [24]

Parameter	Estimation	Resolution	Note		
Range	$R = \frac{c f_b}{2S}$	(1)	$R_{res} = \frac{c}{2B}$	(2)	<ul style="list-style-type: none"> c is the speed of the light ($3 * 10^8 m/s$). f_b is the instantaneous frequency difference at the mixers from TX-chirp and RX-chirp. S is the slope of a chirp. B refers to the frequency variation range.
Doppler Velocity	$V = \frac{\lambda \Delta \phi}{4\pi T_c}$	(3)	$V_{res} = \frac{\lambda}{2T_f}$	(4)	<ul style="list-style-type: none"> λ is the wavelength of the light. $\Delta \phi$ is a shift in phase. T_f is cycle time of a frame.
Azimuth Angle	$\theta = \sin^{-1}(\frac{\lambda \Delta \phi}{2\pi l})$	(5)	$\theta_{res} = \frac{\lambda}{N_{RX} l \cos(\theta)}$	(6)	<ul style="list-style-type: none"> l is the length between RX antennas. N_{RX} is the number of RX antennas.

Recently, transformer-based segmentation models (e.g., SETR [108], Segmenter [109], SegFormer [110], Lawin [111] and MaskFormer [112]) extract global contextual features based on self-attention and achieve remarkable results.

III. RADAR DATA PROCESSING

In this section, we review the radar signal processing for radar parameters, including range, Doppler velocity and azimuth angle. Subsequently, RCS measurement is analyzed to approximate the target's size, shape and material composition, thereby characterizing its reflection properties. To filter out clutters during the radar signal processing stage, we research the workflow of Constant False Alarm Rate (CFAR) processing and explore representative CFAR processors. According to the different signal processing stages, we categorize the radar representations into five types and research their composition process and algorithms, as well as their advantages and disadvantages.

A. Radar Signal Processing

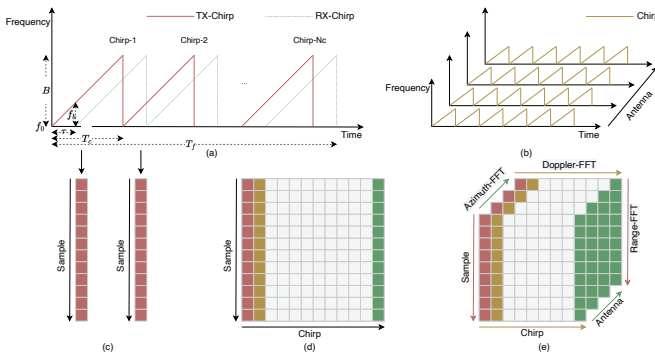


Fig. 5. Pipeline of radar signal processing. (a) Frequency of chirps emitted by a TX antenna and received by an RX antenna. (b) Frequency of chirps received by multiple RX antennas. (c) Sampling performed on each chirp. (d) Sample-Chirp map generated from sampling on all chirps. (e) Simple-Chirp-Antenna tensor generated from Sample-Chirp maps based on multiple RX antennas.

1) *Parameter Estimation*: Frequency-Modulated Continuous Wave (FMCW) is a special millimeter wave technology that continuously transmits frequency-modulated signals to measure the attributes of objects. The estimation and resolution of each attribute are summarized in Table I. As is described in Fig. 5(a), the frequency of the chirp emitted by the TX antenna increases linearly over time, leading to the corresponding frequency of the chirp reflected by the RX antenna. The IF signal containing information on objects is determined by calculating the difference of the instantaneous frequency of the TX-chirp and RX-chirp, expressed by the variable f_b .

a) *Range*: Among each chirp signal, sampling is conducted as depicted in Fig. 5(c). Then, Fast Fourier Transform (FFT) is performed to produce a spectrum with different peaks, representing different objects at different ranges. Given that FFT operation is utilized to obtain values of ranges, it is also called “Range-FFT”. From Equation 1, we know that the range of a target is determined by the difference in the frequency and the slope of a chirp. Range resolution refers to the ability to distinguish two objects located extremely close together along the range dimension. Fourier transform theory states that the range resolution can be improved by extending the IF signal [113]. Extending the IF signal requires increasing the signal bandwidth, which results in range resolution being proportional to the signal bandwidth (B), as shown in Equation 2.

b) *Doppler Velocity*: To measure the Doppler velocity of an object, two chirps separated by time T_c are transmitted. For each chirp, the spectrum after Range-FFT peaks at the same position but with different phases. The difference of the measured phase $\Delta \phi$ contains the velocity of an object, as noted in Equation 3. For multiple objects at the same range, it is difficult to identify their velocities as the peaks are located at the same position. Thus, a sequence of signals consisting of N_c chirps is employed, formulating a Simple-Chirp map shown in Fig. 5(d). Doppler-FFT is then performed on the phasors generated by Range-FFT to separate objects since the phase differences between consecutive chirps are different. Velocity resolution is the minimum difference in velocity at which a radar can distinguish between two targets at the same range.

As expressed in Equation 4, velocity resolution is inversely proportional to the cycle time of a frame (T_f).

c) *Azimuth Angle*: Estimating the azimuth angle is accomplished using at least two RX antennas separated by l . The resulting difference in distances from the target to each RX antenna causes a phase change in the FFT spectrum, from which the Angle of Arrival (AoA) can be obtained, as outlined in Equation 5. To measure the azimuth angle of multiple objects located at the same range and moving at the same velocity, multiple RX antennas are needed, as illustrated in Fig. 5(b). In this way, the radar signal is described in a Simple-Chirp-Antenna dimension, as shown in Fig. 5(e). Then, an Azimuth-FFT is performed on the phasor sequences corresponding to the peaks after 2D-FFT (Range-FFT and Doppler-FFT) to resolve azimuth angles. Azimuth angle resolution θ_{res} is the minimum angle separation for two objects appearing as separated peaks in the spectrum after Azimuth-FFT. It can be justified from Equation 6 that the azimuth angle resolution is maximum when measured perpendicular to the radar system's axis ($\theta = 0$). Additionally, it is necessary to increase the number of RX antennas to enhance azimuth angle resolution.

2) *RCS Measurement*: Radar Cross-Section (RCS) denotes the ability of an object to reflect a radar signal, and a higher RCS value corresponds to an increased likelihood of detection. The value of RCS is expressed as an area in m^2 [114]. However, this value does not simply represent the surface area of the object being detected, but depends on multiple factors, including the target's material, physical geometry, and exterior features of the target, as well as the direction and frequency of the illuminating radar.

In terms of mathematical calculations, RCS measures the ratio between the scattered density in the direction of the radar and the power density intercepted by the object. Since the power is distributed over a sphere, only a small part of this ($4\pi r^2$) can be received by the radar. Hence, the expression for RCS takes the form:

$$\sigma = \frac{4\pi r^2 S_r}{S_t}, \quad (7)$$

where r is the range from the radar to the target, S_r is the scattered power density at the radar, and S_t represents the incident power density the target intercepts.

3) *CFAR Processing*: The radar sensors not only receive the reflected signals from the objects of interest, but also encounter the internal receiver noise and external interfering signals. Signals generated by these unwanted sources are commonly called **clutters**. Traditional methods like removing signals with zero Doppler and fixing signal thresholds all have drawbacks that lead to false alarms. Consequently, dynamic thresholding, which involves using adaptive threshold values, plays a crucial role in mitigating false alarms and spurious radar detections attributable to noise signals. Compared to fixed thresholds, varied thresholds are involved in reducing false alarms and erroneous radar detections caused by noise. CFAR is the most commonly used method of dynamic thresholding [115], [116], which enables the radar system to automatically adjust its sensitivity level to changes in the strength of external interference, thereby maintaining a steady false alarm rate.

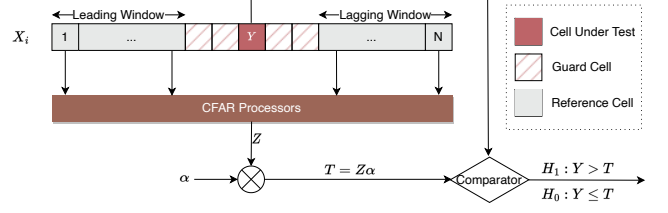


Fig. 6. Overview of CFAR processing. Set of X_1, X_2, \dots, X_N represents the detection window, Y is the value of CUT, Z represents the clutter background level of the CUT, T is the detection threshold, α denotes a scaling factor, H_1 declares that an object is located within the CUT, H_0 indicates that there is no object in the current CUT.

Fig. 6 describes the overview processing flow of CFAR processors. Before feeding the data into the CFAR processor, a square law detector is applied to convert the real and imaginary parts of the radar data into a real-valued square of its power [117]. The radar signal then runs through a sliding window comprising reference cells, guard cells, and Cell Under Test (CUT). For estimating the clutter background level, it is reasonable to use the surrounding reference cells of the CUT due to the spatial-temporal correlation of radar echo. Then, with the samples in the reference window, the clutter background level of the CUT (labeled as Z) can be evaluated based on different detectors. The threshold value T is calculated by multiplying Z by a scaling factor α . If the value of the CUT (labeled as Y) exceeds the threshold value T , the comparator will declare that an object is located within the CUT (expressed as H_1). Otherwise, there is no object in the current CUT (expressed as H_0).

A reasonable selection of processors for the clutter statistical model in the CFAR clutter window can significantly mitigate the issues of false alarms and missed alarms caused by complex situations, such as uniform clutter, multiple targets, and clutter edges in radar signals. As a result of the multitude of techniques available for estimating clutter within the CFAR framework, a variety of CFAR methods are proposed. These methods can be broadly classified into three types:

a) *Mean-level Processors*: The first type of processor comprises mean-level estimators, including Cell Averaging CFAR (CA-CFAR) [118], Greatest-of CFAR (GO-CFAR) [119] and Smallest-of CFAR (SO-CFAR) [120]. These processors obtain the estimated clutter power level by taking the average value, maximum value and minimum value of the reference cells, respectively. However, the detection mechanism in mean-level processors is not optimized for multiple objects. Other objects within the reference window distort the noise estimation and lead to an increased threshold value, thereby causing potential target detections to be missed.

b) *Sorting-based Processors*: The second category of the processor is exemplified by Ordered Statistics CFAR (OS-CFAR) [115], which sorts the reference cells in ascending order and selects the k^{th} value as the estimated clutter power level. After that, numerous methods based on ordered statistics have emerged, called OS-like methods, such as Censored Mean Level Detector CFAR (CMLD-CFAR) [121], Trimmed

Mean CFAR (TM-CFAR) [116]. However, since the sorting-based processors retain only one ordered reference sample, they rely heavily on prior knowledge about the number and distribution of interference objects.

c) *Neural Network-based Processors*: Recently, with the rapid development of machine learning and deep learning, traditional CFAR processors have evolved into neural network-based methods. A representative example of this method is DBSCAN-CFAR [122], which combines Artificial Neural Network (ANN) and a clustering algorithm of Density-Based Spatial Clustering of Applications with Noise (DBSCAN) [123]. Unlike conventional methods, DBSCAN-CFAR is able to learn the potential relationship between normal data and outliers without labels and a specific number of clusters in advance. In simulations with different object numbers, shape parameters, and false alarm probabilities, DBSCAN-CFAR exhibits superiority and robustness, outperforming conventional processors, including CA-CFAR, SO-CFAR, GO-CFAR, OS-CFAR, and CMLD-CFAR. However, to achieve the advantages mentioned above, DBSCAN-CFAR suffers from a higher computational burden and time consumption than other processors.

B. Radar Data Representations

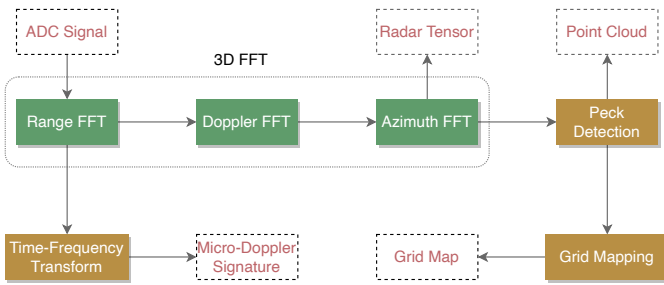


Fig. 7. Radar signal processing chain.

As depicted in Fig. 7, the raw output of a radar sensor is the ADC signal, which is hardly readable for human observers. Thus, some researchers apply 3D FFT along the sample, chirp and antenna dimensions to get an image-like representation named radar tensor. Furthermore, peak detection is carried out on the radar tensor to filter out clutter, resulting in a sparse point-like representation called the point cloud. By applying grid mapping methods to point clouds accumulated over a given period, a grid map for identifying static objects is generated. In addition, some researchers perform Time-Frequency transform [124] after the Range-FFT to obtain the micro-Doppler signature, which is utilized to recognize objects with tiny motion features. In the following contents, we elaborate on the formation process, algorithms, advantages and disadvantages associated with each of these representations.

1) *ADC Signal*: When an analog signal is sampled and quantized by an ADC, it produces a sequential data stream called the ADC signal. At this stage, the signal lacks spatial coherence between the values as all the information exists in the time domain [125]. To represent the ADC signal in a more structured form, it is usually transformed into

a 3D Sample-Chirp-Antenna (SCA) tensor, as described in Fig. 7(e). Since the ADC signal consists of raw data from the object reflection, it inherently contains rich information about the object, which can be employed for various fine-grained feature recognition tasks, such as human detection [126], human activities classification [127], gait classification [128], and hand or arm gesture recognition [129], [130]. Stephan *et al.* [126] presented a human detection approach that utilizes deep learning as a substitute for traditional signal processing procedures. The proposed solution significantly reduces the computational requirements by replacing the FFT that consumes most of the operations and simplifying the data flow in the embedded implementation. Stadelmayer *et al.* [127] applied Deep Convolutional Neural Networks (DCNN) on ADC signals to implicitly learn features for classification of human activities, including walking, standing idle, arm movement, waving, and working on a laptop. Later, they improved the approach for classifying multiple activities among multiple objects and applied it to the field of gait classification in [128]. For gesture recognition tasks, Zhao *et al.* [129] introduced a learnable CubeLearn module to extract more distinguishable features, while Arsalan *et al.* [130] used Spiking Neural Networks (SNNs) that are event-driven and energy-efficient.

Given the tasks outlined by the algorithms discussed above, neural networks that process ADC signals directly are suitable for classification tasks in closed environments, such as determining the presence or absence of objects and distinguishing between different types of objects. However, in open environments, various distracting factors may lead to inaccurate identification of object features. Therefore, the use of ADC signals for conducting object detection or semantic segmentation tasks by discerning the shape of an object is not feasible. Moreover, ADC signals require a developer kit for data acquisition and are challenging for data processing.

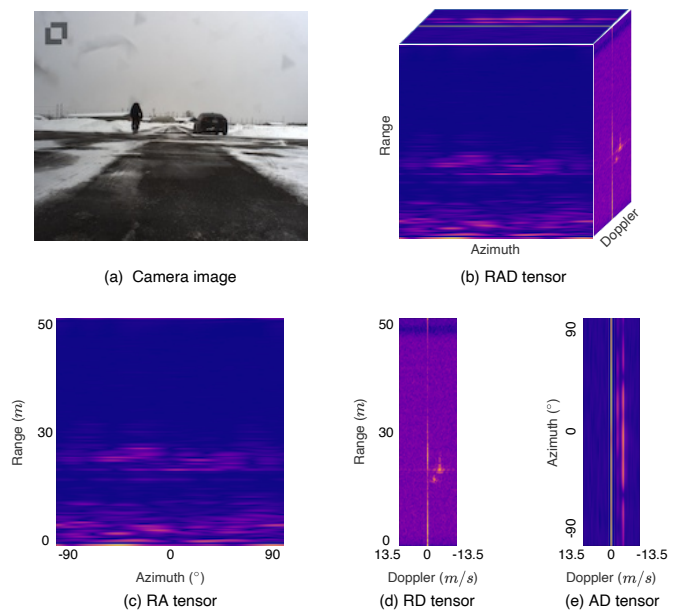


Fig. 8. Representation of radar tensor. (a) Image from the camera sensor. (b) 3D RAD tensor. (c) 2D RA tensor. (d) 2D RD tensor. (e) 2D AD tensor. Images are generated from the CARRADA [131] dataset.

2) *Radar Tensor*: As mentioned before, performing 3D FFT on ADC signals along the sample, chirp and antenna dimensions yields 3D tensors in Range-Azimuth-Doppler (RAD) coordinates, which are referred to as radar tensors. As is shown in Fig. 8, with these three features, two forms of radar tensors are formed: one is in 2D including the Range-Azimuth (RA) tensor, Range-Doppler (RD) tensor and Azimuth-Doppler (AD) tensor; the other is the whole 3D RAD tensor, with each side consisting of a 2D tensor. Specifically, each 2D tensor represents a 2D pseudo-image that describes the spatial pattern of the received echo. In particular, the brighter colors within the tensor represent greater reflection amplitude at that location [132].

To conduct object detection on radar tensors, specific neural network architectures take 2D views of the tensor as input, as has been demonstrated in various studies using RA tensors [16], [132], [133] or RD tensors [134], [135]. In addition, specific architectures have been developed to process aggregated views of RAD tensors for object detection [15], [136]–[138] and semantic segmentation [125], [139], [140]. Gao *et al.* [132] initiated the object detection process by defining a fixed-size bounding box for each detected object on the RA tensor. In addition, they extracted the radar data within the bounding box from multiple RA tensors and arranged this data in the form of radar data cubes. With the temporal information and object movement pattern, the data cubes serve as features for classifying different objects, such as pedestrians, cars and cyclists. Dong *et al.* [133] applied ResNet [141] architecture on RA tensors for object detection. They also introduced uncertainty estimation for oriented bounding box localization further to enhance the accuracy of the object detection process. Ng *et al.* [134] performed simulation object detection on RD tensors using a 2D U-Net [98] as the network architecture. Furthermore, Decourt *et al.* [135] proposed a lightweight architecture derived from Faster R-CNN [51] and extended the RD tensor-based object detection task to datasets obtained from real scenarios.

In addition to using 2D tensors, some researchers have extended the input data to 3D tensors. Major *et al.* [15] first demonstrated the effectiveness of a deep learning-based object detection model that operated on the RAD tensor and proved that the Doppler dimension helps increase detection performance. They proposed two approaches for handling the RAD tensor. The first method is to compress along the Doppler dimension, followed by mean pooling to obtain the RA model. The second approach involves enlarging the tensor by including two additional 2D tensors: the RD tensor and AD tensor, obtained by compressing along the azimuth angle and range dimensions separately. Feature maps from the three 2D tensors are concatenated together after being resized to the same size. By processing three 2D tensors instead of directly processing the whole 3D tensor, the computational complexity is reduced. Similarly to the approach proposed by Major *et al.* [15], Gao *et al.* [136] decomposed the RAD tensor into three parts separately before combining them. The primary distinction between the two approaches is that the RA tensor in [136] is comprised of complex values that aid in recognizing objects using spatial patterns. Moreover, Palfy *et al.* [137] mapped

the radar targets into radar RAD tensors and cropped the 3D radar tensors originating from each object for classification. Combining features from radar targets and radar cubes demonstrated that the proposed Radar Target Classification Network (RTCnet) outperforms previous target-wise and object-wise methods. Zhang *et al.* [138] suggested a dual detection head based on YOLOv4 [56] to enable both 3D detection on RAD tensors and 2D detection in Cartesian coordinates. Ouaknine *et al.* [140] introduced a lightweight segmentation architecture specialized for RAD tensors to deduce objects' localization and relative speed. To identify the performance of different radar tensors, Nowruzi *et al.* [125] compared three distinct input modalities: RAD, RA and Direction of Arrival (DoA) on various algorithms. In their approach, both RAD tensors and RA tensors are in polar coordinates, while DoA tensors are Bird's Eye View (BEV) maps in Cartesian coordinates generated from RA tensors. Experimental results illustrate that utilizing RAD tensors as input results in the best performance. Additionally, RA tensors outperform the DoA representation because the BEV map's far points in the DoA tensors are sparser than that of the near points. Later, they proposed an encoder-decoder network named PolarNet [139], with RA tensors serving as input. PolarNet outperforms the prior experiments utilizing DeepLabv3+ [103], FCN [96] and FCN_tiny algorithms. Furthermore, some researchers replaced FFT operations with neural networks to extract velocity and azimuth information, while retaining the chirp and antenna dimensions. For example, in RODNet [16], FFT is applied only to the sample and antenna dimensions, while the chirp dimension is preserved to construct the Range-Azimuth-Chirp (RAC) tensor. Next, a neural network named M-Net is utilized to process the chirp dimension for the extraction of Doppler features.

Compared to ADC signals that only permit the utilization of object classification tasks, radar tensors facilitate object detection and semantic segmentation tasks through combined labeling with cameras or LiDARs. They retain more comprehensive information about an object, while also reserving interference information around it. Nevertheless, the radar tensor representation requires considerable memory storage as well as large bandwidth.

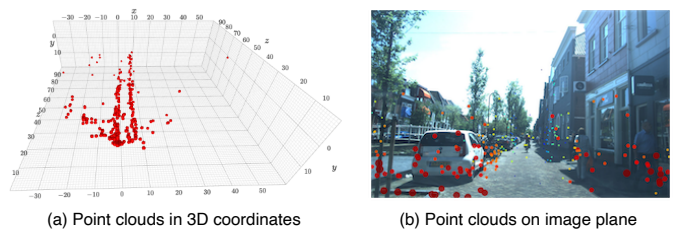


Fig. 9. Representation of point cloud. (a) Radar point clouds in 3D coordinates. (b) Point clouds projection on 2D image plane. Images are generated from the View-of-Delft [142] dataset.

3) *Point Cloud*: By CFAR processing on the radar tensor, data in the format of a group of points is obtained, which we refer to as a point cloud. As illustrated in Fig. 9, the point cloud provides a rough indication of an object's location, yet it can-

not accurately indicate the outline information of the object. Point cloud-based radar algorithms for object detection [143]–[145] and semantic segmentation [143], [146]–[150] generally draw inspiration from LiDAR-based algorithms, such as PointNet [151], PointNet++ [152] and Frustum PointNets [153].

Nabati *et al.* [9] presented Radar Region Proposal Network (RRPN), a real-time RPN with an attention mechanism for radar object detection. RRPN relies only on radar detections to propose Regions of Interest (RoI), which is extremely fast while still achieving higher precision and recall than the Selective Search algorithm. In Radar TrackNet [144], authors leveraged radar point clouds collected from multiple frames to detect and track road users. Radar feature extraction in their method is based on PointNet++ [152] and FPN [52]. Results indicate that the Doppler velocity is crucial information for radar object detection. Interestingly, Scheiner *et al.* [145] demonstrated that radar point clouds could be exploited to detect and track hidden objects in Non-Line-Of-Sight (NLOS) environments. By converting BEV radar point clouds into pseudo-images and applying a pyramid network and a zoom-in network, they estimated the geometry and velocity of collision objects before seeing them.

Schumann *et al.* [146] proposed a structure based on PointNet++ [152] for semantic segmentation on radar point clouds. The Multi-Scale Grouping (MSG) module in PointNet++ [152] helps in grouping and generating features for a center point and its neighborhoods. They demonstrated that incorporating the RCS value and compensated Doppler velocity significantly improved classification accuracy, with the Doppler velocity having a considerable impact on the results. Inspired by [146], Danzer *et al.* [143] adopted a two-stage method using PointNets [151], [153] for 2D car detection and segmentation. They considered each point as a proposal and adjusted the proposal size according to the object's prior knowledge. Then PointNet [151] and Frustum PointNets [153] are used to classify the proposals and each point in the proposal. Finally, the bounding box prediction is executed only for the proposals that are objects. Feng *et al.* [147] leveraged PointNet [151] and PointNet++ [152] architectures to present the potential of neural networks in radar point cloud segmentation. Their approach primarily emphasizes the tasks of lane, guardrail and road marking segmentation. To avoid expensive and time-consuming manual labeling of radar points, Kaul *et al.* [154] presented a weakly-supervised multi-class semantic segmentation method by combining segmented images with LiDAR points.

Since radar point clouds are generated by filtering techniques (e.g., CFAR), they have advantages in filtering noise, yet some potential information within the raw data may inevitably be lost [15]. Additionally, some small objects or objects with weak reflections may not be rendered as point clouds. Currently, most point cloud detection and segmentation algorithms in radar are based on LiDAR algorithms. Point clouds in LiDARs are dense and can describe the outline of surrounding objects. Conversely, radar point clouds are incredibly sparse, posing challenges to developing effective algorithms. To address this issue, point cloud algorithms need to explore the intrinsic relationships between point clouds and

leverage velocity and RCS information to provide additional features.

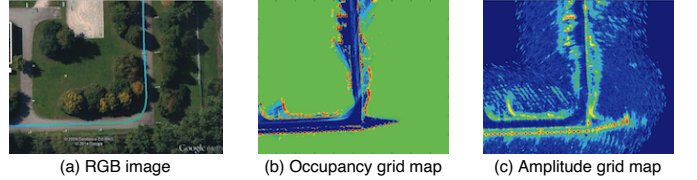


Fig. 10. Representation of grid map. (a) RGB image from BEV. (b) Occupancy grid map representing obstacles and free-space. (c) Amplitude grid map representing RCS values. Images are from [155].

4) *Grid Map*: Leveraging multi-frame point clouds, some researchers transform spatially inhomogeneous radar reflections into a BEV pseudo-image, commonly called a grid map [146]. As the grid map has the same structure as the 2D image, deep learning-based algorithms can be directly implemented for detection and segmentation tasks.

There are two main grid maps: one is the occupancy-based grid map [155]–[164], which represents the obstacles and free-space derived from the radar data; the other is the amplitude-based grid map [155], [156], which displays the reflected RCS values for each cell. As can be seen from Fig. 10(b), an occupancy-based grid map has clearer and more distinguishable outline, which makes it more feasible for outline-based detection tasks (e.g., parking spaces) or free-space segmentation. An amplitude-based grid map shown in Fig. 10(c) emphasizes the reflective characteristics of different objects, rendering it more appropriate for rural roads with a few distinct objects. Werber *et al.* [155] presented occupancy-based grid maps and amplitude-based grid maps, both designed for self-localization tasks. Experiments indicate that both occupancy-based and amplitude-based algorithms successfully provide adequate representations of surrounding environments. After that, they employed a CNN named LeNet-5 [165] to classify vehicles and non-vehicles [156]. Furthermore, based on classification research on the occupancy-based grid map [166], [167], Lombacher *et al.* [157] applied a pixel-based algorithm [168] to classify each grid, demonstrating the likelihood of gaining semantic knowledge through radar grid maps. Dreher *et al.* [169] converted the point clouds into grid maps with a maximum of one point per grid and employed YOLOv3 [55] for detection. In addition to 2D grid maps, [158]–[160] focused on segmenting vehicles using 3D occupancy grid maps, in which the third dimension is encapsulated by height information and represented through distinct colors in the respective grid. Apart from segmentation on vehicles, [161], [162] utilized grid maps to segment the free-space of drivable areas, which are valuable to vehicle trajectory planning.

Depending on specific scenarios and contexts, different algorithms offer suitable gridding and mapping solutions. Wen *et al.* [170] conducted research on grid mapping comparison and evaluated the map quality through quantitative simulations and experiments. New studies attempted to construct grid maps through deep learning. For example, Sless *et al.* [163] leveraged LiDAR ground truth and supervised learning to achieve occupancy grid mapping for static obstacles. Specifically,

they proposed an occupancy net using an encoder-decoder architecture with skip connections. This approach derives the underlying joint probability function from data and surpasses classic methods.

Above all, the grid map representation is useful for static objects as the velocity information of each object is ignored when constructing the map. To accommodate both static and dynamic objects, Schumann *et al.* [164] introduced a two-branch network, separating static and dynamic objects into distinct branches. One branch performs semantic segmentation on grid maps for identifying static objects, while the other branch carries out instance segmentation on point clouds for detecting moving objects. The outputs of the two branches are then merged to generate semantic point clouds. However, this two-branch structure also results in high computational effort and increased memory consumption. In another aspect, as grid maps are constructed from a series of radar point clouds, they are unsuitable for real-time mapping. Additionally, the sparsity of the point clouds still influences the accuracy of detection and segmentation performed on the grid map.

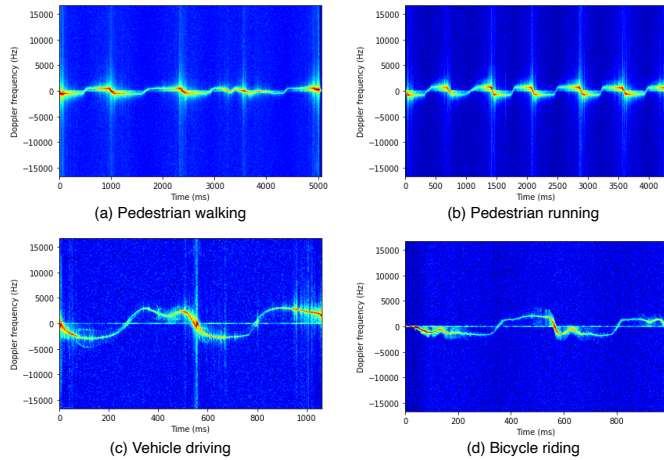


Fig. 11. Representation of micro-Doppler signature. (a) Spectrogram showing a pedestrian walking. (b) Spectrogram showing a pedestrian running. (c) Spectrogram showing a vehicle driving. (d) Spectrogram showing a bicycle riding. Images are generated from the Open Radar Datasets [171].

5) *Micro-Doppler Signature*: Micro-Doppler Signature (MDS) refers to the representation of micro-motion, such as rotation and vibration caused by object parts, resulting in a characteristic representation that differs from the Doppler frequency variation. It is generated by the Time-Frequency transform methods (e.g., Short Time Fourier Transform (STFT), Wavelet Transform (WT)) on Range-FFT results. As illustrated in Fig. 11, the spectrograms of walking and running pedestrians reveal different features. Specifically, the period of the micro-Doppler for a running pedestrian is shorter than that for a walking pedestrian. Moreover, the spectrograms between different types of objects (e.g., vehicles and bicycles) are unique, making them powerful features for object classification.

Over the past few years, significant research attention has been paid to the classification and recognition of objects' postures and activities through MDS-based methods, particularly in the areas of object classification [132], [172], human

activity and gait recognition [173]–[175], and human gesture recognition [176]. Gao *et al.* [132] generated STFT maps from the cropped radar RA tensor and fed them to the VGG16 [177] deep learning classifier for MDS extraction. A decision tree algorithm was then used to evaluate three classes: car, pedestrian and cyclist. Moreover, Angelov *et al.* [172] converted the raw ADC signal into spectrograms and performed object classification among persons, bicycles and cars. They conducted a comparative evaluation of diverse neural network architectures on MDS, including VGG-like CNN, convolutional residual network, and the combination of convolutional and recurrent Long Short-Term Memory (LSTM) network. The findings of their study suggest that residual networks are more effective than simple CNN in the radar MDS classification task among diverse spectrograms. Gurbuz and Amin [173] also demonstrated that data-driven approaches outperform conventional classification methods using handcrafted features. Kim and Moon [174] applied DCNN to human detection and activity classification tasks. They conducted STFT on the self-collected data and generated spectrograms for four objects and seven human activities. Additionally, they pointed out that MDS shapes are crucial to classification. If the motions are irregular, the model's classification performance is adversely affected. Seifert *et al.* [175] extracted features from the time-scale domain by forming a feature vector for each detected frame, and then analyzed the features among normal walking, abnormal walking and the use of assistive walking devices. The resultant features provide valuable insights for monitoring the recovery progress from physical and possible cognitive impairment.

Apart from the spectrogram presenting Doppler information in the time domain, another representation of MDS that exists in the frequency domain is the Cadence-Velocity Diagram (CVD), which is derived by taking the Fourier transform of the spectrogram along the time axis [178]–[180]. Based on [175], to distinguish among distinct walking styles, Seifert *et al.* [178] used pre-defined features and Principal Component Analysis (PCA) in a periodically frequency-modulated signal. Kim *et al.* [179] proposed a pseudo-image by merging spectrograms and CVDs, and then utilized GoogLeNet [181] for drone classification. Furthermore, Chen *et al.* [180] combined spectrograms and CVDs with an attention-based network for gait recognition. They split spectrograms and CVDs into patches while embedding their positions using the vision transformer. By integrating the discriminant features from these two representations, their proposed attention-based fusion scheme outperformed SOTA solutions.

MDS recognizes targets by observing minute movement characteristics of objects. This representation enables not only the distinction of different object categories (e.g., pedestrians, bicycles and vehicles), but also the recognition of complex object behaviors, such as gait and gesture recognition. However, the transformation to the frequency domain via Time-Frequency transform suffers from the superposition of target components, leading to suboptimal feature extraction for subsequent computational tasks [128]. Similar to the ADC signal representation, since MDS is insufficient in delineating an object's spatial coordinates required for object detection

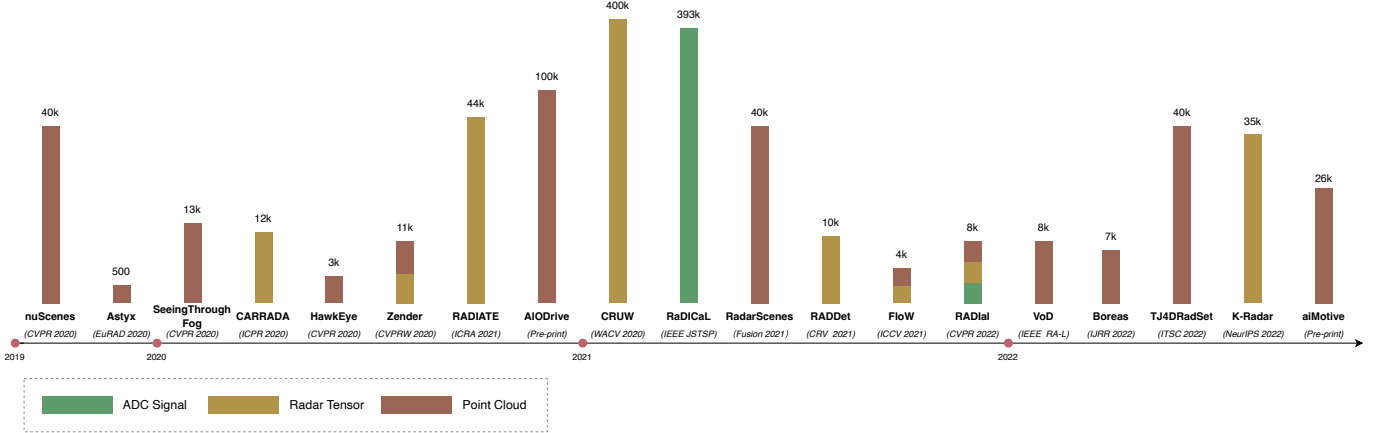


Fig. 12. Overview of radar-camera fusion datasets. Color of the bar denotes different radar representations, and height of the bar represents the size of each dataset.

and semantic segmentation, it is commonly employed for classification tasks.

IV. FUSION DATASETS

High-quality and large-scale data are fundamental for deep learning-based perception algorithms in autonomous driving. Datasets containing data from LiDARs and cameras, such as KITTI [182], Oxford RobotCar [183], ApolloScape [184], and Waymo [185], have been widely used for LiDAR-camera fusion in autonomous driving. As radar research continues in-depth, dozens of radar and camera datasets have been released in recent years. In this section, we analyze and summarize these datasets designed explicitly for tasks related to object detection and semantic segmentation. Fig. 12 presents clear statistics of radar-camera fusion datasets with their radar representations and dataset sizes. We also provide a table for retrieval and comparison of different datasets (see Table II).

A. Dataset Tasks

According to the dimension of bounding boxes and masks, datasets that incorporate radar and camera modalities in object detection and semantic segmentation are categorized into four groups:

- **2D object detection:** SeeingThroughFog [31], CARRADA [131], Zender [186], RADIATE [187], AIODrive [188], CRUW [189], RaDICaL [190], RadarScenes [191], RADDet [138], FloW [192], RADial [193], VoD [142] and Boreas [194];
- **3D object detection:** nuScenes [5], Astyx [195], SeeingThroughFog [31], AIODrive [188], VoD [142], TJ4DRadSet [196], K-Radar [197] and aiMotive [198];
- **2D semantic segmentation:** CARRADA [131] and RADial [193];
- **3D semantic segmentation:** HawkEye [199] and RadarScenes [191].

Regarding dataset tasks, most datasets are oriented toward object detection, whereas comparatively fewer datasets are employed for semantic segmentation tasks. Notably, CARRADA [131], RadarScenes [191] and RADial [193] can be applied

to both object detection and semantic segmentation tasks. As to those datasets that contribute to multiple tasks, nuScenes [5] is the most widely used dataset in radar-camera fusion algorithms, supporting tasks of detection, tracking, prediction and localization. In addition to object detection, RADIATE [187] involves object tracking, scene understanding and SLAM tasks. Moreover, datasets like Zender [186] and Boreas [194] are available for localization and odometry.

B. Sensing Modalities

In radar-camera fusion datasets, the data produced by the camera sensor is either a single image or a video over a while, both of which are essentially 2D images. In comparison, data produced by the radar sensor is rich in representations, which can be grouped into ADC signal, radar tensor, and point cloud according to the stages of data processing.

1) *ADC Signal*: As the raw data produced by radar sensors, ADC signals retain all semantic information and can be highly valuable in deep learning applications. Up to now, only two radar-camera fusion datasets provide raw ADC signal data: RaDICaL [190] and RADial [193]. RaDICaL [190] is the first dataset providing raw ADC signal data, specialized for object detection tasks involving pedestrians and vehicles. The authors encouraged researchers to further design their own processing methods by providing the raw radar measurements. RADial [193] is the richest dataset regarding radar data representations, offering not only ADC signals, but also processed data after ADC signals, including radar tensors and point clouds.

2) *Radar Tensor*: After multiple FFTs, radar tensors are obtained from ADC signals. They can be classified into three categories: 2D tensors (e.g., RADIATE [187], CRUW [189], FloW [192]), 3D tensors (e.g., CARRADA [131], Zender [186], RADDet [138], RADial [193]) and 4D tensors (e.g., K-Radar [197]). Both RADIATE [187] and CRUW [189] are in range-azimuth coordinates, presenting the BEV position of objects, while the FloW [192] dataset is in range-Doppler coordinates, illustrating the relationship between range and Doppler velocity of each object. CARRADA [131] is the first dataset that combines synchronized stereo RGB images and

3D radar RAD tensors in autonomous driving. As far as we are aware, K-Radar [197] is the only dataset containing 4D radar tensors, with full information on range, Doppler, azimuth and elevation.

3) *Point Cloud*: Compared to radar tensors, point clouds serve as a lighter and more intuitive representation of objects. They are also the format of data output from commercial radars. Conventional 3D radars produce sparse point clouds, such as data in nuScenes [5], Zender [186], SeeingThroughFog [31], HawkEye [199], AIODrive [188], RADlal [193], FloW [192], RadarScenes [191] and aiMotive [198] dataset. In recent years, the radar sensor has advanced from 3D to 4D with improvements in resolution and elevation measurement capabilities. Consequently, public 4D radar-camera fusion datasets are emerging, with examples such as Astyx [195], VoD [142] and TJ4DRadSet [196]. Although Astyx [195] is the first 4D point cloud dataset, it is limited by the data size, containing only 500 frames. VoD [142] and TJ4DRadSet [196] datasets are improved in terms of data categories and data size, with the former consisting of 13 types and 8,693 frames, and the latter containing eight types and 40k frames. Meanwhile, these two datasets also contain simultaneous LiDAR data, facilitating comparison between the 4D radar point clouds and LiDAR point clouds.

C. Dataset Categories

For autonomous driving, it is critical to identify Vulnerable Road Users (VRU) on roads. Therefore, the most common categories in these datasets are pedestrians, bicycles, and cars [131], [142], [187]–[189], [191], [195]. Datasets such as nuScenes [5], AIODrive [188], RadarScenes [191], VoD [142] and aiMotive [198] have studied more than ten categories. nuScenes [5] provides precision in its classifications, with 23 object categories refining certain ambiguous categories. For instance, the pedestrian category is sub-categorized into groups such as adult and child, while the vehicle category is subclassed into the car, ambulance, police, motorcycle, trailer and truck. Except for the category of pedestrian, RADlalate [187] and RadarScenes [191] include a class called pedestrian group. AIODrive [188] and VoD [142] classify stationary objects on the roadside, such as building, road, wall, traffic sign, unused bicycle and bicycle rack. Furthermore, apart from objects on road surfaces, FloW [192] is a floating waste dataset containing the category of bottle that can be utilized for Unmanned Surface Vehicles (USVs) on water surfaces.

In addition to the primary object categories, some specific attributes of the object are also labeled in some datasets. Examples can be found in nuScenes [5], in which vehicles are labeled as moving, stopped or parked, while pedestrians are marked as moving or standing. Besides, in VoD [142] dataset, two types of occlusions (“spatial” and “lighting”) and attributes related to an object’s activity (“stopped”, “moving”, “parked”, “pushed” and “sitting”) are also annotated. All these specific attributes are essential for scene understanding.

D. Dataset Size

The reviewed datasets differ significantly in size, ranging from 500 to 1.4 million frames. nuScenes [5] is the largest

dataset with 1.4 million images, radar frames and object bounding boxes in 40k keyframes. These data frames are split from 15 hours and 242 kilometers of driving data. On the other hand, Astyx [195] provides only 500 frames, containing around 3k labeled 3D object annotations. Others like CRUW [189], CARRADA [131], RADlalate [187], AIODrive [188], SeeingThroughFog [31], CRUW [189], RADlalate [138] and RADlal [193] all contribute hundreds of thousands of frames.

In addition to data in frames, some datasets deliver videos for researchers to split keyframes and conduct further research on videos. For example, RadarScenes [191] offers 158 individual sequences with a total length of over four hours. Similarly, CRUW [189] and CARRADA [131] datasets provide videos of 3.5 hours and 21.2 minutes, respectively.

E. Recording Scenarios

A rich data collection environment is crucial for training robust models in autonomous driving. Generally, datasets for autonomous driving are collected in road environments like urban streets, country roads, highways and parking lots, which are all represented in datasets like CARRADA [131], RADlalate [187], RadarScenes [191], RADlal [193], and K-Radar [197]. However, it is not enough to collect data in common areas. nuScenes [5], Zender [186], SeeingThroughFog [31], AIODrive [188] and CRUW [189] involve dense traffic and challenging driving situations, including urban roads, residential areas and industrial areas. Moreover, RadarScenes [191] offers data for selected particular scenarios, such as T-junctions, commercial areas and road works. All the datasets mentioned above are from outdoor environments, and as to indoor scenarios, HawkEye [199] and RaDICaL [190] are collected in indoor parking garages. These indoor environments present unique challenges and can help advance research in indoor autonomous vehicle navigation.

In terms of weather and lighting conditions, related data can be found in nuScenes [5], SeeingThroughFog [31], CARRADA [131], RADlalate [187], K-Radar [197], AIODrive [188], CRUW [189], TJ4DRadSet [196] and aiMotive [198]. In particular, SeeingThroughFog [31] focuses on extreme weather conditions, like fog, snow and rain. This dataset highlights the importance of data fusion and the redundancy of multiple sensors in adverse weather environments. In addition to adverse weather conditions, RADlalate [187], K-Radar [197] and aiMotive [198] involve conditions for the night. AIODrive [188], CRUW [189] and TJ4DRadSet [196] supply data in specific vision-fail scenarios, such as darkness, bright light and blur, where the images are pretty bad in quality. These datasets provide valuable information about how autonomous driving technology operates in low visibility and low light scenarios. Boreas [194] is a dataset involving data taken from specific routes through one-year repeat collection. It can be leveraged to study the effects of seasonal variation on self-localization and object detection.

Since it is time-cost and resource-cost for data collection on roads, some researchers have adopted simulated data to generate datasets. In HawkEye [199], raw low-resolution heatmaps are transformed into high-frequency shapes. Additionally, the

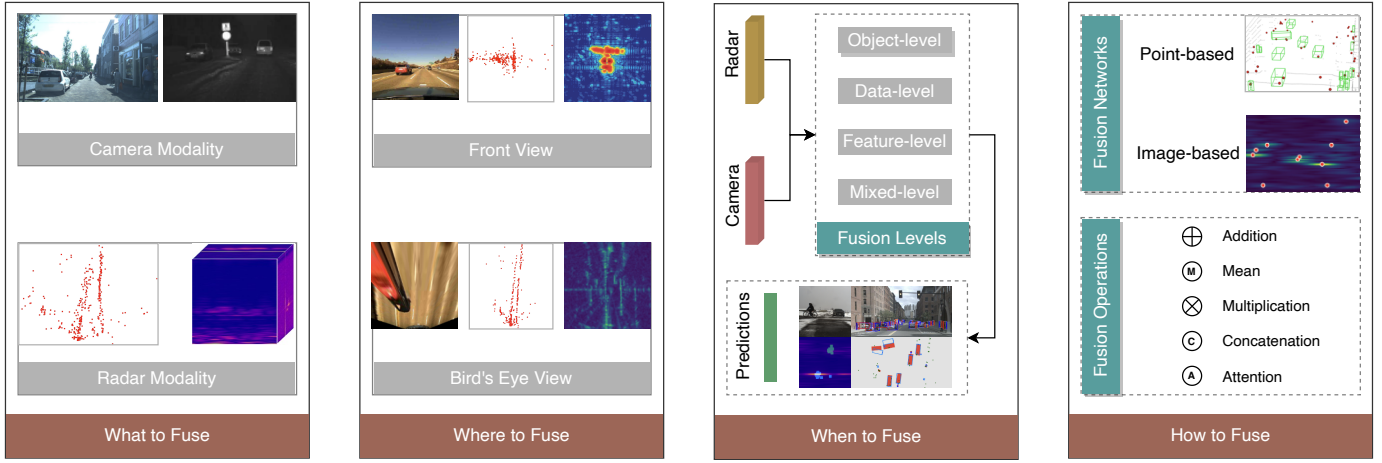


Fig. 13. Methodologies of radar-camera fusion. (a) “What to fuse”: the input modalities for radar-camera fusion, such as RGB images, near-infrared images, point clouds, and radar tensors. (b) “Where to fuse”: the position transformation for radar-camera fusion, including two perspectives: front view and bird’s eye view. (c) “When to fuse”: at which stage the two modalities are fused, encompassing the fusion of final objects, raw data, extracted features and mixed representations. (d) “How to fuse”: the architecture of fusion networks and fusion operations, comprising of two types of networks, namely point-based and image-based, and five types of fusion operations, namely addition, mean, multiplication, concatenation and attention.

authors developed a data synthesizer to simulate radar signals from the created 3D point reflector models of cars. Meanwhile, Weng *et al.* [188] used Carla [200] simulator to create different driving scenarios with various sensors. With the annotation data generated by combining and post-processing Carla outputs, they presented AIODrive [188], a large-scale synthetic dataset for all mainstream perception tasks.

V. FUSION METHODOLOGIES

In this section, we delve into the methodologies related to radar-camera fusion, starting with “why to fuse”, that is, the purpose and advantages of fusion. Subsequently, we analyze “what to fuse”, covering diverse representations of both radar and camera modalities implicated in fusion. Next, we investigate “where to fuse”, describing the coordinate relations between the two modalities before fusion. In the section on “when to fuse”, we categorize the current fusion levels and illustrate their differences. Last but not least, we explore the specifics of “how to fuse”, including temporal-spatial synchronization, fusion operations, network architectures and model evaluations. An overview of radar-camera fusion methodologies is demonstrated in Fig. 13.

A. Why to fuse

The integration of radar and camera sensors is intended to enhance the perception outcomes by capitalizing on the advantages of both sensing modalities. As illustrated in Fig. 4 in Section II-A3, the combination of a radar sensor and a camera sensor enables the measurement of rich object attributes such as color, shape, range, and velocity. In addition, with the ability to perceive in darkness and adverse weather conditions, the fusion of radar and camera can work all day in autonomous driving.

Numerous studies have also demonstrated that radar-camera fusion improves the accuracy and robustness of the network.

As it is difficult for image-based detectors to detect distant objects, Chadwick *et al.* [201] combined a radar sensor and sets of camera sensors in their experiments. Results exceed the performance of the camera detector, as the radar sensor persists in delivering a potent indication of motion for faraway objects. Major *et al.* [15] also proved that the velocity dimension derived from the radar sensor could be leveraged to increase detection performance. Additionally, Nabati and Qi [17] utilized radar features (e.g., depth, rotation, velocity) to complement the image features, resulting in an improvement of the overall nuScenes Detection Score (NDS) by more than 12% compared to the SOTA camera-based algorithm including OFT [202], MonoDIS [203] and CenterNet [204]. In noisy circumstances, Yadav *et al.* [205] discovered that radar data exhibit robustness in detection, and integration of radar data could enhance performance in these challenging scenarios.

B. What to fuse

The objective of radar-camera fusion is the output data from the radar sensor and camera sensor, which are presented in different modalities at various fusion stages and via different fusion techniques. For the camera sensor, the output data is typically presented as 2D images. In radar-camera fusion, there are mainly two kinds of images. One type is the RGB image with rich color information, such as images in nuScenes [5] dataset. The other is the infrared image captured with infrared cameras (including Far Infrared (FIR) and Near Infrared (NIR)), as illustrated in the images from SeeingThroughFog [31] dataset. Though in lower resolutions, these images contain specific advantages in temperature differences and night visibility. The data structure of an image is relatively simple, with low data dimensionality and high correlations between neighboring pixels. The simplicity of this structure allows deep neural networks to learn the fundamental representations of images, thus enabling them to detect objects within the images [197].

As mentioned in Section III-B, radar data can be classified into different representations depending on the level of processing. ADC Signals, the underlying digital signals of the radar, cannot be marked with the location information of an object. MDS, a Time-Frequency representation, consists of consecutive radar frames and does not correspond to a single image frame. As a result, ADC Signals and MDS are commonly used for identifying the presence of objects and discriminating between different objects [127], [129], [174], [180]. With the ability to describe the shape of an object, radar tensors and point clouds are commonly leveraged for object detection and semantic segmentation tasks.

C. Where to fuse

1) *Front View*: Fusion at the Front View (FV) involves projecting the radar data onto an image plane, where the radar data can be 3D point clouds, partial point cloud information or radar tensors. Around the projected area, proposals that indicate potential objects are generated [9], [205]–[208]. In this way, a large number of non-object regions are excluded, thus reducing the computational burden and increasing recognition speed. Radar data mapped to the image plane can also be utilized to create feature maps for complementing the image-based features [17], [201], [209], [210]. These methods improve the detection accuracy by leveraging the additional input, including ranges, velocities and RCS values. Moreover, some researchers project radar point clouds onto the image plane to form a radar pseudo-image [28], [211], [212]. For example, In RVNet [28] and SO-Net [211], a pseudo-image named “Sparse Radar Image” is generated from radar data, containing information regarding depth, lateral velocity and longitudinal velocity. Besides, Dong *et al.* [212] projected both radar point clouds and 2D bounding boxes onto the image plane, forming new pseudo-images from camera RGB images.

Projecting radar data onto the image plane assists in providing proposals and features. However, due to the low resolution in the azimuth angle provided by the radar as well as camera calibration errors, projected radar point clouds may deviate from the object. While increasing the RoI could potentially address the issue, it results in multiple objects within the same region, and consequently being detected repeatedly, causing confusion in object matching. Moreover, due to the occlusion of objects, the projection of radar data onto the image perspective may be limited.

2) *Bird’s Eye View*: Another fusion position is to convert radar data or camera images into Bird’s Eye View (BEV) coordinates. For example, radar point clouds from each frame generate a BEV image of six height maps and one density map in [195]. Besides, Cui *et al.* [207] projected radar point clouds to both FV and BEV, and proposed a 3D region proposal network to generate proposals from both camera images and radar BEV images. Compared with generating proposals directly from point clouds, the CNN-based proposal generation approach increases the quality of proposals by leveraging the network’s ability to extract deeper and richer information. Problems come that BEV images discretize the sensing space into grids, which may lead to the loss of valuable information

necessary to refine bounding boxes. To address this issue, Bansal *et al.* [213] added additional point-based features (e.g., velocities, RCS values) to the BEV map. Harley *et al.* [214] converted all radar point clouds from multiple radar sensors into BEV coordinates to yield high-dimensional BEV feature maps.

Apart from projecting radar data into BEV, Inverse Projection Mapping (IPM) [215], [216] method can be utilized to convert camera images from FV to BEV with a homography matrix. For instance, Lim *et al.* [217] transformed the camera images into Cartesian coordinates using IPM and then combined them with 2D radar RA tensors. In addition, both radar point clouds and camera images are projected onto BEV in [218], where the independent feature extractors learn shared features. Consequently, projecting data on BEV offers several advantages over FV, particularly in the case of occlusion [219]. Nonetheless, since IPM is based on an assumption of flat road surfaces, it often produces distortions of dynamic objects when applied to real-world scenarios [218].

D. When to fuse

When to fuse refers to at which stage the radar and camera data are fused in the network. Based on the occasion of the fusion process, we classify radar-camera fusion stages into object-level, data-level, feature-level and mixed-level. Fig. 14 illustrates the overview and difference between the four fusion levels.

1) *Object-level Fusion*: For object-level fusion (also known as decision-level fusion or late-level fusion), the independent objects acquired from the radar and camera sensors are fused at a later stage of the network to obtain the final integrated results, as demonstrated in Fig. 14(a). In object-level fusion, how to match the results from the two different modalities is worth considering. One way is to calculate the similarity (e.g., location, size, category) and then employ methods such as the Kalman filter, Bayesian theory, Hungarian algorithm and Bipartite Matching to match the outputs. Another approach involves utilizing the transformation matrix between the radar and camera to determine the position relationships between the two modalities. For example, Jha *et al.* [220] projected the radar detections onto the image plane using the transformation matrix, and then aligned independent detection objects from the two sensors. Moreover, after completing the association of radar point clouds with camera images, Dong *et al.* [212] proposed AssociationNet for learning the semantic representation information from the two sensors. This network improves the accuracy of association by calculating and minimizing Euclidean distance between the representations from the pair of radar point clouds and image bounding boxes.

Object-level fusion is commonly used in conventional radars and cameras, which offers high flexibility and modularity [221]. However, it also relies heavily on the accuracy of outputs from individual modules. For example, in scenarios where the camera sensor is obstructed, object-level fusion exclusively depends on the final objects detected by the radar sensor. Besides, rich intermediate features are discarded due to the sensing modality’s weaknesses or errors in the sensors. As

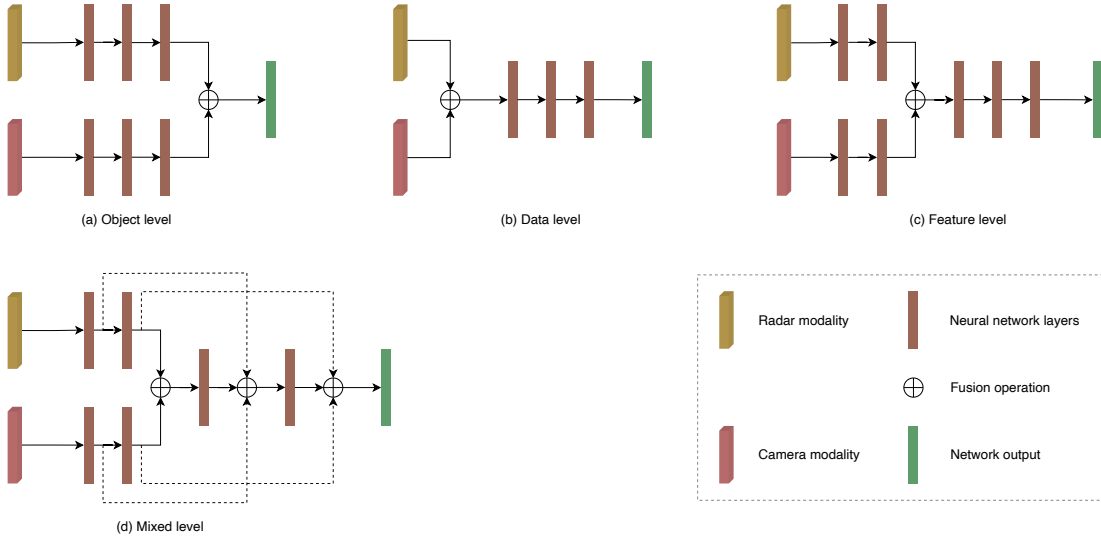


Fig. 14. Taxonomy of radar-camera fusion levels. (a) Object-level fusion. (b) Data-level fusion. (c) Feature-level fusion. (d) Mixed-level fusion.

a result, object-level fusion methods can only utilize limited information obtained from the detection results.

2) *Data-level Fusion*: For data-level fusion (also referred to as low-level fusion or early-level fusion), the raw data or pre-processing data from radar and camera sensors are fused at the early stage of deep learning models, illustrated in Fig. 14(b). Nobis *et al.* [222] fed the concatenated camera and radar point clouds into the network and then employed VGG [177] to extract features from the combined data. Moreover, Bansal *et al.* [213] created a Semantic-Point-Grid (SPG) representation from camera semantic maps, radar point clouds and radar BEV grid maps. In their method, the SPG representation is then fed into SPG encoding to extract semantic information from cameras, aiding in the identification of radar points associated with objects of interest. Instead of fusing radar point clouds with camera images, Nabati and Qi [9] proposed an RRPN, which generates object proposals to narrow the scope of detection on the camera images. However, if there is no radar point on an object, this object will be ignored. To solve the difficulty of associating radar point clouds with image pixels, Long *et al.* [223] presented Radar-Camera Pixel Depth Association (RC-PDA), a learned method that associates radar point clouds with nearby image pixels to enhance and densify the radar image.

With the input of raw data, it is possible to exploit complete characteristics and learn a joint representation from these two modalities. However, data-level fusion methods tend to be sensitive to temporal or spatial misalignment within the data. Precise external calibration of the two sensors is essential for data-level fusion. Besides, as radar data representations are not consistent with the object's shape, it is difficult to match the radar tensors or radar point clouds with the image pixels.

3) *Feature-level Fusion*: In feature-level fusion (also called middle-level fusion), features extracted from separate radar data and camera images are combined at an intermediate stage in deep learning-based fusion networks, as shown in Fig. 14(c). In [201], features from both radar and camera

branches are generated by ResNet [141] blocks and then fused by concatenation and addition operations. CenterFusion [17] detects objects by locating their center points in the image using CenterNet [204]. After that, it utilizes a frustum-based association strategy to accurately match radar detections with objects in the image, generating radar-based feature maps to augment the image features. Chang *et al.* [224] introduced the attention mechanism for weighting different positions of the feature maps. Specifically, they applied a Spatial Attention Fusion (SAF) block to merge the feature maps from radar and camera. In the SAF block, the radar image's feature maps are encoded as a spatial attention weight matrix, which is then applied to all channels to re-weight the feature maps extracted by the camera sensor. In fact, attention maps can be generated from various sensors. Bijelic *et al.* [31] extended the sensors to RGB camera, gated camera, LiDAR and radar by transforming all sensor data into uniform image coordinates. The feature maps of different sensors are then superimposed together by concatenation and multiplied with the sigmoid-processed entropy map for the final feature output.

For feature-level fusion, it is possible to design appropriate feature extractors for each modality according to its specific characteristics. Neural networks can also learn features jointly across modalities, making them complementary to each other. However, it is worth noting that feature extraction and feature fusion do not address scenarios where camera sensors become unreliable [221].

4) *Mixed-level Fusion*: Apart from equally fusing final objects, raw data or features from two modalities, some fusion methods combine different stages of data, which we define as mixed-level fusion, shown in Fig. 14(d). In [206], radar proposals are first generated from radar point clouds and 3D anchors derived from camera images. Then a Radar Proposal Refinement (RPR) network is proposed to fuse the radar proposals with camera image features, which enables the adjustment of the size and location of the radar proposals in the image. Besides, the RPR network also estimates an

objectness score for each radar proposal, as some radar point clouds are caused by background noise. Similarly, Cui *et al.* [207] generated proposals based on camera images and radar BEV point clouds, followed by projecting the proposals onto three feature maps from camera images, radar BEV point clouds and radar FV point clouds. A Self-Supervised Model Adaptation (SSMA) block [225] is utilized to fuse the proposals with features, which leverages an attention scheme for better correlation. Furthermore, HRFuser [226] introduces ideas from HRNet [99] and HRFFormer [227], adopting an asymmetric Multi-Window Cross-Attention (MWCA) to fuse the features captured by the RGB camera, LiDAR, radar and gated camera.

Compared with data-level and feature-level fusion, fusion from both proposals and features leads to more accurate proposals, producing better features for the two-stage network. Generally, different modalities have different contributions to radar-camera fusion. One modality dominates, while the other provides supplementary information to refine the features. Thus, mixed-level fusion takes advantage of different data levels and effectively preserves information at various stages. However, mixed-level fusion should consider the importance of different modalities, which also pose implementation challenges. Since most implementations of mixed-level fusion are based on experience and lack explainability to some extent, conducting numerous ablation experiments is needed to validate the efficiency of mixed-level fusion. Moreover, models based on mixed-level fusion typically have more branches in neural networks, dramatically slowing down the inference time.

E. How to fuse

In this section, we present how to fuse radar data with camera images. First of all, the primary consideration is the temporal and spatial alignment between the two sensors. Then, in fusion operations, we compare five operations and analyze their advantages and disadvantages. As far as network architectures for fusion are concerned, we categorize them into two architectures: point-based and image-based, followed by elaborating on the main ideas in these architectures. Finally, we also review various metrics for model evaluation.

1) *Temporal Alignment*: Temporal alignment in sensor fusion refers to synchronizing the temporal sequences of data from different sensors. To obtain high-quality fusion results, the data collected by each sensor must be synchronized with the same time dimension. However, there may be time offsets between these sensors due to the differences in set-up time, crystal oscillator frequencies and measurement latency. Depending on the object of the temporal alignment methods, we categorize them into two types: estimating temporal latency between sensors and estimating temporal offset within the same frame.

a) *Estimating Temporal Latency*: Generally, temporal latency consists of the measurement latency between sensors and the drift between different frames. Measurement latency mainly stems from computer scheduling, measurement acquisition, pre-processing, and communication transfer time. In

aligning cycle time, drift is caused by the offset between the internal clock and the Coordinated Universal Time (UTC).

A software-based technique for reducing temporal error is periodically estimating the maximum measurement latency and drift time [228]–[230]. Another alternative approach is to predict the future latency between sensors using Kalman filters [231] or Bayesian estimation [232] based on prior knowledge of the sensors' latency. These methods improve the synchronization result and are suitable for most applications. Since trigger signals for sensors are not initiated simultaneously, there inevitably remains some degree of unknown latency, which can cause variations in acquisition times during data fusion. Thus, some researchers proposed solutions by combining a hardware controller trigger with the software strategy to reduce the execution time of activation threads in software [233]–[235]. These approaches communicate with hardware synchronization components at a low level to eliminate the data acquisition latency. However, standard commercial hardware often lacks hardware synchronization interfaces [236]. When using such methods, the complexity and portability of the system design should be considered.

b) *Estimating Temporal Offset*: As the temporal offset between sensors directly affects the fusion quality, some studies proposed temporal calibration strategies based on aligning the same objects from camera and radar sensors to extract timestamp offset. For example, Du *et al.* [237] aligned the frames that a vehicle passes the detection line and then estimated the temporal offset between these two frames. Moreover, some researchers [222], [238], [239] suggested employing real-time pre-processing buffers that leverage algorithms like YOLOv3 [55] and DBSCAN [123] to reorganize the same frame.

2) *Spatial Alignment*: Spatial alignment between radar and camera sensors involves transformation operations that map 3D or 2D radar point clouds to camera image pixels. As the spatial calibration between radar and camera is a fundamental task for information fusion, several methods of joint calibration have been proposed. Among these approaches, whether a specially designed calibration target is needed in the calibration process is an important indicator, leading to different calibration design strategies.

a) *Target-based Approaches*: For target-based calibration approaches, specific calibration targets are utilized so that sensors can get precise locations of the target. These locations estimate the rigid transformation relations between the radar and camera sensors. The triangular corner reflector is the most common choice for radar calibration, reflecting specific RCS values for the positional information. Moreover, to obtain positions of the calibrated targets from both the radar sensor and camera sensor, some novel designed calibration boards are proposed. For example, a corner reflector and a styrofoam board are combined as the calibration target in [240], [241]. The styrofoam board is applied for visual recognition in camera sensors without affecting the radar signals. Wang *et al.* [240] designed a calibration board consisting of a styrofoam board with four holes and a corner reflector in the center of these holes. The Perspective-n-Point (PnP) [242] algorithm is then used to extract the 3D location of holes and estimate the

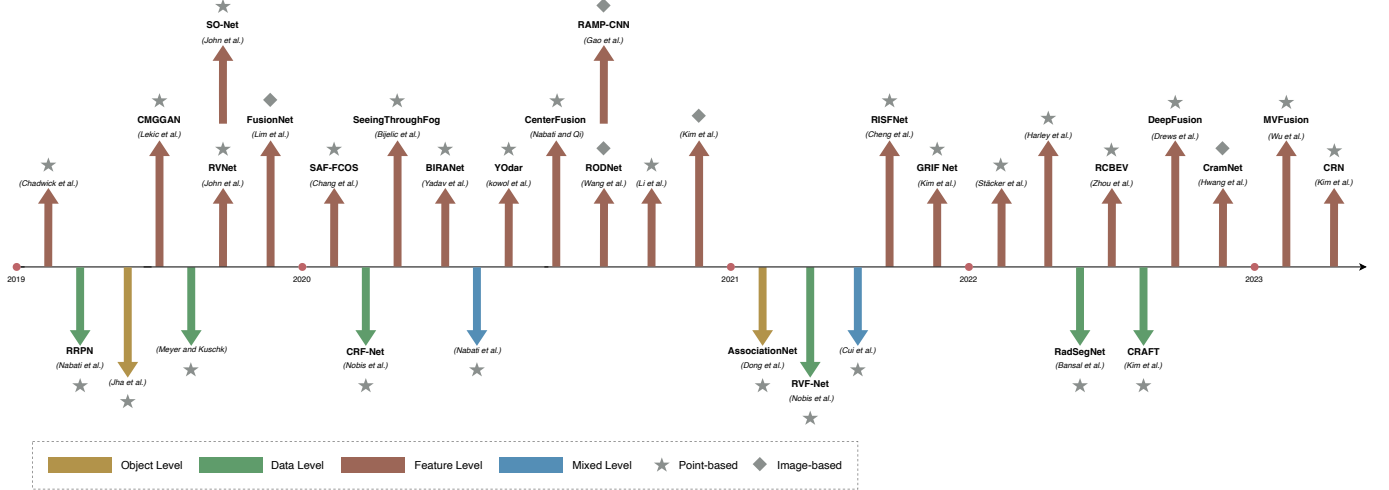


Fig. 15. Chronological overview of radar-camera fusion algorithms. Color of the arrow represents different fusion levels, and shape of the icon represents different network architectures.

location of the corner reflector. Moreover, Peršić *et al.* [241] introduced a calibration board consisting of a corner reflector and a styrofoam triangle adorned with a checkerboard, from which both radar and camera sensors can obtain accurate target positional readings. Based on the paired set of image pixels and radar points for the same targets in different locations, the transformation matrix between the radar coordinates and camera coordinates is calculated.

b) *Target-less Approaches*: On the other hand, target-less calibration approaches do not rely on specific checkerboards, thus improving the portability of calibration. However, the uncertainty of environmental factors when extracting the same features from multiple sensors is a common drawback in target-less calibration methods. Some researchers utilize precise radar velocity measurements based on the moving objects and the camera pose to implement radar-to-camera extrinsic calibration algorithms [241], [243]–[246]. Besides, machine learning algorithms are also utilized in [240], [247]–[249] to predict calibration parameters based on improving the consistency of radar point clouds and camera images.

3) *Fusion Operations*: In radar-camera fusion, different fusion operations are used to fuse data from the two modalities. Specifically, for object-level and data-level fusion networks, a transformation matrix is commonly used to align final objects or raw data [220], [250]. In contrast, feature-level and mixed-level fusion networks tend to utilize addition and concatenation operations. In the **addition** operation, element-wise features in the feature maps are added. Thus, each channel in the feature map contains more feature information, making the classifier comprehend the feature details. Similarly to the addition operation, the **mean** and **multiplication** operations calculate the average mean and multiplication of the element-wise feature maps, respectively. In the **concatenation** operation, the feature maps are flattened into vectors and then concatenated along the rows. The primary objective of the concatenation operation is to enrich feature diversity, enabling the classifier to recognize objects with higher accuracy.

Given that the features of radars and cameras are heteroge-

neous, and the above fusion operations are sensitive to changes in the input data, the effectiveness of the modalities in particular scenarios is ignored. For example, the performance of the camera sensor tends to reduce in adverse weather conditions, while the radar sensor continues to work properly. Thus, the **attention** operation is proposed to re-calculate the weights of the feature maps from two modalities. One example of such an approach is Spatial Attention Fusion (SAF), proposed by Chang *et al.* [224]. SAF extracts the spatial attention matrix from the radar images and then employs it to re-weight the feature maps from the image branch. Other approaches leverage the Mixture of Expert (MoE) [251], [252] to extract feature maps from respective expert networks and calculate the attention weights by a gating network. After that, based on these weights, the feature maps are re-assigned to optimize fusion performance.

4) *Network Architectures*: Generally, networks for radar-camera fusion are structured with dual input branches, where the data from radar and camera is input separately. Depending on the desired fusion stage, raw data, feature maps or final objects are fused in the designed network for fusion results. Based on the representations of radar data, we classify the radar-camera fusion networks into point-based and image-based networks. We also provide a chronological overview of radar-camera fusion algorithms in Fig. 15, and summarize the comparable contents in Table III.

a) *Point-based Networks*: In point-based radar-camera fusion networks, radar point clouds are mostly projected onto the image plane to provide proposals or features. Then networks such as VGG [177], ResNet [141], U-Net [98], YOLOv3 [55] and YOLOv4 [56] are used for feature extraction. Chadwick *et al.* [201] projected the radar point clouds onto the camera plane and generated two kinds of radar images: range image and range-rate image. Then they integrated an additional radar input branch upon the SSD [61] network, and used both concatenation and element-wise addition operations to fuse the radar features after the image block. The branch structure exhibits potential flexibility in

re-calculating weights between the camera image and radar representations. Besides, Meyer and Kuschk [195] generated a BEV image with six height maps and one density map from the point clouds of each frame. The authors also proposed a 3D region proposal network based on VGG [177] to predict the position of boxes and the front angle of the detected object. RVNet [28], a one-stage object detection network based on the YOLOv3 [55], contains two input branches for radar and camera, and two output branches for small obstacles and big obstacles. Specifically, radar point clouds are transformed into sparse radar images in the image coordinate system via the intrinsic matrix from the camera sensor. Each sparse radar image consists of three channels, namely depth, lateral velocity and longitudinal velocity. Based on RVNet [28], SO-Net [211] is presented, focusing on multi-task learning within a single network. In RVNet, the two output branches are modified for vehicle detection and free-space segmentation. CRF-Net [222] projects the radar point clouds onto the image plane and feeds the concatenated camera and radar data into a designed VGG-based network. This network enables learning which layer fusion would yield the best benefits by adjusting the weights to radar features on different layers. In fact, particular objects in camera images tend to remain undetected in night-time scenarios, even when using standard object detection frameworks like YOLOv3 [55]. YOdar [209] involves lowering the score threshold and assigning radar point clouds to image slices, which are then combined through an aggregated output. Finally, a gradient-boosting classifier is employed to minimize the number of false positive predictions, improving the detection accuracy at night conditions.

Since image-based CNN networks cannot directly learn original radar point clouds, some studies convert radar point clouds into radar pseudo-images and then utilize image-based methods to extract features. Based on the distant object detection method in [201], Chang *et al.* [224] proposed a radar pseudo-image generation model. Apart from transforming radar point clouds from 3D coordinates into 2D camera coordinates, they also converted the depth, longitudinal velocity and lateral velocity to a real pixel value in RGB channels. Then they introduced a Spatial Attention Fusion-based Fully Convolutional One-Stage (SAF-FCOS) network using a SAF block to merge feature maps derived from radar and camera sensors. In the SAF block, features of radar images are encoded as a spatial attention weight matrix, which is employed to re-weight the feature maps from the image branch. SeeingThroughFog [31] introduces a measurement entropy to fuse features from multiple sensors adaptively. Specifically, it applies convolution and sigmoid to the input entropy for a multiplication matrix. The matrix is then utilized to scale the concatenated features from different sensors. This approach adaptively fuses features in the feature extraction stack with the most accurate information. In CenterFusion [17], a novel frustum-based radar association method is proposed to correlate radar detections with preliminary image results. Notably, the authors generated a heat map using depth and radial velocity channels to produce complementary features for the image. After that, they fed the concatenated features into the regression heads to refine the preliminary detection by re-

calculating the object’s depth, rotation, velocity and attributes. Finally, the results from the regression heads are decoded into 3D bounding boxes. Harley *et al.* [214] focused on BEV maps from multiple cameras and radars. Their method generates a 3D volume with features by projecting 3D coordinates around the ego-vehicle camera images and bilinearly sampling features at projected locations. Later, a BEV feature map is produced by concatenating the 3D features with a rasterized radar image.

Apart from projecting radar point clouds onto the camera plane and transforming them into pseudo-images, some researchers extract features directly from 3D radar point clouds to complement the image features. This approach exploits the rich information from the radar point clouds, but requires more sophisticated processing techniques to handle the high-dimensional and unstructured nature of the data. In GRIF Net [252], an FPN [52] and a Sparse Block Network (SBNet) [253] are used as radar backbones to achieve superior performance with low computational resources. Specifically, in point cloud processing, GRIF Net converts point clouds into voxels. As the point clouds are sparse and most voxels are empty, it leverages SBNet to convolve only on masked areas, avoiding ineffective blank areas. In the fusion module, RoI features from image and radar feature maps are combined by convolutional MoE, demonstrating the effectiveness of radar sensors in detecting vehicles at longer distances than cameras.

Recently, architectures utilizing BEV representations and transformer networks exhibited impressive performance. CRAFT [254] refines image proposals by radar point clouds via a Spatio-Contextual Fusion Transformer (SCFT). The SCFT aims to leverage cross-attention layers to exchange spatial and contextual information, enabling the fusion network to learn where and what information should be extracted from camera and radar modalities. MVFusion [255] employs multi-view camera images to obtain semantic-aligned radar features, and subsequently integrates these features in a robust fusion transformer to optimize the cross-modal information interaction. CRN [256] introduces multi-modal deformable attention to tackle the spatial misalignment between radar and camera feature maps. With its aggregated semantic features and accurate BEV representations, CRN [256] currently ranks first among all radar-camera fusion detectors in the nuScenes [5] dataset.

b) Image-based Networks: Due to the potential loss of crucial information concerning objects or the surrounding environment during the processing of radar point clouds after CFAR detection, several researchers have put forward a fusion scheme that involves the fusion of radar tensors with camera images. FusionNet [217] converts both radar RA tensors and camera images into Cartesian coordinates, followed by projecting camera images onto the radar plane using a homography transformation. Upon passing through the independent feature extractor branches, features of the two modalities are passed through the additional fusion layers to form a unified feature map. RODNet [16], [189] is a radar object detection network using a camera-radar fusion strategy to cross-supervised 3D localization of detected objects during the training stage. It takes sequences of RA tensors as input and uses a neural

network-based approach to extract the Doppler information. Specifically, to handle multi-chirp merging information and dynamic object motion, RODNet introduces two customized modules, namely M-Net and Temporal Deformable Convolution (TDC).

Moreover, Gao *et al.* [136] fed sequences of RD tensor, RA tensor and AD tensor into convolutional autoencoders. They proposed a Radar Multiple-Perspectives Convolutional Neural Network (RAMP-CNN) that utilizes the temporal information in the chirps within a single frame, along with the change in spatial information between frames. In RAMP-CNN, features of these three tensors are then fused in a fusion module to generate new range-azimuth features. Compared to RODNet [16], [189], RAMP-CNN achieves significant performance and maintains the same detection accuracy in night scenes as in the daytime. Recently, as it is challenging to fuse radar tensors and camera images in 3D coordinates, Hwang *et al.* [257] proposed a radar-camera matching network named CramNet. CramNet overcomes the uncertainties in the geometric correspondences between the camera and radar through a ray-constrained cross-attention mechanism. Specifically, since a peak in the radar returns usually accompanies the optimal 3D position corresponding to the foreground pixel of an image, CramNet utilizes radar features along the pixel rays to estimate the depth and refine the 3D locations of camera pixels. Experiments on the RADIATE [187] dataset demonstrate that the CramNet outperforms the baseline results from the Faster R-CNN [51] detector. Additionally, by conducting experiments on the filtering of RA tensors via varying intensity thresholds, radar RA tensors prove to contain more meaningful information for 3D object detection than sparse point clouds.

5) *Model Evaluations:* Various evaluation metrics are adopted or newly proposed to evaluate the performance of radar-camera fusion models, as summarized in Table IV. Similar to image-based object detection and semantic segmentation tasks, in radar-camera fusion, commonly used evaluation metrics are precision, recall, Average Precision (AP), Average Recall (AR), mean Average Precision (mAP) and mean Intersection over Union (mIoU). However, these metrics only calculate the prediction accuracy on a given test dataset. Attributes in multi-modal datasets, such as velocity, range, size and orientation, are ignored. Besides, for multi-modal networks, the IoU thresholds should depend on object distance and occlusion, as well as the type of sensors [3].

To overcome these drawbacks, the nuScenes [5] dataset introduces mATE, mASE, mAOE, mAVE and mAAE, which stand for mean average translation, scale, orientation, velocity and attribute errors, respectively. Furthermore, they presented nuScenes Detection Score (NDS), half based on the mAP, half quantifying the previous five metrics. To evaluate how well a detection result matches the ground truth, Wang *et al.* [16] defined Object Location Similarity (OLS) that quantifies the correlation between two detections concerning their distance, classes and scale information. Additionally, some metrics designed for LiDAR object detection are also adopted in radar point clouds. For example, Cui *et al.* [207] utilized Average Heading Similarity (AHS) to calculate the accuracy, which is formulated initially to calculate the average orientation angle

in 3D LiDAR IoU defined in AVOD [7].

VI. CHALLENGES AND RESEARCH DIRECTIONS

It is a challenging problem to balance the performance of different modalities so that all of them can perform at their best level and thus improve the overall performance. As described in Section I, radar-camera fusion faces numerous challenges. If these challenges are not properly addressed in sensor perception, they may also affect the subsequent tasks such as localization, prediction, planning and control. In this section, we focus on improving the accuracy and robustness of radar-camera fusion, with discussions on the critical challenges and possible research directions from two aspects: multi-modal data and fusion architectures.

A. Multi-modal Data

1) *Data Quality:* Unlike uni-modal data, multi-modal data requires consideration of each modality's native characteristics. The information within an image is structured and regular, with partial information being associated with the whole image. In contrast, the spatial information embodied in radar point clouds tends to be disordered. As a result, handling radar data poses a more significant challenge in the context of radar-camera fusion. We categorize these challenges related to data quality into three directions: sparsity, inaccuracy, and noise.

a) *Sparsity:* The sparsity of radar point clouds poses a challenge for neural networks to learn features effectively. Besides, as these point clouds do not comprehensively represent an object's shape, a fixed-size bounding box approach would be impractical. To address the issue of sparsity, researchers usually combine multiple frames (from 0.25 seconds to 1 second) of radar data to get denser point clouds, making it conducive to improving accuracy [17], [142], [146], [214], [222], [223], [252]. However, the time-dependent approach also causes system delays. Nowadays, the 4D radar sensor is a potential research direction as it produces denser point clouds, reaching hundreds of points on a car. The spatial distribution of objects is effectively represented in 4D radar datasets, including Astyx [195], VoD [142] and TJ4DRadSet [196]. Experiments also indicate that the 4D radar is helpful in radar detection. For example, Zheng *et al.* [196] proved that 4D radar has potential in 3D perception as the points get dense. Palffy *et al.* [142] pointed out that the additional elevation data increases object detection performance (from 31.9 to 38.0 in mAP) in their VoD [142] dataset.

b) *Inaccuracy:* Aside from the sparsity of radar point clouds, the points may not be located at the object's center, but may be at any corner of the object or even outside of it [195]. To make the radar points located on or close to the object, Chadwick *et al.* [201] marked each radar point on the image as a small circle instead of a single pixel. Nabati and Qi [9] proposed RRPN to generate several anchors with different sizes and aspect ratios centered at the points of interest. These translated anchors are employed to achieve more precise bounding boxes where the points of interest are mapped to the object's right, left, or bottom.

Researchers have employed column and pillar expansion techniques to improve the accuracy of radar point clouds in the vertical dimension. For example, Nobis *et al.* [222] assumed a height extension of three meters on each radar detection to associate camera pixels with radar data. Nabati and Qi [17] used pillar expansion to expand each radar point to a fixed-size pillar. In their experiment, the size of a pillar is set to $[0.2, 0.2, 1.5]$ meters along the $[x, y, z]$ directions. Notably, the column size should be different for different types of objects. In [208], the authors utilized a clustering approach to group ground truth bounding boxes of vehicles into three distinct height categories. Following this, radar points are assigned a scale based on boundary edge values in each category.

In our opinion, column or pillar expansion is effective but still hardly convincing. The distribution of point clouds is a direction worth investigating. For example, Stäcker *et al.* [258] assumed a Gaussian distribution to measure the azimuth angle. According to the resulting Gaussian density curve, they generated denser radar point clouds, horizontally distributed over multiple pixels.

c) *Noise*: Actually, the radar sensor returns noisy data from irrelevant objects, including ghost objects, ground detections and even multi-radar mutual interference [259]. The noise from radars could cause the detection of fake targets, thereby limiting the accuracy of radar-based detection or segmentation.

Conventional methods [260]–[263] for automotive radar denoising are typically based on CFAR and peak detection algorithms, which exhibit poor generalization capabilities. Recently, deep learning methods have provided a key solution to the challenges associated with automotive radar data denoising. In [264], a deep neural network is proposed to enhance the target peaks on RA tensors. Rock *et al.* [265] analyzed the quantization of CNN-based denoising autoencoder for radar interference mitigation on radar RD tensors to guarantee real-time inference on low-performance equipment. Dubey *et al.* [266] realized the multi-radar mutual interference and target detection on RD tensors simultaneously with one one-stage CNN-based neural network. Moreover, in [267]–[271], fully-convolution networks are widely proposed and applied to interference mitigation on RD tensors.

However, conventional radars generally do not provide access to the radar tensor, highlighting the importance of noise mitigation techniques at the level of radar point clouds. For example, Nobis *et al.* [222] designed a ground-truth filter to remove radar detections outside of the 3D ground truth bounding boxes. Cheng *et al.* [272] proposed a cross-modal radar point detector through the assistance of LiDAR, which could also remove the noisy points.

In all, regardless of the stage of denoising in radar tensors or point clouds, a dataset with high-quality annotations is necessary. For the noise removal on radar tensors, researchers may adopt image denoising and restoration principles. For removing noisy point clouds, constructing features based on the physical characteristics of point clouds to guide models separate targets from clutters makes sense. As radar point clouds are sparse and inaccurate, modeling the inherent uncertainty is an open question, which can aid in effectively

distinguishing targets from noise.

2) *Data Diversity*:

a) *Small Size*: Deep learning models rely on large amounts of training data to achieve high levels of accuracy. However, multi-modal datasets consisting of both radar and camera data are much smaller than uni-modal image data. For instance, compared to the ImageNet [273], [274] dataset with over 14 million images and over 20k classes, the largest radar-camera fusion dataset to date named CRUW [189] has only 400k frames and 260k objects. Furthermore, regarding category distribution, most labels are vehicles, while pedestrians and bicycles are far less prevalent. The imbalance in these categories' distribution may result in overfitting designed deep learning networks.

b) *Unrich Conditions*: In real scenarios, 360-degree perception of the surrounding environment is critical in autonomous driving, requiring multiple cameras and radars to work together. Besides, the multi-modal dataset also needs to consider complex weather conditions (e.g., rain, fog, snow) and complex road conditions (e.g., blocked roads, rural paths, intersections), all of which are time-consuming and labor-consuming tasks.

Some studies [188], [199] generate synthetic data via simulation tools (e.g., Carla [200]). Researchers can freely match different sensors and generate different driving conditions with these tools, especially in complex and dangerous scenarios. However, it is also worth noting that although simulators can generate a variety of virtual datasets, the simulated data cannot completely replace the data from real scenarios. Moreover, exploring the appropriate methodology for integrating synthetic data with real-world data is a critical area of inquiry warranting further investigation [275].

Domain adaptation is also a valuable research direction that aims to leverage knowledge learned from a related domain with adequate labeled data. Although domain adaptation has been applied in radar data, including radar tensor reconstruction [126], human sensing [276], human activity recognition [277] and gesture recognition [278], it has not been employed in radar-camera fusion till now.

3) *Data Synchronization*:

a) *High Calibration Requirements*: For radar-camera fusion systems, well-calibrated sensors are the prerequisite. In multi-sensor calibration, LiDAR sensors are typically employed as an essential intermediary component. The LiDAR sensor is calibrated separately from the camera sensor and radar sensor, and then a transformation matrix between the radar and camera can be calculated [194], [196]. In addition to the sensor-to-sensor calibration, calibration between a single sensor and the vehicle coordinate system is also a feasible approach [279]. Although numerous approaches (e.g., [207], [280]) are proposed for calibration between radars and the cameras, the accuracy of the calibration remains a challenge due to the inaccurate and vulnerable radar returns. Besides, as far as we know, [207] is the only method for 4D radar and camera calibration. As 4D radar technologies are developing rapidly, we believe that 4D radar calibration is a potential direction, and more finds will be proposed in the future.

In real scenarios, extrinsic calibration parameters between radar and camera sensors may change from vehicle vibration. Besides, different sampling frequencies of the radar and camera may produce a particular temporal difference between the data from each sensor. The temporal difference would cause data inconsistency, especially when the ego-car or targets move at high speed. Therefore, real-time online calibration and correction are essential research directions in the future.

b) Difficulties in Labeling: The process of labeling data is labor-intensive and time-consuming, especially when dealing with multi-modal data. This is particularly true for radar-camera fusion, where the physical shapes of objects cannot be discerned directly from the radar data representation. In RadarScene [191], all the radar points are labeled by human experts. However, only moving objects are annotated, while the static points are ignored. Auto-labeling radar data is a potential research direction to address the challenge of laborious data labeling. Actually, labels for radar data can be calculated based on the corresponding ground truth from camera images and the extrinsic matrix between the radar sensor and the camera sensor. But the problem is that applying this labeling approach for radar data is not perfect, as radar targets may not always be located in the ground truth from images. Sengupta *et al.* [281] proposed a camera-aided method for automatically labeling radar point clouds, leveraging a pre-trained YOLOv3 [55] network and the Hungarian algorithm for enhanced accuracy and efficiency. However, despite the potential advantages of auto-labeling radar data, filtering out noisy data around the object of interest is still challenging.

For camera image labeling, it is worth considering how to select appropriate labeling data for reducing labor costs. Active learning is a supervised learning method that aims to select the smallest possible training set to achieve the desired data efficiency [282], [283]. The active learning network iteratively queries the most informative samples from the human labelers in an unlabeled data pool and then updates the weights for the network. This approach leads to equivalent performance with less labeled training data, reducing human labeling efforts. Experiments from [284] indicate that using only about 40% of the data in the training set leads to the same classification results as the completely supervised reference experiment. Moreover, Haussmann *et al.* [285] developed a scalable production system for active learning in autonomous driving. From their system, the performance of the automatic selection is improved, with up to four times the relative mAP improvement compared to a manual selection process by domain experts. Furthermore, many other methods would also be used to reduce the burden of data labeling, such as domain adaptation [126], [286], [287], transfer learning [288], semi-supervised learning [289] and lifelong learning [290].

B. Fusion Architectures

1) Feature Extraction: Applying LiDAR-based feature extraction algorithms to radar modality is less effective due to the inherent sparsity of radar point clouds. As an example, PointPillars [291] algorithm converts LiDAR point clouds into pillars and then extracts features from each pillar. When this

algorithm is adapted to radar point clouds, there may be few or even no points in a pillar, which makes it hard to extract features. In fact, results in [145] and [292] also indicate that the average precision of radar point clouds using PointPillars [291] is much lower than using SSD [61] and YOLOv3 [55] detectors. As PointPillars [291] focus on local features, global features are introduced to improve accuracy. For example, RPFA-Net [293] leverages the self-attention mechanism to extract global features (e.g., orientation) from point clouds. These global features enable the network to perform more efficient and effective regression of key object parameters (e.g., heading angle), thereby enhancing the accuracy and reliability of object detection.

To dig deeper into the relationship between sparse point clouds, Graph Neural Network (GNN) [294] is a promising research direction in which each point is considered as a node, and edges are the relationship between the points. GNN adopted for 3D feature extraction of radar point clouds demonstrates that the graph representation produces more effective object proposals than other point cloud encoders by mapping radar point clouds to contextual representations [295]. GNN also shows its advantages in detection from RA tensors. The Graph Tensor Radar Network (GTR-Net) [296] architecture utilizes graph convolutional operations to aggregate information across the point cloud nodes. The process involves weighting the features of connected nodes based on their respective edge weights. In this way, it improves the defective sparse points by aggregating relevant information and thus leads to better performance.

Another potential research opportunity is using neural networks to extract radar information instead of traditional FFT operations, which can reduce the computational requirements that consume most of the operations and simplify the data flow in the embedded implementation. For example, in ROD-Net [16], FFT operations are only performed in sample and antenna dimensions, while the chirp dimension remains to get the range-azimuth-chirp tensor. Then a neural network is employed to process the chirp dimension for extracting Doppler features, enabling end-to-end training of radar features in-depth within the deep learning framework.

2) Data Association: Another significant challenge is the ambiguity in associating radar data with image data, as they are heterogeneous. The typical way is to project radar data onto the image plane and then bind the data in the same position. However, direct projection through a calibration matrix results in poor association with the objects' centers. As aforementioned, radar data is sparse, inaccurate and noisy, making poor association at either the object-level or data-level fusion.

Thus, associating image data with radar data is an open question. Nabati and Qi [206] proposed a Radar Proposal Refinement (RPR) network to match proposals from radars and cameras. Later, they integrated the detection boxes and pillar expansion through frustum association in CenterFusion [17], allowing for the mapping of radar detections to the centers of objects and mitigating the issue of overlapping. Dong *et al.* [212] used AssociationNet to learn the semantic representation information and associate radar point clouds

and image bounding boxes by Euclidean distance. For associating the semantics to radar point clouds, Bansal *et al.* [213] proposed a representation named Semantic-Point-Grid (SPG), which encodes semantic information from camera images into radar point clouds to identify camera pixel correspondences for each radar point.

In our opinion, a potential approach to associate radar data with image data is the attention-based association with adaptive thresholds. For example, Radar-Camera Pixel Depth Association (RC-PDA) is proposed to filter out occluded radar returns and enhance the projected radar depth map by generating a confidence measure for these associations in [223]. Soft Polar Association (SPA) is proposed to associate radar point clouds around the image proposals in polar coordinates [254]. In order to overcome background clutter, it utilized consecutive cross attention-based encoder layers to integrate image proposal features and radar point features.

3) *Data Augmentation*: Numerous data augmentation methods have been proposed to increase the quantity and diversity of data samples, thus preventing network overfitting and enhancing model generalization. For radar data in the form of point clouds, data augmentations such as random rotation, scaling, and flipping shifting are applied to enrich the diversity of samples in [17], [196], [218]. In addition, since radar tensors can be treated as images, existing image-based data augmentation algorithms (e.g., horizontal flipping, translating in range, interpolating, mixing) are tested in experiments and proved to be effective [136].

However, all these data augmentation methods above are based only on the radar modality. In radar-camera fusion perception, designing effective data augmentation methods needs to consider the correlation and interdependence between radar and camera modalities, which means joint data augmentation methods are necessary rather than augmenting each modality separately. Otherwise, the model will learn from incorrect data, whose physical properties are unreliable. For example, when the coordinates of radar data and image are aligned, applying Cutmix [297] on the image and radar feature maps will undoubtedly destroy the target features (e.g., azimuth and elevation) obtained by the radar sensor, leading to incorrect model inferences. Therefore, designing joint data augmentation algorithms for the unique radar representations combined with image modality remains a significant challenge.

4) *Training Strategies*: Since a multi-modal network has additional input information, it should match or outperform the uni-modal network. However, this is not always the case. A multi-modal network is often prone to overfitting and tends to learn to ignore one branch if the hyper-parameters set for training are more suitable for the other branch. Wang *et al.* [298] argued that the rates of overfitting and generalization vary across different modalities, and training a multi-modal network using the uni-modal training strategy may not be optimal for the overall network.

A feasible approach to balance the performance is to add loss functions for each modality. In this way, after one modality converges, the remaining modality can still be generalized. Besides, weighting operations on loss functions could be more beneficial to adapt to the learning rates of each modality. In

recent studies, Wang *et al.* [298] proposed Gradient-Blending, which computes an optimal blending of modalities based on their overfitting behaviors. Although this method achieves SOTA accuracy on audio and vision benchmarks, the idea has yet to be applied in radar and camera modalities. Moreover, dropout operation helps overcome overfitting. Nobis *et al.* [222] introduced BlackIn by deactivating camera image data. The lack of camera input data forces the network to rely more on sparse radar data for specific potential values.

Fine-tuning a multi-modal network over pre-trained uni-modal encoders can also outperform fusion from scratch. Lim *et al.* [217] utilized the weights freezing strategy to train a single branch network using the optimal training hyper-parameters. These weights were subsequently loaded into the corresponding branches to train the fusion network. Experimental results indicate that the best strategy is to train the camera branch in advance and then train the entire network with the gradient propagation disabled through the camera branch. Recently, knowledge distillation has shown its performance in multi-modal networks by distilling the pre-trained uni-modal features to the multi-modal networks [299], [300]. It could also be a potential research direction in radar-camera fusion.

5) *Model Robustness*: Another challenge is how to guarantee the model's robustness when the sensors are degraded, or the autonomous driving vehicles enter into adverse or unseen driving scenarios. Most reviewed methods focus on the accuracy of public datasets, while only a few consider sensor failure with only one modality as the input data. In RadSegNet [213], the SPG encoding independently extracts information from cameras and radar, as well as encodes semantic information from camera images into radar point clouds. Thus in scenarios where the camera input becomes unreliable, the SPG encoding method maintains reliable operation using radar data alone. Bijelic *et al.* [31] introduced an entropy channel for each sensor stream and a feature fusion architecture to exchange features, which still work in unseen weather conditions and sensor failures. Moreover, the attention mechanism is also an effective choice for guiding mixed information from different sensors to fuse features of multiple modalities, as well as handle original features from a single modality. For example, attention maps leverage features learned from different sensors to predict the importance of specific parameters in [301].

It is essential to focus not only on the accuracy of the predicted outcomes, but also on the degree of certainty the model has about them. Uncertainty is a potential direction that can be used to handle unseen driving scenarios. Specifically, a multi-modal network should present higher uncertainty against unseen objects [302]. The Bayesian neural network is a valuable choice for calculating uncertainty. It utilizes a prior distribution of network weights to infer the posterior distribution, thereby estimating the probability associated with a given prediction [3], [303]. In radar-camera fusion, YOdar [209] is an uncertainty-based method in which uncertainty combines outputs of radar and camera networks with a gradient-boosting classifier. Experimental results show that YOdar increases performance significantly at night scenes.

Another way that may be useful to increase the networks'

robustness is generative models. They can detect sensor defects or new scenarios an autonomous vehicle has never entered. Wheeler *et al.* [304] described a methodology for constructing stochastic automotive radar models based on deep learning with adversarial loss connected to real-world data. The resulting model exhibits fundamental radar effects while maintaining real-time capability. Lekic and Babic *et al.* [305] introduced a Conditional Multi-Generator Generative Adversarial Network (CMGGAN) to generate pseudo-images containing all the surrounding objects detected by the radar sensor. In our opinion, designing specific deep generative models for radar-camera fusion is an interesting open question.

6) *Model Evaluations*: Most researchers utilize the nuScenes [5] dataset to evaluate the performance of their algorithms. However, the selected sub-dataset and the evaluation metrics are different, leading to a lack of direct comparisons. As summarized in Table V, some methods [9], [209], [211], [224], [250] use portions of the nuScenes dataset for training, validating and testing, while some others [28], [206], [252], [258] exploit data collected by part of sensors within the nuScenes dataset. In addition, some researchers [205], [208], [222] do not clarify which section of the nuScenes dataset they utilized in their experiments.

In terms of evaluation metrics, even though some studies provide results using AP and mAP metrics, the type and value of the threshold are different. Besides, only a few works provide information on the inference time, which is also calculated by authors on their own devices and lacks uniform hardware measurements. In our opinion, since the nuScenes [5] dataset has been used to evaluate the performance of major algorithms, researchers should validate the performance of their algorithms on the same IoU, metrics and sub-dataset. This would enable a more meaningful and direct comparison of the results obtained from various studies.

Moreover, standard evaluation metrics are not specifically designed for situations where sensors are defective. Metrics related to uncertainties, such as Probability-based Detection Quality (PDQ) [306], may be helpful in radar-camera fusion to compare the robustness of different algorithms. Radar-camera fusion also faces the challenges of unknown objects in the open world. In such scenarios, evaluation metrics proposed in [307], [308] can be utilized for open-set objects in radar-camera fusion.

Furthermore, visualization evaluation techniques are a potential research direction for analyzing and optimizing radar-camera fusion networks. Several methods [309], [310] have been proposed for interpreting and understanding deep neural networks. However, to the best of our knowledge, there has yet to be an investigation of visual analytics in radar-camera fusion. How to design the visual toolkits for radar-camera fusion networks is still an open and challenging question.

7) *Model Deployment*: Radar-camera fusion holds significant potential in practical autonomous driving vehicles, where models of radar-camera fusion are deployed on edge devices. Compared with high computational servers, edge devices are often equipped with limited computational resources in memory, bandwidth, Graphics Processing Unit (GPU) and Central Processing Unit (CPU). Nevertheless, they still need to meet

the low-latency and high-performance requirements. Currently, [311] is the only work that reports on fusion output speed, reaching 11 Hz on an NVIDIA Jetson AGX TX2. The results of fusion algorithms on edge devices are an open question, and how to improve the computational efficiency is worth considering. Some network acceleration schemes (e.g., pruning and quantization [312], [313]) are good choices to be applied to radar-camera fusion models.

It is valuable to implement multiple tasks in a uni-model for real applications. In multi-task learning, the knowledge learned during training for one task can be shared and used to improve performance on the other tasks [4]. Besides, by sharing model features between multiple tasks, the overall number of parameters and computations can be reduced, making it more efficient in real-time autonomous driving applications [206], [314]. Multi-task in radar-camera fusion is still in the preliminary stage, and we believe the multi-task approach in radar-camera fusion is a potential research direction. Nonetheless, combining multiple tasks into a unified optimization objective results in a complex optimization problem, especially when the tasks are related but have different performance metrics. Finding a set of hyper-parameters that can effectively balance the importance of different tasks is challenging.

VII. CONCLUSION

With the rapid development of autonomous driving, radar-camera fusion, a multi-modal and all-weather solution, is gaining more attention in both academic research and industrial applications. This review investigates and discusses radar-camera fusion studies on object detection and semantic segmentation tasks. Starting with the working principles of radar and camera sensors, we gradually introduce the importance of radar-camera fusion in autonomous driving perception. Through the analysis of radar signal processing, we gain a deep understanding of radar representations, which also provides fundamental support for the radar-camera fusion datasets. As to fusion methodologies, we delve into various fusion methods and explore questions about “why to fuse”, “what to fuse”, “where to fuse”, “when to fuse” and “how to fuse”.

Based on the current radar-camera fusion datasets and methods, we discuss the critical challenges and raise possible research directions involving multi-modal data and fusion architectures. In general, radar-camera fusion is moving towards data representations containing rich information. On the one hand, representations such as ADC signals and radar tensors provide more potential information, which is valuable for multi-modal fusion. On the other hand, the new 4D radar sensors provide denser point clouds and higher resolutions, which will become a new trend in autonomous driving. Fusion approaches are evolving towards customizing radar algorithms based on particular radar characteristics. Additionally, methods on multi-frames and multi-tasks in radar-camera fusion are expected in future works. Above all, we hope that our survey serves as a comprehensive reference for researchers and practitioners in developing robust perception in radar-camera fusion.

ACKNOWLEDGMENT

This work received financial support from Jiangsu Industrial Technology Research Institute (JITRI) and Wuxi National Hi-Tech District (WND).

REFERENCES

- [1] B. Paden, M. Čáp, S. Z. Yong, D. Yershov, and E. Fazzoli, “A survey of motion planning and control techniques for self-driving urban vehicles,” *IEEE Transactions on intelligent vehicles*, vol. 1, no. 1, pp. 33–55, 2016.
- [2] Y. Xiao, F. Codevilla, A. Gurram, O. Urfalioglu, and A. M. López, “Multimodal end-to-end autonomous driving,” *IEEE Transactions on Intelligent Transportation Systems*, vol. 23, no. 1, pp. 537–547, 2020.
- [3] D. Feng, C. Haase-Schütz, L. Rosenbaum, H. Hertlein, C. Glaeser, F. Timm, W. Wiesbeck, and K. Dietmayer, “Deep multi-modal object detection and semantic segmentation for autonomous driving: Datasets, methods, and challenges,” *IEEE Transactions on Intelligent Transportation Systems*, vol. 22, no. 3, pp. 1341–1360, 2020.
- [4] M. Liang, B. Yang, Y. Chen, R. Hu, and R. Urtasun, “Multi-task multi-sensor fusion for 3d object detection,” in *Proceedings of the IEEE/CVF Conference on Computer Vision and Pattern Recognition*, 2019, pp. 7345–7353.
- [5] H. Caesar, V. Bankiti, A. H. Lang, S. Vora, V. E. Liong, Q. Xu, A. Krishnan, Y. Pan, G. Baldan, and O. Beijbom, “nuscenes: A multimodal dataset for autonomous driving,” in *Proceedings of the IEEE/CVF conference on computer vision and pattern recognition*, 2020, pp. 11621–11631.
- [6] X. Chen, H. Ma, J. Wan, B. Li, and T. Xia, “Multi-view 3d object detection network for autonomous driving,” in *Proceedings of the IEEE conference on Computer Vision and Pattern Recognition*, 2017, pp. 1907–1915.
- [7] J. Ku, M. Mozifian, J. Lee, A. Harakeh, and S. L. Waslander, “Joint 3d proposal generation and object detection from view aggregation,” in *2018 IEEE/RSJ International Conference on Intelligent Robots and Systems (IROS)*. IEEE, 2018, pp. 1–8.
- [8] B. Li, T. Zhang, and T. Xia, “Vehicle detection from 3d lidar using fully convolutional network,” *arXiv preprint arXiv:1608.07916*, 2016.
- [9] R. Nabati and H. Qi, “Rrpn: Radar region proposal network for object detection in autonomous vehicles,” in *2019 IEEE International Conference on Image Processing (ICIP)*. IEEE, 2019, pp. 3093–3097.
- [10] R. Zhang, S. A. Candra, K. Vetter, and A. Zakhori, “Sensor fusion for semantic segmentation of urban scenes,” in *2015 IEEE international conference on robotics and automation (ICRA)*. IEEE, 2015, pp. 1850–1857.
- [11] R. Yin, Y. Cheng, H. Wu, Y. Song, B. Yu, and R. Niu, “Fusionlane: Multi-sensor fusion for lane marking semantic segmentation using deep neural networks,” *IEEE Transactions on Intelligent Transportation Systems*, vol. 23, no. 2, pp. 1543–1553, 2020.
- [12] A. Asvadi, P. Girao, P. Peixoto, and U. Nunes, “3d object tracking using rgb and lidar data,” in *2016 IEEE 19th International Conference on Intelligent Transportation Systems (ITSC)*. IEEE, 2016, pp. 1255–1260.
- [13] Y. Fang, H. Zhao, H. Zha, X. Zhao, and W. Yao, “Camera and lidar fusion for on-road vehicle tracking with reinforcement learning,” in *2019 IEEE Intelligent Vehicles Symposium (IV)*. IEEE, 2019, pp. 1723–1730.
- [14] P. Li, P. Wang, K. Berntorp, and H. Liu, “Exploiting temporal relations on radar perception for autonomous driving,” in *Proceedings of the IEEE/CVF Conference on Computer Vision and Pattern Recognition*, 2022, pp. 17071–17080.
- [15] B. Major, D. Fontijne, A. Ansari, R. Teja Sukhavasi, R. Gowaikar, M. Hamilton, S. Lee, S. Grzechnik, and S. Subramanian, “Vehicle detection with automotive radar using deep learning on range-azimuth-doppler tensors,” in *Proceedings of the IEEE/CVF International Conference on Computer Vision Workshops*, 2019, pp. 0–0.
- [16] Y. Wang, Z. Jiang, Y. Li, J.-N. Hwang, G. Xing, and H. Liu, “Rodnet: A real-time radar object detection network cross-supervised by camera-radar fused object 3d localization,” *IEEE Journal of Selected Topics in Signal Processing*, vol. 15, no. 4, pp. 954–967, 2021.
- [17] R. Nabati and H. Qi, “Centerfusion: Center-based radar and camera fusion for 3d object detection,” in *Proceedings of the IEEE/CVF Winter Conference on Applications of Computer Vision*, 2021, pp. 1527–1536.
- [18] E. Arnold, O. Y. Al-Jarrah, M. Dianati, S. Fallah, D. Oxtoby, and A. Mouzakitis, “A survey on 3d object detection methods for autonomous driving applications,” *IEEE Transactions on Intelligent Transportation Systems*, vol. 20, no. 10, pp. 3782–3795, 2019.
- [19] Y. Cui, R. Chen, W. Chu, L. Chen, D. Tian, Y. Li, and D. Cao, “Deep learning for image and point cloud fusion in autonomous driving: A review,” *IEEE Transactions on Intelligent Transportation Systems*, vol. 23, no. 2, pp. 722–739, 2021.
- [20] K. Huang, B. Shi, X. Li, S. Huang, and Y. Li, “Multi-modal sensor fusion for auto driving perception: A survey,” *arXiv preprint arXiv:2202.02703*, 2022.
- [21] S. Jusoh and S. Almajali, “A systematic review on fusion techniques and approaches used in applications,” *IEEE Access*, vol. 8, pp. 14424–14439, 2020.
- [22] Z. Wang, Y. Wu, and Q. Niu, “Multi-sensor fusion in automated driving: A survey,” *Ieee Access*, vol. 8, pp. 2847–2868, 2019.
- [23] Z. Wei, F. Zhang, S. Chang, Y. Liu, H. Wu, and Z. Feng, “Mmwave radar and vision fusion for object detection in autonomous driving: A review,” *Sensors*, vol. 22, no. 7, p. 2542, 2022.
- [24] C. Iovescu and S. Rao, “The fundamentals of millimeter wave sensors,” *Texas Instruments*, pp. 1–8, 2017.
- [25] S. Saponara, M. S. Greco, and F. Gini, “Radar-on-chip/in-package in autonomous driving vehicles and intelligent transport systems: Opportunities and challenges,” *IEEE Signal Processing Magazine*, vol. 36, no. 5, pp. 71–84, 2019.
- [26] R. Appleby and R. N. Anderton, “Millimeter-wave and submillimeter-wave imaging for security and surveillance,” *Proceedings of the IEEE*, vol. 95, no. 8, pp. 1683–1690, 2007.
- [27] P. Fritzsche, S. Kueppers, G. Briese, and B. Wagner, “Radar and lidar sensorfusion in low visibility environments.” in *ICINCO (2)*, 2016, pp. 30–36.
- [28] V. John and S. Mita, “Rvnet: Deep sensor fusion of monocular camera and radar for image-based obstacle detection in challenging environments,” in *Image and Video Technology: 9th Pacific-Rim Symposium, PSIVT 2019, Sydney, NSW, Australia, November 18–22, 2019, Proceedings 9*. Springer, 2019, pp. 351–364.
- [29] Wikipedia contributors, “Image sensor — Wikipedia, the free encyclopedia,” 2023, [Online; accessed 10-April-2023]. [Online]. Available: https://en.wikipedia.org/w/index.php?title=Image_sensor&oldid=1146373856
- [30] T. Gruber, F. Julca-Aguilar, M. Bijelic, and F. Heide, “Gated2depth: Real-time dense lidar from gated images,” in *Proceedings of the IEEE/CVF International Conference on Computer Vision*, 2019, pp. 1506–1516.
- [31] M. Bijelic, T. Gruber, F. Mannan, F. Kraus, W. Ritter, K. Dietmayer, and F. Heide, “Seeing through fog without seeing fog: Deep multimodal sensor fusion in unseen adverse weather,” in *Proceedings of the IEEE/CVF Conference on Computer Vision and Pattern Recognition*, 2020, pp. 11682–11692.
- [32] S. Inbar and O. David, “Laser gated camera imaging system and method,” May 27 2008, uS Patent 7,379,164.
- [33] C. Michaelis, B. Mitzkus, R. Geirhos, E. Rusak, O. Bringmann, A. S. Ecker, M. Bethge, and W. Brendel, “Benchmarking robustness in object detection: Autonomous driving when winter is coming,” *arXiv preprint arXiv:1907.07484*, 2019.
- [34] S. Saponara and B. Neri, “Radar sensor signal acquisition and multi-dimensional fft processing for surveillance applications in transport systems,” *IEEE Transactions on Instrumentation and Measurement*, vol. 66, no. 4, pp. 604–615, 2017.
- [35] S. Sun, A. P. Petropulu, and H. V. Poor, “Mimo radar for advanced driver-assistance systems and autonomous driving: Advantages and challenges,” *IEEE Signal Processing Magazine*, vol. 37, no. 4, pp. 98–117, 2020.
- [36] B. Li, “3d fully convolutional network for vehicle detection in point cloud,” in *2017 IEEE/RSJ International Conference on Intelligent Robots and Systems (IROS)*. IEEE, 2017, pp. 1513–1518.
- [37] X. Chen, K. Kundu, Z. Zhang, H. Ma, S. Fidler, and R. Urtasun, “Monocular 3d object detection for autonomous driving,” in *Proceedings of the IEEE conference on computer vision and pattern recognition*, 2016, pp. 2147–2156.
- [38] S. Zhang, R. Benenson, M. Omran, J. Hosang, and B. Schiele, “Towards reaching human performance in pedestrian detection,” *IEEE transactions on pattern analysis and machine intelligence*, vol. 40, no. 4, pp. 973–986, 2017.
- [39] L. Zhang, L. Lin, X. Liang, and K. He, “Is faster r-cnn doing well for pedestrian detection?” in *Computer Vision–ECCV 2016: 14th*

European Conference, Amsterdam, The Netherlands, October 11-14, 2016, Proceedings, Part II 14. Springer, 2016, pp. 443–457.

[40] X. Chen, K. Kundu, Y. Zhu, H. Ma, S. Fidler, and R. Urtasun, “3d object proposals using stereo imagery for accurate object class detection,” *IEEE transactions on pattern analysis and machine intelligence*, vol. 40, no. 5, pp. 1259–1272, 2017.

[41] M. Weber, P. Wolf, and J. M. Zöllner, “Deeptrt: A single deep convolutional network for detection and classification of traffic lights,” in *2016 IEEE intelligent vehicles symposium (IV)*. IEEE, 2016, pp. 342–348.

[42] J. Müller and K. Dietmayer, “Detecting traffic lights by single shot detection,” in *2018 21st International Conference on Intelligent Transportation Systems (ITSC)*. IEEE, 2018, pp. 266–273.

[43] M. Bach, S. Reuter, and K. Dietmayer, “Multi-camera traffic light recognition using a classifying labeled multi-bernoulli filter,” in *2017 IEEE Intelligent Vehicles Symposium (IV)*. IEEE, 2017, pp. 1045–1051.

[44] K. Behrendt, L. Novak, and R. Botros, “A deep learning approach to traffic lights: Detection, tracking, and classification,” in *2017 IEEE International Conference on Robotics and Automation (ICRA)*. IEEE, 2017, pp. 1370–1377.

[45] Z. Zhu, D. Liang, S. Zhang, X. Huang, B. Li, and S. Hu, “Traffic-sign detection and classification in the wild,” in *Proceedings of the IEEE conference on computer vision and pattern recognition*, 2016, pp. 2110–2118.

[46] H. S. Lee and K. Kim, “Simultaneous traffic sign detection and boundary estimation using convolutional neural network,” *IEEE Transactions on Intelligent Transportation Systems*, vol. 19, no. 5, pp. 1652–1663, 2018.

[47] H. Luo, Y. Yang, B. Tong, F. Wu, and B. Fan, “Traffic sign recognition using a multi-task convolutional neural network,” *IEEE Transactions on Intelligent Transportation Systems*, vol. 19, no. 4, pp. 1100–1111, 2017.

[48] R. Girshick, J. Donahue, T. Darrell, and J. Malik, “Rich feature hierarchies for accurate object detection and semantic segmentation,” in *Proceedings of the IEEE conference on computer vision and pattern recognition*, 2014, pp. 580–587.

[49] K. He, X. Zhang, S. Ren, and J. Sun, “Spatial pyramid pooling in deep convolutional networks for visual recognition,” *IEEE transactions on pattern analysis and machine intelligence*, vol. 37, no. 9, pp. 1904–1916, 2015.

[50] R. Girshick, “Fast r-cnn,” in *Proceedings of the IEEE international conference on computer vision*, 2015, pp. 1440–1448.

[51] S. Ren, K. He, R. Girshick, and J. Sun, “Faster r-cnn: Towards real-time object detection with region proposal networks,” *Advances in neural information processing systems*, vol. 28, 2015.

[52] T.-Y. Lin, P. Dollár, R. Girshick, K. He, B. Hariharan, and S. Belongie, “Feature pyramid networks for object detection,” in *Proceedings of the IEEE conference on computer vision and pattern recognition*, 2017, pp. 2117–2125.

[53] J. Redmon, S. Divvala, R. Girshick, and A. Farhadi, “You only look once: Unified, real-time object detection,” in *Proceedings of the IEEE conference on computer vision and pattern recognition*, 2016, pp. 779–788.

[54] J. Redmon and A. Farhadi, “Yolo9000: better, faster, stronger,” in *Proceedings of the IEEE conference on computer vision and pattern recognition*, 2017, pp. 7263–7271.

[55] J. Redmon and A. Farhadi, “Yolov3: An incremental improvement,” *arXiv preprint arXiv:1804.02767*, 2018.

[56] A. Bochkovski, C.-Y. Wang, and H.-Y. M. Liao, “Yolov4: Optimal speed and accuracy of object detection,” *arXiv preprint arXiv:2004.10934*, 2020.

[57] G. Jocher, “YOLOv5 by Ultralytics,” 5 2020. [Online]. Available: <https://github.com/ultralytics/yolov5>

[58] C. Li, L. Li, H. Jiang, K. Weng, Y. Geng, L. Li, Z. Ke, Q. Li, M. Cheng, W. Nie *et al.*, “Yolov6: A single-stage object detection framework for industrial applications,” *arXiv preprint arXiv:2209.02976*, 2022.

[59] C.-Y. Wang, A. Bochkovski, and H.-Y. M. Liao, “Yolov7: Trainable bag-of-freebies sets new state-of-the-art for real-time object detectors,” *arXiv preprint arXiv:2207.02696*, 2022.

[60] G. Jocher, A. Chaurasia, and J. Qiu, “YOLO by Ultralytics,” Jan. 2023. [Online]. Available: <https://github.com/ultralytics/ultralytics>

[61] W. Liu, D. Anguelov, D. Erhan, C. Szegedy, S. Reed, C.-Y. Fu, and A. C. Berg, “Ssd: Single shot multibox detector,” in *Computer Vision–ECCV 2016: 14th European Conference, Amsterdam, The Netherlands, October 11–14, 2016, Proceedings, Part I 14*. Springer, 2016, pp. 21–37.

[62] T.-Y. Lin, P. Goyal, R. Girshick, K. He, and P. Dollár, “Focal loss for dense object detection,” in *Proceedings of the IEEE international conference on computer vision*, 2017, pp. 2980–2988.

[63] L. Huang, Y. Yang, Y. Deng, and Y. Yu, “Densebox: Unifying landmark localization with end to end object detection,” *arXiv preprint arXiv:1509.04874*, 2015.

[64] Z. Tian, C. Shen, H. Chen, and T. He, “Fcos: Fully convolutional one-stage object detection,” in *Proceedings of the IEEE/CVF international conference on computer vision*, 2019, pp. 9627–9636.

[65] Z. Tian, C. Shen, H. Chen, and T. He, “Fcos: A simple and strong anchor-free object detector,” *IEEE Transactions on Pattern Analysis and Machine Intelligence*, vol. 44, no. 4, pp. 1922–1933, 2020.

[66] B. Zhu, J. Wang, Z. Jiang, F. Zong, S. Liu, Z. Li, and J. Sun, “Autotassign: Differentiable label assignment for dense object detection,” *arXiv preprint arXiv:2007.03496*, 2020.

[67] H. Law and J. Deng, “Cornernet: Detecting objects as paired keypoints,” in *Proceedings of the European conference on computer vision (ECCV)*, 2018, pp. 734–750.

[68] K. Duan, S. Bai, L. Xie, H. Qi, Q. Huang, and Q. Tian, “Centernet: Keypoint triplets for object detection,” in *Proceedings of the IEEE/CVF international conference on computer vision*, 2019, pp. 6569–6578.

[69] X. Zhou, J. Zhuo, and P. Krahenbuhl, “Bottom-up object detection by grouping extreme and center points,” in *Proceedings of the IEEE/CVF conference on computer vision and pattern recognition*, 2019, pp. 850–859.

[70] Z. Yang, S. Liu, H. Hu, L. Wang, and S. Lin, “Reppoints: Point set representation for object detection,” in *Proceedings of the IEEE/CVF international conference on computer vision*, 2019, pp. 9657–9666.

[71] F. Wei, X. Sun, H. Li, J. Wang, and S. Lin, “Point-set anchors for object detection, instance segmentation and pose estimation,” in *Computer Vision–ECCV 2020: 16th European Conference, Glasgow, UK, August 23–28, 2020, Proceedings, Part X 16*. Springer, 2020, pp. 527–544.

[72] N. Carion, F. Massa, G. Synnaeve, N. Usunier, A. Kirillov, and S. Zagoruyko, “End-to-end object detection with transformers,” in *Computer Vision–ECCV 2020: 16th European Conference, Glasgow, UK, August 23–28, 2020, Proceedings, Part I 16*. Springer, 2020, pp. 213–229.

[73] X. Zhu, W. Su, L. Lu, B. Li, X. Wang, and J. Dai, “Deformable detr: Deformable transformers for end-to-end object detection,” *arXiv preprint arXiv:2010.04159*, 2020.

[74] W. Lv, S. Xu, Y. Zhao, G. Wang, J. Wei, C. Cui, Y. Du, Q. Dang, and Y. Liu, “Detr beat yolos on real-time object detection,” 2023.

[75] F. Liu, H. Wei, W. Zhao, G. Li, J. Peng, and Z. Li, “Wb-detr: transformer-based detector without backbone,” in *Proceedings of the IEEE/CVF International Conference on Computer Vision*, 2021, pp. 2979–2987.

[76] Z. Liu, Y. Lin, Y. Cao, H. Hu, Y. Wei, Z. Zhang, S. Lin, and B. Guo, “Swin transformer: Hierarchical vision transformer using shifted windows,” in *Proceedings of the IEEE/CVF international conference on computer vision*, 2021, pp. 10 012–10 022.

[77] Y. Fang, B. Liao, X. Wang, J. Fang, J. Qi, R. Wu, J. Niu, and W. Liu, “You only look at one sequence: Rethinking transformer in vision through object detection,” *Advances in Neural Information Processing Systems*, vol. 34, pp. 26 183–26 197, 2021.

[78] Z. Peng, W. Huang, S. Gu, L. Xie, Y. Wang, J. Jiao, and Q. Ye, “Conformer: Local features coupling global representations for visual recognition,” in *Proceedings of the IEEE/CVF international conference on computer vision*, 2021, pp. 367–376.

[79] J. Pan, A. Bulat, F. Tan, X. Zhu, L. Dudziak, H. Li, G. Tzimiropoulos, and B. Martinez, “Edgevits: Competing light-weight cnns on mobile devices with vision transformers,” in *Computer Vision–ECCV 2022: 17th European Conference, Tel Aviv, Israel, October 23–27, 2022, Proceedings, Part XI*. Springer, 2022, pp. 294–311.

[80] S. Mehta and M. Rastegari, “Mobilevit: light-weight, general-purpose, and mobile-friendly vision transformer,” *arXiv preprint arXiv:2110.02178*, 2021.

[81] Y. Xu, Q. Zhang, J. Zhang, and D. Tao, “Vitae: Vision transformer advanced by exploring intrinsic inductive bias,” *Advances in Neural Information Processing Systems*, vol. 34, pp. 28 522–28 535, 2021.

[82] Z. Chen, L. Xie, J. Niu, X. Liu, L. Wei, and Q. Tian, “Visformer: The vision-friendly transformer,” in *Proceedings of the IEEE/CVF international conference on computer vision*, 2021, pp. 589–598.

[83] S. Tsutsui, T. Kerola, and S. Saito, “Distantly supervised road segmentation,” in *Proceedings of the IEEE International Conference on Computer Vision Workshops*, 2017, pp. 174–181.

[84] S. Tsutsui, T. Kerola, S. Saito, and D. J. Crandall, “Minimizing supervision for free-space segmentation,” in *Proceedings of the IEEE*

Conference on Computer Vision and Pattern Recognition Workshops, 2018, pp. 988–997.

[85] Y.-C. Chan, Y.-C. Lin, and P.-C. Chen, “Lane mark and drivable area detection using a novel instance segmentation scheme,” in *2019 IEEE/SICE International Symposium on System Integration (SII)*. IEEE, 2019, pp. 502–506.

[86] Y. Qian, J. M. Dolan, and M. Yang, “Dlt-net: Joint detection of drivable areas, lane lines, and traffic objects,” *IEEE Transactions on Intelligent Transportation Systems*, vol. 21, no. 11, pp. 4670–4679, 2019.

[87] H. Wang, R. Fan, P. Cai, and M. Liu, “Sne-roadseg+: Rethinking depth-normal translation and deep supervision for freespace detection,” in *2021 IEEE/RSJ International Conference on Intelligent Robots and Systems (IROS)*. IEEE, 2021, pp. 1140–1145.

[88] M.-E. Shao, M. A. Haq, D.-Q. Gao, P. Chondro, and S.-J. Ruan, “Semantic segmentation for free space and lane based on grid-based interest point detection,” *IEEE Transactions on Intelligent Transportation Systems*, vol. 23, no. 7, pp. 8498–8512, 2021.

[89] J. Kim and C. Park, “End-to-end ego lane estimation based on sequential transfer learning for self-driving cars,” in *Proceedings of the IEEE conference on computer vision and pattern recognition workshops*, 2017, pp. 30–38.

[90] D. Neven, B. De Brabandere, S. Georgoulis, M. Proesmans, and L. Van Gool, “Towards end-to-end lane detection: an instance segmentation approach,” in *2018 IEEE intelligent vehicles symposium (IV)*. IEEE, 2018, pp. 286–291.

[91] Z. Wang, W. Ren, and Q. Qiu, “Lanenet: Real-time lane detection networks for autonomous driving,” *arXiv preprint arXiv:1807.01726*, 2018.

[92] Q. Zou, H. Jiang, Q. Dai, Y. Yue, L. Chen, and Q. Wang, “Robust lane detection from continuous driving scenes using deep neural networks,” *IEEE transactions on vehicular technology*, vol. 69, no. 1, pp. 41–54, 2019.

[93] X. Chen, Y. Liu, and K. Achuthan, “Wodis: water obstacle detection network based on image segmentation for autonomous surface vehicles in maritime environments,” *IEEE Transactions on Instrumentation and Measurement*, vol. 70, pp. 1–13, 2021.

[94] B. Bovcon and M. Kristan, “Wasr—a water segmentation and refinement maritime obstacle detection network,” *IEEE Transactions on Cybernetics*, vol. 52, no. 12, pp. 12 661–12 674, 2021.

[95] B. Bovcon, J. Muhović, D. Vranac, D. Mozetič, J. Perš, and M. Kristan, “Mod3—a usv-oriented object detection and obstacle segmentation benchmark,” *IEEE Transactions on Intelligent Transportation Systems*, vol. 23, no. 8, pp. 13 403–13 418, 2021.

[96] J. Long, E. Shelhamer, and T. Darrell, “Fully convolutional networks for semantic segmentation,” in *Proceedings of the IEEE conference on computer vision and pattern recognition*, 2015, pp. 3431–3440.

[97] V. Badrinarayanan, A. Kendall, and R. Cipolla, “Segnet: A deep convolutional encoder-decoder architecture for image segmentation,” *IEEE transactions on pattern analysis and machine intelligence*, vol. 39, no. 12, pp. 2481–2495, 2017.

[98] O. Ronneberger, P. Fischer, and T. Brox, “U-net: Convolutional networks for biomedical image segmentation,” in *Medical Image Computing and Computer-Assisted Intervention—MICCAI 2015: 18th International Conference, Munich, Germany, October 5–9, 2015, Proceedings, Part III 18*. Springer, 2015, pp. 234–241.

[99] Y. Yuan, X. Chen, and J. Wang, “Object-contextual representations for semantic segmentation,” in *Computer Vision—ECCV 2020: 16th European Conference, Glasgow, UK, August 23–28, 2020, Proceedings, Part VI 16*. Springer, 2020, pp. 173–190.

[100] L.-C. Chen, G. Papandreou, I. Kokkinos, K. Murphy, and A. L. Yuille, “Semantic image segmentation with deep convolutional nets and fully connected crfs,” *arXiv preprint arXiv:1412.7062*, 2014.

[101] L.-C. Chen, G. Papandreou, I. Kokkinos, K. Murphy, and A. L. Yuille, “Deeplab: Semantic image segmentation with deep convolutional nets, atrous convolution, and fully connected crfs,” *IEEE transactions on pattern analysis and machine intelligence*, vol. 40, no. 4, pp. 834–848, 2017.

[102] L.-C. Chen, G. Papandreou, F. Schroff, and H. Adam, “Rethinking atrous convolution for semantic image segmentation,” *arXiv preprint arXiv:1706.05587*, 2017.

[103] L.-C. Chen, Y. Zhu, G. Papandreou, F. Schroff, and H. Adam, “Encoder-decoder with atrous separable convolution for semantic image segmentation,” in *Proceedings of the European conference on computer vision (ECCV)*, 2018, pp. 801–818.

[104] A. Paszke, A. Chaurasia, S. Kim, and E. Culurciello, “Enet: A deep neural network architecture for real-time semantic segmentation,” *arXiv preprint arXiv:1606.02147*, 2016.

[105] H. Zhao, J. Shi, X. Qi, X. Wang, and J. Jia, “Pyramid scene parsing network,” in *Proceedings of the IEEE conference on computer vision and pattern recognition*, 2017, pp. 2881–2890.

[106] P. Wang, P. Chen, Y. Yuan, D. Liu, Z. Huang, X. Hou, and G. Cottrell, “Understanding convolution for semantic segmentation,” in *2018 IEEE winter conference on applications of computer vision (WACV)*. IEEE, 2018, pp. 1451–1460.

[107] M. Yang, K. Yu, C. Zhang, Z. Li, and K. Yang, “Denseaspp for semantic segmentation in street scenes,” in *Proceedings of the IEEE conference on computer vision and pattern recognition*, 2018, pp. 3684–3692.

[108] S. Zheng, J. Lu, H. Zhao, X. Zhu, Z. Luo, Y. Wang, Y. Fu, J. Feng, T. Xiang, P. H. Torr *et al.*, “Rethinking semantic segmentation from a sequence-to-sequence perspective with transformers,” in *Proceedings of the IEEE/CVF conference on computer vision and pattern recognition*, 2021, pp. 6881–6890.

[109] R. Strudel, R. Garcia, I. Laptev, and C. Schmid, “Segmenter: Transformer for semantic segmentation,” in *Proceedings of the IEEE/CVF international conference on computer vision*, 2021, pp. 7262–7272.

[110] E. Xie, W. Wang, Z. Yu, A. Anandkumar, J. M. Alvarez, and P. Luo, “Segformer: Simple and efficient design for semantic segmentation with transformers,” *Advances in Neural Information Processing Systems*, vol. 34, pp. 12 077–12 090, 2021.

[111] H. Yan, C. Zhang, and M. Wu, “Lawin transformer: Improving semantic segmentation transformer with multi-scale representations via large window attention,” *arXiv preprint arXiv:2201.01615*, 2022.

[112] B. Cheng, A. Schwing, and A. Kirillov, “Per-pixel classification is not all you need for semantic segmentation,” *Advances in Neural Information Processing Systems*, vol. 34, pp. 17 864–17 875, 2021.

[113] K. M. Cuomo, J. E. Pion, and J. T. Mayhan, “Ultrawide-band coherent processing,” *IEEE Transactions on Antennas and Propagation*, vol. 47, no. 6, pp. 1094–1107, 1999.

[114] E. F. Knott, J. F. Schaeffer, and M. T. Tulley, *Radar cross section*. SciTech Publishing, 2004.

[115] H. Rohling, “Radar cfar thresholding in clutter and multiple target situations,” *IEEE transactions on aerospace and electronic systems*, no. 4, pp. 608–621, 1983.

[116] P. P. Gandhi and S. A. Kassam, “Analysis of cfar processors in nonhomogeneous background,” *IEEE Transactions on Aerospace and Electronic systems*, vol. 24, no. 4, pp. 427–445, 1988.

[117] A. Melebari, A. K. Mishra, and M. A. Gaffar, “Comparison of square law, linear and bessel detectors for ca and os cfar algorithms,” in *2015 IEEE Radar Conference*. IEEE, 2015, pp. 383–388.

[118] M. Weiss, “Analysis of some modified cell-averaging cfar processors in multiple-target situations,” *IEEE Transactions on Aerospace and Electronic Systems*, no. 1, pp. 102–114, 1982.

[119] V. G. Hansen and J. H. Sawyers, “Detectability loss due to “greatest of” selection in a cell-averaging cfar,” *IEEE Transactions on Aerospace and Electronic Systems*, no. 1, pp. 115–118, 1980.

[120] G. V. Trunk, “Range resolution of targets using automatic detectors,” *IEEE Transactions on Aerospace and Electronic Systems*, no. 5, pp. 750–755, 1978.

[121] J. T. Rickard and G. M. Dillard, “Adaptive detection algorithms for multiple-target spectral data,” in *1977 IEEE Conference on Decision and Control including the 16th Symposium on Adaptive Processes and A Special Symposium on Fuzzy Set Theory and Applications*. IEEE, 1977, pp. 515–518.

[122] J. Zhao, R. Jiang, X. Wang, and H. Gao, “Robust cfar detection for multiple targets in k-distributed sea clutter based on machine learning,” *Symmetry*, vol. 11, no. 12, p. 1482, 2019.

[123] M. Ester, H.-P. Kriegel, J. Sander, X. Xu *et al.*, “A density-based algorithm for discovering clusters in large spatial databases with noise.” in *kdd*, vol. 96, no. 34, 1996, pp. 226–231.

[124] V. C. Chen and H. Ling, *Time-frequency transforms for radar imaging and signal analysis*. Artech house, 2002.

[125] F. E. Nowruzi, D. Kolhatkar, P. Kapoor, F. Al Hassanat, E. J. Heravi, R. Lagnaniere, J. Rebut, and W. Malik, “Deep open space segmentation using automotive radar,” in *2020 IEEE MTT-S International Conference on Microwaves for Intelligent Mobility (ICMIM)*. IEEE, 2020, pp. 1–4.

[126] M. Stephan, T. Stadelmayer, A. Santra, G. Fischer, R. Weigel, and F. Lurz, “Radar image reconstruction from raw adc data using parametric variational autoencoder with domain adaptation,” in *2020 25th International Conference on Pattern Recognition (ICPR)*. IEEE, 2021, pp. 9529–9536.

[127] T. Stadelmayer, A. Santra, R. Weigel, and F. Lurz, “Data-driven radar processing using a parametric convolutional neural network for human

activity classification,” *IEEE Sensors Journal*, vol. 21, no. 17, pp. 19 529–19 540, 2021.

[128] T. Stadelmayer, A. Santra, M. Stadelmayer, R. Weigel, and F. Lurz, “Improved target detection and feature extraction using a complex-valued adaptive sine filter on radar time domain data,” in *2021 29th European Signal Processing Conference (EUSIPCO)*. IEEE, 2021, pp. 1745–1749.

[129] P. Zhao, C. X. Lu, B. Wang, N. Trigoni, and A. Markham, “Cubelearn: End-to-end learning for human motion recognition from raw mmwave radar signals,” *IEEE Internet of Things Journal*, 2023.

[130] M. Arsalan, A. Santra, and V. Issakov, “Spiking neural network-based radar gesture recognition system using raw adc data,” *IEEE Sensors Letters*, vol. 6, no. 6, pp. 1–4, 2022.

[131] A. Ouaknine, A. Newson, J. Rebut, F. Tupin, and P. Pérez, “Carrada dataset: Camera and automotive radar with range-angle-doppler annotations,” in *2020 25th International Conference on Pattern Recognition (ICPR)*. IEEE, 2021, pp. 5068–5075.

[132] X. Gao, G. Xing, S. Roy, and H. Liu, “Experiments with mmwave automotive radar test-bed,” in *2019 53rd asilomar conference on signals, systems, and computers*. IEEE, 2019, pp. 1–6.

[133] X. Dong, P. Wang, P. Zhang, and L. Liu, “Probabilistic oriented object detection in automotive radar,” in *Proceedings of the IEEE/CVF Conference on Computer Vision and Pattern Recognition Workshops*, 2020, pp. 102–103.

[134] W. Ng, G. Wang, Z. Lin, B. J. Dutta *et al.*, “Range-doppler detection in automotive radar with deep learning,” in *2020 International Joint Conference on Neural Networks (IJCNN)*. IEEE, 2020, pp. 1–8.

[135] C. Decourt, R. VanRullen, D. Salle, and T. Oberlin, “Darod: A deep automotive radar object detector on range-doppler maps,” in *2022 IEEE Intelligent Vehicles Symposium (IV)*. IEEE, 2022, pp. 112–118.

[136] X. Gao, G. Xing, S. Roy, and H. Liu, “Ramp-cnn: A novel neural network for enhanced automotive radar object recognition,” *IEEE Sensors Journal*, vol. 21, no. 4, pp. 5119–5132, 2020.

[137] A. Palfy, J. Dong, J. F. Kooij, and D. M. Gavrila, “Cnn based road user detection using the 3d radar cube,” *IEEE Robotics and Automation Letters*, vol. 5, no. 2, pp. 1263–1270, 2020.

[138] A. Zhang, F. E. Nowruzi, and R. Laganière, “Raddet: Range-azimuth-doppler based radar object detection for dynamic road users,” in *2021 18th Conference on Robots and Vision (CRV)*. IEEE, 2021, pp. 95–102.

[139] F. E. Nowruzi, D. Kolhatkar, P. Kapoor, E. J. Heravi, F. A. Hassamat, R. Laganière, J. Rebut, and W. Malik, “Polarnet: Accelerated deep open space segmentation using automotive radar in polar domain,” *arXiv preprint arXiv:2103.03387*, 2021.

[140] A. Ouaknine, A. Newson, P. Pérez, F. Tupin, and J. Rebut, “Multi-view radar semantic segmentation,” in *Proceedings of the IEEE/CVF International Conference on Computer Vision*, 2021, pp. 15 671–15 680.

[141] K. He, X. Zhang, S. Ren, and J. Sun, “Deep residual learning for image recognition,” in *Proceedings of the IEEE conference on computer vision and pattern recognition*, 2016, pp. 770–778.

[142] A. Palfy, E. Pool, S. Baratam, J. F. Kooij, and D. M. Gavrila, “Multi-class road user detection with 3+ 1d radar in the view-of-delft dataset,” *IEEE Robotics and Automation Letters*, vol. 7, no. 2, pp. 4961–4968, 2022.

[143] A. Danzer, T. Griebel, M. Bach, and K. Dietmayer, “2d car detection in radar data with pointnets,” in *2019 IEEE Intelligent Transportation Systems Conference (ITSC)*. IEEE, 2019, pp. 61–66.

[144] J. F. Tilly, S. Haag, O. Schumann, F. Weishaupt, B. Duraisamy, J. Dickmann, and M. Fritzsche, “Detection and tracking on automotive radar data with deep learning,” in *2020 IEEE 23rd International Conference on Information Fusion (FUSION)*. IEEE, 2020, pp. 1–7.

[145] N. Scheiner, F. Kraus, F. Wei, B. Phan, F. Mannan, N. Appenrodt, W. Ritter, J. Dickmann, K. Dietmayer, B. Sick *et al.*, “Seeing around street corners: Non-line-of-sight detection and tracking in-the-wild using doppler radar,” in *Proceedings of the IEEE/CVF Conference on Computer Vision and Pattern Recognition*, 2020, pp. 2068–2077.

[146] O. Schumann, M. Hahn, J. Dickmann, and C. Wöhler, “Semantic segmentation on radar point clouds,” in *2018 21st International Conference on Information Fusion (FUSION)*. IEEE, 2018, pp. 2179–2186.

[147] Z. Feng, S. Zhang, M. Kunert, and W. Wiesbeck, “Point cloud segmentation with a high-resolution automotive radar,” in *AmE 2019- Automotive meets Electronics; 10th GMM-Symposium*. VDE, 2019, pp. 1–5.

[148] O. Schumann, M. Hahn, J. Dickmann, and C. Wöhler, “Supervised clustering for radar applications: On the way to radar instance segmentation,” in *2018 IEEE MTT-S International Conference on Microwaves for Intelligent Mobility (ICMIM)*. IEEE, 2018, pp. 1–4.

[149] F. Nobis, F. Fent, J. Betz, and M. Lienkamp, “Kernel point convolution lstm networks for radar point cloud segmentation,” *Applied Sciences*, vol. 11, no. 6, p. 2599, 2021.

[150] J. Liu, W. Xiong, L. Bai, Y. Xia, T. Huang, W. Ouyang, and B. Zhu, “Deep instance segmentation with automotive radar detection points,” *IEEE Transactions on Intelligent Vehicles*, 2022.

[151] C. R. Qi, H. Su, K. Mo, and L. J. Guibas, “Pointnet: Deep learning on point sets for 3d classification and segmentation,” in *Proceedings of the IEEE conference on computer vision and pattern recognition*, 2017, pp. 652–660.

[152] C. R. Qi, L. Yi, H. Su, and L. J. Guibas, “Pointnet++: Deep hierarchical feature learning on point sets in a metric space,” *Advances in neural information processing systems*, vol. 30, 2017.

[153] C. R. Qi, W. Liu, C. Wu, H. Su, and L. J. Guibas, “Frustum pointnets for 3d object detection from rgb-d data,” in *Proceedings of the IEEE conference on computer vision and pattern recognition*, 2018, pp. 918–927.

[154] P. Kaul, D. De Martini, M. Gadd, and P. Newman, “Rss-net: weakly-supervised multi-class semantic segmentation with fmcw radar,” in *2020 IEEE Intelligent Vehicles Symposium (IV)*. IEEE, 2020, pp. 431–436.

[155] K. Werber, M. Rapp, J. Klappstein, M. Hahn, J. Dickmann, K. Dietmayer, and C. Waldschmidt, “Automotive radar gridmap representations,” in *2015 IEEE MTT-S International Conference on Microwaves for Intelligent Mobility (ICMIM)*. IEEE, 2015, pp. 1–4.

[156] J. Lombacher, M. Hahn, J. Dickmann, and C. Wöhler, “Detection of arbitrarily rotated parked cars based on radar sensors,” in *2015 16th International Radar Symposium (IRS)*. IEEE, 2015, pp. 180–185.

[157] J. Lombacher, K. Laudt, M. Hahn, J. Dickmann, and C. Wöhler, “Semantic radar grids,” in *2017 IEEE intelligent vehicles symposium (IV)*. IEEE, 2017, pp. 1170–1175.

[158] J. Degerman, T. Pernstål, and K. Alenljung, “3d occupancy grid mapping using statistical radar models,” in *2016 IEEE Intelligent Vehicles Symposium (IV)*. IEEE, 2016, pp. 902–908.

[159] R. Prophet, G. Li, C. Sturm, and M. Vossiek, “Semantic segmentation on automotive radar maps,” in *2019 IEEE Intelligent Vehicles Symposium (IV)*. IEEE, 2019, pp. 756–763.

[160] R. Prophet, A. Deligiannis, J.-C. Fuentes-Michel, I. Weber, and M. Vossiek, “Semantic segmentation on 3d occupancy grids for automotive radar,” *IEEE Access*, vol. 8, pp. 197 917–197 930, 2020.

[161] R. Prophet, H. Stark, M. Hoffmann, C. Sturm, and M. Vossiek, “Adaptions for automotive radar based occupancy gridmaps,” in *2018 IEEE MTT-S International Conference on Microwaves for Intelligent Mobility (ICMIM)*. IEEE, 2018, pp. 1–4.

[162] M. Li, Z. Feng, M. Stolz, M. Kunert, R. Henze, and F. Küçükay, “High resolution radar-based occupancy grid mapping and free space detection,” in *VEHITS*, 2018, pp. 70–81.

[163] L. Sless, B. El Shlomo, G. Cohen, and S. Oron, “Road scene understanding by occupancy grid learning from sparse radar clusters using semantic segmentation,” in *Proceedings of the IEEE/CVF International Conference on Computer Vision Workshops*, 2019, pp. 0–0.

[164] O. Schumann, J. Lombacher, M. Hahn, C. Wöhler, and J. Dickmann, “Scene understanding with automotive radar,” *IEEE Transactions on Intelligent Vehicles*, vol. 5, no. 2, pp. 188–203, 2019.

[165] Y. LeCun, L. Bottou, Y. Bengio, and P. Haffner, “Gradient-based learning applied to document recognition,” *Proceedings of the IEEE*, vol. 86, no. 11, pp. 2278–2324, 1998.

[166] J. Lombacher, M. Hahn, J. Dickmann, and C. Wöhler, “Potential of radar for static object classification using deep learning methods,” in *2016 IEEE MTT-S International Conference on Microwaves for Intelligent Mobility (ICMIM)*. IEEE, 2016, pp. 1–4.

[167] J. Lombacher, M. Hahn, J. Dickmann, and C. Wöhler, “Object classification in radar using ensemble methods,” in *2017 IEEE MTT-S International Conference on Microwaves for Intelligent Mobility (ICMIM)*. IEEE, 2017, pp. 87–90.

[168] M. Thom and F. Gritschneider, “Rapid exact signal scanning with deep convolutional neural networks,” *IEEE Transactions on Signal Processing*, vol. 65, no. 5, pp. 1235–1250, 2016.

[169] M. Dreher, E. Erçelik, T. Bänziger, and A. Knol, “Radar-based 2d car detection using deep neural networks,” in *2020 IEEE 23rd International Conference on Intelligent Transportation Systems (ITSC)*. IEEE, 2020, pp. 1–8.

[170] Z. Wen, D. Li, and W. Yu, “A quantitative evaluation for radar grid map construction,” in *2019 International Conference on Electromagnetics in Advanced Applications (ICEAA)*. IEEE, 2019, pp. 0794–0796.

[171] D. Gusland, J. M. Christiansen, B. Torvik, F. Fioranelli, S. Z. Gurbuz, and M. Ritchie, "Open radar initiative: Large scale dataset for benchmarking of micro-doppler recognition algorithms," in *2021 IEEE Radar Conference (RadarConf21)*. IEEE, 2021, pp. 1–6.

[172] A. Angelov, A. Robertson, R. Murray-Smith, and F. Fioranelli, "Practical classification of different moving targets using automotive radar and deep neural networks," *IET Radar, Sonar & Navigation*, vol. 12, no. 10, pp. 1082–1089, 2018.

[173] S. Z. Gurbuz and M. G. Amin, "Radar-based human-motion recognition with deep learning: Promising applications for indoor monitoring," *IEEE Signal Processing Magazine*, vol. 36, no. 4, pp. 16–28, 2019.

[174] Y. Kim and T. Moon, "Human detection and activity classification based on micro-doppler signatures using deep convolutional neural networks," *IEEE geoscience and remote sensing letters*, vol. 13, no. 1, pp. 8–12, 2015.

[175] A.-K. Seifert, M. G. Amin, and A. M. Zoubir, "New analysis of radar micro-doppler gait signatures for rehabilitation and assisted living," in *2017 IEEE International Conference on Acoustics, Speech and Signal Processing (ICASSP)*. IEEE, 2017, pp. 4004–4008.

[176] J. Zhang, J. Tao, and Z. Shi, "Doppler-radar based hand gesture recognition system using convolutional neural networks," in *Communications, Signal Processing, and Systems: Proceedings of the 2017 International Conference on Communications, Signal Processing, and Systems*. Springer, 2019, pp. 1096–1113.

[177] K. Simonyan and A. Zisserman, "Very deep convolutional networks for large-scale image recognition," *arXiv preprint arXiv:1409.1556*, 2014.

[178] A.-K. Seifert, M. G. Amin, and A. M. Zoubir, "Toward unobtrusive in-home gait analysis based on radar micro-doppler signatures," *IEEE Transactions on Biomedical Engineering*, vol. 66, no. 9, pp. 2629–2640, 2019.

[179] B. K. Kim, H.-S. Kang, and S.-O. Park, "Drone classification using convolutional neural networks with merged doppler images," *IEEE Geoscience and Remote Sensing Letters*, vol. 14, no. 1, pp. 38–42, 2016.

[180] S. Chen, W. He, J. Ren, and X. Jiang, "Attention-based dual-stream vision transformer for radar gait recognition," in *ICASSP 2022-2022 IEEE International Conference on Acoustics, Speech and Signal Processing (ICASSP)*. IEEE, 2022, pp. 3668–3672.

[181] C. Szegedy, W. Liu, Y. Jia, P. Sermanet, S. Reed, D. Anguelov, D. Erhan, V. Vanhoucke, and A. Rabinovich, "Going deeper with convolutions," in *Proceedings of the IEEE conference on computer vision and pattern recognition*, 2015, pp. 1–9.

[182] A. Geiger, P. Lenz, and R. Urtasun, "Are we ready for autonomous driving? the kitti vision benchmark suite," in *2012 IEEE conference on computer vision and pattern recognition*. IEEE, 2012, pp. 3354–3361.

[183] W. Maddern, G. Pascoe, C. Linegar, and P. Newman, "1 year, 1000 km: The oxford robotcar dataset," *The International Journal of Robotics Research*, vol. 36, no. 1, pp. 3–15, 2017.

[184] X. Huang, P. Wang, X. Cheng, D. Zhou, Q. Geng, and R. Yang, "The apolloscape open dataset for autonomous driving and its application," *IEEE transactions on pattern analysis and machine intelligence*, vol. 42, no. 10, pp. 2702–2719, 2019.

[185] P. Sun, H. Kretzschmar, X. Dotiwalla, A. Chouard, V. Patnaik, P. Tsui, J. Guo, Y. Zhou, Y. Chai, B. Caine *et al.*, "Scalability in perception for autonomous driving: Waymo open dataset," in *Proceedings of the IEEE/CVF conference on computer vision and pattern recognition*, 2020, pp. 2446–2454.

[186] M. Mostajabi, C. M. Wang, D. Ranjan, and G. Hsyz, "High-resolution radar dataset for semi-supervised learning of dynamic objects," in *Proceedings of the IEEE/CVF Conference on Computer Vision and Pattern Recognition Workshops*, 2020, pp. 100–101.

[187] M. Sheeny, E. De Pellegrin, S. Mukherjee, A. Ahrabian, S. Wang, and A. Wallace, "Radiate: A radar dataset for automotive perception in bad weather," in *2021 IEEE International Conference on Robotics and Automation (ICRA)*. IEEE, 2021, pp. 1–7.

[188] X. Weng, Y. Man, D. Cheng, J. Park, M. O'Toole, K. Kitani, J. Wang, and D. Held, "All-in-one drive: A large-scale comprehensive perception dataset with high-density long-range point clouds," *arXiv*, 2020.

[189] Y. Wang, G. Wang, H.-M. Hsu, H. Liu, and J.-N. Hwang, "Rethinking of radar's role: A camera-radar dataset and systematic annotator via coordinate alignment," in *Proceedings of the IEEE/CVF Conference on Computer Vision and Pattern Recognition*, 2021, pp. 2815–2824.

[190] T.-Y. Lim, S. A. Markowitz, and M. N. Do, "Radical: A synchronized fmcw radar, depth, imu and rgb camera data dataset with low-level fmcw radar signals," *IEEE Journal of Selected Topics in Signal Processing*, vol. 15, no. 4, pp. 941–953, 2021.

[191] O. Schumann, M. Hahn, N. Scheiner, F. Weishaupt, J. F. Tilly, J. Dickmann, and C. Wöhler, "Radarscenes: A real-world radar point cloud data set for automotive applications," in *2021 IEEE 24th International Conference on Information Fusion (FUSION)*. IEEE, 2021, pp. 1–8.

[192] Y. Cheng, J. Zhu, M. Jiang, J. Fu, C. Pang, P. Wang, K. Sankaran, O. Onabola, Y. Liu, D. Liu *et al.*, "Flow: A dataset and benchmark for floating waste detection in inland waters," in *Proceedings of the IEEE/CVF International Conference on Computer Vision*, 2021, pp. 10953–10962.

[193] J. Rebut, A. Ouaknine, W. Malik, and P. Pérez, "Raw high-definition radar for multi-task learning," in *Proceedings of the IEEE/CVF Conference on Computer Vision and Pattern Recognition*, 2022, pp. 17021–17030.

[194] K. Burnett, D. J. Yoon, Y. Wu, A. Z. Li, H. Zhang, S. Lu, J. Qian, W.-K. Tseng, A. Lambert, K. Y. Leung *et al.*, "Boreas: A multi-season autonomous driving dataset," *arXiv preprint arXiv:2203.10168*, 2022.

[195] M. Meyer and G. Kuschk, "Deep learning based 3d object detection for automotive radar and camera," in *2019 16th European Radar Conference (EuRAD)*. IEEE, 2019, pp. 133–136.

[196] L. Zheng, Z. Ma, X. Zhu, B. Tan, S. Li, K. Long, W. Sun, S. Chen, L. Zhang, M. Wan *et al.*, "Tj4dradset: A 4d radar dataset for autonomous driving," in *2022 IEEE 25th International Conference on Intelligent Transportation Systems (ITSC)*. IEEE, 2022, pp. 493–498.

[197] D.-H. Paek, S.-H. Kong, and K. T. Wijaya, "K-radar: 4d radar object detection dataset and benchmark for autonomous driving in various weather conditions," *arXiv preprint arXiv:2206.08171*, 2022.

[198] T. Matuszka, I. Barton, Á. Butykai, P. Hajas, D. Kiss, D. Kovács, S. Kunsági-Máté, P. Lengyel, G. Németh, L. Pető *et al.*, "aimotive dataset: A multimodal dataset for robust autonomous driving with long-range perception," *arXiv preprint arXiv:2211.09445*, 2022.

[199] J. Guan, S. Madani, S. Jog, S. Gupta, and H. Hassanieh, "Through fog high-resolution imaging using millimeter wave radar," in *Proceedings of the IEEE/CVF Conference on Computer Vision and Pattern Recognition*, 2020, pp. 11464–11473.

[200] A. Dosovitskiy, G. Ros, F. Codevilla, A. Lopez, and V. Koltun, "Carla: An open urban driving simulator," in *Conference on robot learning*. PMLR, 2017, pp. 1–16.

[201] S. Chadwick, W. Maddern, and P. Newman, "Distant vehicle detection using radar and vision," in *2019 International Conference on Robotics and Automation (ICRA)*. IEEE, 2019, pp. 8311–8317.

[202] T. Roddick, A. Kendall, and R. Cipolla, "Orthographic feature transform for monocular 3d object detection," *arXiv preprint arXiv:1811.08188*, 2018.

[203] A. Simonelli, S. R. Bulo, L. Porzi, M. López-Antequera, and P. Kuntschieder, "Disentangling monocular 3d object detection," in *Proceedings of the IEEE/CVF International Conference on Computer Vision*, 2019, pp. 1991–1999.

[204] X. Zhou, D. Wang, and P. Krähenbühl, "Objects as points," *arXiv preprint arXiv:1904.07850*, 2019.

[205] R. Yadav, A. Vierling, and K. Berns, "Radar+rgb attentive fusion for robust object detection in autonomous vehicles," *arXiv preprint arXiv:2008.13642*, 2020.

[206] R. Nabati and H. Qi, "Radar-camera sensor fusion for joint object detection and distance estimation in autonomous vehicles," *arXiv preprint arXiv:2009.08428*, 2020.

[207] H. Cui, J. Wu, J. Zhang, G. Chowdhary, and W. R. Norris, "3d detection and tracking for on-road vehicles with a monovision camera and dual low-cost 4d mmwave radars," in *2021 IEEE International Intelligent Transportation Systems Conference (ITSC)*. IEEE, 2021, pp. 2931–2937.

[208] L.-q. Li and Y.-l. Xie, "A feature pyramid fusion detection algorithm based on radar and camera sensor," in *2020 15th IEEE International Conference on Signal Processing (ICSP)*, vol. 1. IEEE, 2020, pp. 366–370.

[209] K. Kowol, M. Rottmann, S. Bracke, and H. Gottschalk, "Yodar: uncertainty-based sensor fusion for vehicle detection with camera and radar sensors," *arXiv preprint arXiv:2010.03320*, 2020.

[210] Y. Cheng, H. Xu, and Y. Liu, "Robust small object detection on the water surface through fusion of camera and millimeter wave radar," in *Proceedings of the IEEE/CVF International Conference on Computer Vision*, 2021, pp. 15263–15272.

[211] V. John, M. Nithilan, S. Mita, H. Tehrani, R. Sudheesh, and P. Lalu, "So-net: Joint semantic segmentation and obstacle detection using deep fusion of monocular camera and radar," in *Image and Video Technology: PSIVT 2019 International Workshops, Sydney, NSW, Australia, November 18–22, 2019, Revised Selected Papers 9*. Springer, 2020, pp. 138–148.

[212] X. Dong, B. Zhuang, Y. Mao, and L. Liu, "Radar camera fusion via representation learning in autonomous driving," in *Proceedings of the IEEE/CVF Conference on Computer Vision and Pattern Recognition*, 2021, pp. 1672–1681.

[213] K. Bansal, K. Rungta, and D. Bharadia, "Radsegnet: A reliable approach to radar camera fusion," *arXiv preprint arXiv:2208.03849*, 2022.

[214] A. W. Harley, Z. Fang, J. Li, R. Ambrus, and K. Fragkiadaki, "A simple baseline for bev perception without lidar," *arXiv e-prints*, pp. arXiv–2206, 2022.

[215] M. Bertozzi, A. Broggi, and A. Fascioli, "Stereo inverse perspective mapping: theory and applications," *Image and vision computing*, vol. 16, no. 8, pp. 585–590, 1998.

[216] M. Oliveira, V. Santos, and A. D. Sappa, "Multimodal inverse perspective mapping," *Information Fusion*, vol. 24, pp. 108–121, 2015.

[217] T.-Y. Lim, A. Ansari, B. Major, D. Fontijne, M. Hamilton, R. Gowaikar, and S. Subramanian, "Radar and camera early fusion for vehicle detection in advanced driver assistance systems," in *Machine learning for autonomous driving workshop at the 33rd conference on neural information processing systems*, vol. 2, 2019, p. 7.

[218] T. Zhou, J. Chen, Y. Shi, K. Jiang, M. Yang, and D. Yang, "Bridging the view disparity between radar and camera features for multi-modal fusion 3d object detection," *IEEE Transactions on Intelligent Vehicles*, vol. 8, no. 2, pp. 1523–1535, 2023.

[219] Y. Wang, W.-L. Chao, D. Garg, B. Hariharan, M. Campbell, and K. Q. Weinberger, "Pseudo-lidar from visual depth estimation: Bridging the gap in 3d object detection for autonomous driving," in *Proceedings of the IEEE/CVF Conference on Computer Vision and Pattern Recognition*, 2019, pp. 8445–8453.

[220] H. Jha, V. Lodhi, and D. Chakravarty, "Object detection and identification using vision and radar data fusion system for ground-based navigation," in *2019 6th International Conference on Signal Processing and Integrated Networks (SPIN)*. IEEE, 2019, pp. 590–593.

[221] J. Kim, Y. Kim, and D. Kum, "Low-level sensor fusion network for 3d vehicle detection using radar range-azimuth heatmap and monocular image," in *Proceedings of the Asian Conference on Computer Vision*, 2020.

[222] F. Nobis, M. Geisslinger, M. Weber, J. Betz, and M. Lienkamp, "A deep learning-based radar and camera sensor fusion architecture for object detection," in *2019 Sensor Data Fusion: Trends, Solutions, Applications (SDF)*. IEEE, 2019, pp. 1–7.

[223] Y. Long, D. Morris, X. Liu, M. Castro, P. Chakravarty, and P. Narayanan, "Radar-camera pixel depth association for depth completion," in *Proceedings of the IEEE/CVF Conference on Computer Vision and Pattern Recognition*, 2021, pp. 12507–12516.

[224] S. Chang, Y. Zhang, F. Zhang, X. Zhao, S. Huang, Z. Feng, and Z. Wei, "Spatial attention fusion for obstacle detection using mmwave radar and vision sensor," *Sensors*, vol. 20, no. 4, p. 956, 2020.

[225] A. Valada, R. Mohan, and W. Burgard, "Self-supervised model adaptation for multimodal semantic segmentation," *International Journal of Computer Vision*, vol. 128, no. 5, pp. 1239–1285, 2020.

[226] T. Broedermann, C. Sakaridis, D. Dai, and L. Van Gool, "Hrfuser: A multi-resolution sensor fusion architecture for 2d object detection," *arXiv preprint arXiv:2206.15157*, 2022.

[227] Y. Yuan, R. Fu, L. Huang, W. Lin, C. Zhang, X. Chen, and J. Wang, "Hrformer: High-resolution transformer for dense prediction," *arXiv preprint arXiv:2110.09408*, 2021.

[228] E. Olson, "A passive solution to the sensor synchronization problem," in *2010 IEEE/RSJ International Conference on Intelligent Robots and Systems*. IEEE, 2010, pp. 1059–1064.

[229] A. Westenberger, T. Huck, M. Fritzsche, T. Schwarz, and K. Dietmayer, "Temporal synchronization in multi-sensor fusion for future driver assistance systems," in *2011 IEEE International Symposium on Precision Clock Synchronization for Measurement, Control and Communication*. IEEE, 2011, pp. 93–98.

[230] P. Furgale, J. Rehder, and R. Siegwart, "Unified temporal and spatial calibration for multi-sensor systems," in *2013 IEEE/RSJ International Conference on Intelligent Robots and Systems*. IEEE, 2013, pp. 1280–1286.

[231] T. Huck, A. Westenberger, M. Fritzsche, T. Schwarz, and K. Dietmayer, "Precise timestamping and temporal synchronization in multi-sensor fusion," in *2011 IEEE intelligent vehicles symposium (IV)*. IEEE, 2011, pp. 242–247.

[232] J. E. Guijant, S. Marden, and K. Pereida, "Distributed multi sensor data fusion for autonomous 3d mapping," in *2012 International Conference on Indoor Positioning and Indoor Navigation (IPIN)*. IEEE, 2012, pp. 1–11.

[233] J. Steinbaeck, C. Steger, E. Brenner, and N. Druml, "A hybrid timestamping approach for multi-sensor perception systems," in *2020 23rd Euromicro Conference on Digital System Design (DSD)*. IEEE, 2020, pp. 447–454.

[234] A. English, P. Ross, D. Ball, B. Upcroft, and P. Corke, "Triggersync: A time synchronisation tool," in *2015 IEEE International Conference on Robotics and Automation (ICRA)*. IEEE, 2015, pp. 6220–6226.

[235] L. Lu, C. Zhang, Y. Liu, W. Zhang, and Y. Xia, "Ieee 1588-based general and precise time synchronization method for multiple sensors," in *2019 IEEE International Conference on Robotics and Biomimetics (ROBIO)*. IEEE, 2019, pp. 2427–2432.

[236] M. Huber, M. Schlegel, and G. Klinker, "Temporal calibration in multisensor tracking setups," in *2009 8th IEEE International Symposium on Mixed and Augmented Reality*. IEEE, 2009, pp. 195–196.

[237] Y. Du, B. Qin, C. Zhao, Y. Zhu, J. Cao, and Y. Ji, "A novel spatio-temporal synchronization method of roadside asynchronous mmw radar-camera for sensor fusion," *IEEE transactions on intelligent transportation systems*, vol. 23, no. 11, pp. 22278–22289, 2021.

[238] Y. Fu, D. Tian, X. Duan, J. Zhou, P. Lang, C. Lin, and X. You, "A camera-radar fusion method based on edge computing," in *2020 IEEE International Conference on Edge Computing (EDGE)*. IEEE, 2020, pp. 9–14.

[239] F. Liu, J. Sparbert, and C. Stiller, "Immpda vehicle tracking system using asynchronous sensor fusion of radar and vision," in *2008 IEEE Intelligent Vehicles Symposium*. IEEE, 2008, pp. 168–173.

[240] L. Wang, Z. Zhang, X. Di, and J. Tian, "A roadside camera-radar sensing fusion system for intelligent transportation," in *2020 17th European Radar Conference (EuRAD)*. IEEE, 2020, pp. 282–285.

[241] J. Peršić, L. Petrović, I. Marković, and I. Petrović, "Spatiotemporal multisensor calibration via gaussian processes moving target tracking," *IEEE Transactions on Robotics*, vol. 37, no. 5, pp. 1401–1415, 2021.

[242] S. Li, C. Xu, and M. Xie, "A robust o (n) solution to the perspective-n-point problem," *IEEE transactions on pattern analysis and machine intelligence*, vol. 34, no. 7, pp. 1444–1450, 2012.

[243] E. Wise, J. Peršić, C. Grebe, I. Petrović, and J. Kelly, "A continuous-time approach for 3d radar-to-camera extrinsic calibration," in *2021 IEEE International Conference on Robotics and Automation (ICRA)*. IEEE, 2021, pp. 13164–13170.

[244] J. Peršić, L. Petrović, I. Marković, and I. Petrović, "Online multi-sensor calibration based on moving object tracking," *Advanced Robotics*, vol. 35, no. 3-4, pp. 130–140, 2021.

[245] K. Qiu, T. Qin, J. Pan, S. Liu, and S. Shen, "Real-time temporal and rotational calibration of heterogeneous sensors using motion correlation analysis," *IEEE Transactions on Robotics*, vol. 37, no. 2, pp. 587–602, 2020.

[246] X.-p. Guo, J.-s. Du, J. Gao, and W. Wang, "Pedestrian detection based on fusion of millimeter wave radar and vision," in *Proceedings of the 2018 International Conference on Artificial Intelligence and Pattern Recognition*, 2018, pp. 38–42.

[247] G. Iyer, R. K. Ram, J. K. Murthy, and K. M. Krishna, "Calibnet: Geometrically supervised extrinsic calibration using 3d spatial transformer networks," in *2018 IEEE/RSJ International Conference on Intelligent Robots and Systems (IROS)*. IEEE, 2018, pp. 1110–1117.

[248] C. Schöller, M. Schnettler, A. Krämer, G. Hinz, M. Bakovic, M. Güzet, and A. Knoll, "Targetless rotational auto-calibration of radar and camera for intelligent transportation systems," in *2019 IEEE Intelligent Transportation Systems Conference (ITSC)*. IEEE, 2019, pp. 3934–3941.

[249] G. Zhao, J. Hu, S. You, and C.-C. J. Kuo, "Calibdnn: multimodal sensor calibration for perception using deep neural networks," in *Signal Processing, Sensor/Information Fusion, and Target Recognition XXX*, vol. 11756. SPIE, 2021, pp. 324–335.

[250] F. Nobis, E. Shafiei, P. Karle, J. Betz, and M. Lienkamp, "Radar voxel fusion for 3d object detection," *Applied Sciences*, vol. 11, no. 12, p. 5598, 2021.

[251] R. A. Jacobs, M. I. Jordan, S. J. Nowlan, and G. E. Hinton, "Adaptive mixtures of local experts," *Neural computation*, vol. 3, no. 1, pp. 79–87, 1991.

[252] Y. Kim, J. W. Choi, and D. Kum, "Grif net: Gated region of interest fusion network for robust 3d object detection from radar point cloud and monocular image," in *2020 IEEE/RSJ International Conference on Intelligent Robots and Systems (IROS)*. IEEE, 2020, pp. 10857–10864.

[253] M. Ren, A. Pokrovsky, B. Yang, and R. Urtasun, "Sbnet: Sparse blocks network for fast inference," in *Proceedings of the IEEE Conference on Computer Vision and Pattern Recognition*, 2018, pp. 8711–8720.

[254] Y. Kim, S. Kim, J. W. Choi, and D. Kum, "Craft: Camera-radar 3d object detection with spatio-contextual fusion transformer," *arXiv preprint arXiv:2209.06535*, 2022.

[255] Z. Wu, G. Chen, Y. Gan, L. Wang, and J. Pu, "Mvfusion: Multi-view 3d object detection with semantic-aligned radar and camera fusion," *arXiv preprint arXiv:2302.10511*, 2023.

[256] Y. Kim, S. Kim, J. Shin, J. W. Choi, and D. Kum, "Crn: Camera radar net for accurate, robust, efficient 3d perception," *arXiv preprint arXiv:2304.00670*, 2023.

[257] J.-J. Hwang, H. Kretzschmar, J. Manela, S. Rafferty, N. Armstrong-Crews, T. Chen, and D. Anguelov, "Cramnet: Camera-radar fusion with ray-constrained cross-attention for robust 3d object detection," in *Computer Vision–ECCV 2022: 17th European Conference, Tel Aviv, Israel, October 23–27, 2022, Proceedings, Part XXXVIII*. Springer, 2022, pp. 388–405.

[258] L. Stäcker, P. Heidenreich, J. Rambach, and D. Stricker, "Fusion point pruning for optimized 2d object detection with radar-camera fusion," in *Proceedings of the IEEE/CVF Winter Conference on Applications of Computer Vision*, 2022, pp. 3087–3094.

[259] C. X. Lu, S. Rosa, P. Zhao, B. Wang, C. Chen, J. A. Stankovic, N. Trigoni, and A. Markham, "See through smoke: robust indoor mapping with low-cost mmwave radar," in *Proceedings of the 18th International Conference on Mobile Systems, Applications, and Services*, 2020, pp. 14–27.

[260] J. Wang, "Cfar-based interference mitigation for fmew automotive radar systems," *IEEE Transactions on Intelligent Transportation Systems*, vol. 23, no. 8, pp. 12 229–12 238, 2021.

[261] R. Zhang and S. Cao, "Support vector machines for classification of automotive radar interference," in *2018 IEEE Radar Conference (RadarConf18)*. IEEE, 2018, pp. 0366–0371.

[262] F. Jin and S. Cao, "Automotive radar interference mitigation using adaptive noise canceller," *IEEE Transactions on Vehicular Technology*, vol. 68, no. 4, pp. 3747–3754, 2019.

[263] M. Alhumaidi and M. Wintermantel, "Interference avoidance and mitigation in automotive radar," in *2020 17th European Radar Conference (EurRAD)*. IEEE, 2021, pp. 172–175.

[264] C. Schüßler, M. Hoffmann, I. Ullmann, R. Ebelt, and M. Vossiek, "Deep learning based image enhancement for automotive radar trained with an advanced virtual sensor," *IEEE Access*, vol. 10, pp. 40 419–40 431, 2022.

[265] J. Rock, W. Roth, M. Toth, P. Meissner, and F. Pernkopf, "Resource-efficient deep neural networks for automotive radar interference mitigation," *IEEE Journal of Selected Topics in Signal Processing*, vol. 15, no. 4, pp. 927–940, 2021.

[266] A. Dubey, J. Fuchs, V. Madhavan, M. Lübke, R. Weigel, and F. Lurz, "Region based single-stage interference mitigation and target detection," in *2020 IEEE Radar Conference (RadarConf20)*. IEEE, 2020, pp. 1–5.

[267] N.-C. Ristea, A. Anghel, and R. T. Ionescu, "Fully convolutional neural networks for automotive radar interference mitigation," in *2020 IEEE 92nd Vehicular Technology Conference (VTC2020-Fall)*. IEEE, 2020, pp. 1–5.

[268] J. Fuchs, A. Dubey, M. Lübke, R. Weigel, and F. Lurz, "Automotive radar interference mitigation using a convolutional autoencoder," in *2020 IEEE International Radar Conference (RADAR)*. IEEE, 2020, pp. 315–320.

[269] S. Chen, J. Taghia, T. Fei, U. Kühnau, N. Pohl, and R. Martin, "A dnn autoencoder for automotive radar interference mitigation," in *ICASSP 2021-2021 IEEE International Conference on Acoustics, Speech and Signal Processing (ICASSP)*. IEEE, 2021, pp. 4065–4069.

[270] S. Chen, J. Taghia, U. Kühnau, N. Pohl, and R. Martin, "A two-stage dnn model with mask-gated convolution for automotive radar interference detection and mitigation," *IEEE Sensors Journal*, vol. 22, no. 12, pp. 12 017–12 027, 2022.

[271] M. L. L. de Oliveira and M. J. Bekooij, "Deep convolutional autoencoder applied for noise reduction in range-doppler maps of fmew radars," in *2020 IEEE International Radar Conference (RADAR)*. IEEE, 2020, pp. 630–635.

[272] Y. Cheng, J. Su, H. Chen, and Y. Liu, "A new automotive radar 4d point clouds detector by using deep learning," in *ICASSP 2021-2021 IEEE International Conference on Acoustics, Speech and Signal Processing (ICASSP)*. IEEE, 2021, pp. 8398–8402.

[273] J. Deng, W. Dong, R. Socher, L.-J. Li, K. Li, and L. Fei-Fei, "Imagenet: A large-scale hierarchical image database," in *2009 IEEE conference on computer vision and pattern recognition*. Ieee, 2009, pp. 248–255.

[274] O. Russakovsky, J. Deng, H. Su, J. Krause, S. Satheesh, S. Ma, Z. Huang, A. Karpathy, A. Khosla, M. Bernstein *et al.*, "Imagenet large scale visual recognition challenge," *International journal of computer vision*, vol. 115, pp. 211–252, 2015.

[275] F. E. Nowruzi, P. Kapoor, D. Kolhatkar, F. A. Hassanat, R. Laganiere, and J. Rebut, "How much real data do we actually need: Analyzing object detection performance using synthetic and real data," *arXiv preprint arXiv:1907.07061*, 2019.

[276] T. Li, L. Fan, Y. Yuan, and D. Katabi, "Unsupervised learning for human sensing using radio signals," in *Proceedings of the IEEE/CVF Winter Conference on Applications of Computer Vision*, 2022, pp. 3288–3297.

[277] X. Li, Y. He, F. Fioranelli, and X. Jing, "Semisupervised human activity recognition with radar micro-doppler signatures," *IEEE Transactions on Geoscience and Remote Sensing*, vol. 60, pp. 1–12, 2021.

[278] Y. Li, D. Zhang, J. Chen, J. Wan, D. Zhang, Y. Hu, Q. Sun, and Y. Chen, "Towards domain-independent and real-time gesture recognition using mmwave signal," *IEEE Transactions on Mobile Computing*, 2022.

[279] G. Yan, Z. Luo, Z. Liu, and Y. Li, "Sensorx2car: Sensors-to-car calibration for autonomous driving in road scenarios," *arXiv preprint arXiv:2301.07279*, 2023.

[280] J. Domhof, J. F. Kooij, and D. M. Gavrila, "A joint extrinsic calibration tool for radar, camera and lidar," *IEEE Transactions on Intelligent Vehicles*, vol. 6, no. 3, pp. 571–582, 2021.

[281] A. Sengupta, A. Yoshizawa, and S. Cao, "Automatic radar-camera dataset generation for sensor-fusion applications," *IEEE Robotics and Automation Letters*, vol. 7, no. 2, pp. 2875–2882, 2022.

[282] P. Ren, Y. Xiao, X. Chang, P.-Y. Huang, Z. Li, B. B. Gupta, X. Chen, and X. Wang, "A survey of deep active learning," *ACM computing surveys (CSUR)*, vol. 54, no. 9, pp. 1–40, 2021.

[283] X. Zhan, Q. Wang, K.-h. Huang, H. Xiong, D. Dou, and A. B. Chan, "A comparative survey of deep active learning," *arXiv preprint arXiv:2203.13450*, 2022.

[284] T. Winterling, J. Lombacher, M. Hahn, J. Dickmann, and C. Wöhler, "Optimizing labelling on radar-based grid maps using active learning," in *2017 18th International Radar Symposium (IRS)*. IEEE, 2017, pp. 1–6.

[285] E. Haussmann, M. Fenzi, K. Chitta, J. Ivanecky, H. Xu, D. Roy, A. Mittel, N. Koumchatzky, C. Farabet, and J. M. Alvarez, "Scalable active learning for object detection," in *2020 IEEE intelligent vehicles symposium (iv)*. IEEE, 2020, pp. 1430–1435.

[286] V. M. Patel, R. Gopalan, R. Li, and R. Chellappa, "Visual domain adaptation: A survey of recent advances," *IEEE signal processing magazine*, vol. 32, no. 3, pp. 53–69, 2015.

[287] Y. Chen, W. Li, X. Chen, and L. V. Gool, "Learning semantic segmentation from synthetic data: A geometrically guided input-output adaptation approach," in *Proceedings of the IEEE/CVF conference on computer vision and pattern recognition*, 2019, pp. 1841–1850.

[288] S. J. Pan and Q. Yang, "A survey on transfer learning," *IEEE Transactions on knowledge and data engineering*, vol. 22, no. 10, pp. 1345–1359, 2010.

[289] D. P. Kingma, S. Mohamed, D. Jimenez Rezende, and M. Welling, "Semi-supervised learning with deep generative models," *Advances in neural information processing systems*, vol. 27, 2014.

[290] G. I. Parisi, R. Kemker, J. L. Part, C. Kanan, and S. Wermter, "Continual lifelong learning with neural networks: A review," *Neural networks*, vol. 113, pp. 54–71, 2019.

[291] A. H. Lang, S. Vora, H. Caesar, L. Zhou, J. Yang, and O. Beijbom, "Pointpillars: Fast encoders for object detection from point clouds," in *Proceedings of the IEEE/CVF conference on computer vision and pattern recognition*, 2019, pp. 12 697–12 705.

[292] N. Scheiner, F. Kraus, N. Appenrodt, J. Dickmann, and B. Sick, "Object detection for automotive radar point clouds—a comparison," *AI Perspectives*, vol. 3, no. 1, pp. 1–23, 2021.

[293] B. Xu, X. Zhang, L. Wang, X. Hu, Z. Li, S. Pan, J. Li, and Y. Deng, "Rpfa-net: A 4d radar pillar feature attention network for 3d object detection," in *2021 IEEE International Intelligent Transportation Systems Conference (ITSC)*. IEEE, 2021, pp. 3061–3066.

[294] F. Scarselli, M. Gori, A. C. Tsoi, M. Hagenbuchner, and G. Monfardini, "The graph neural network model," *IEEE transactions on neural networks*, vol. 20, no. 1, pp. 61–80, 2008.

[295] P. Svennbergsson, F. Fioranelli, and A. Yarovoy, "Radar-pointggn: Graph based object recognition for unstructured radar point-cloud data," in *2021 IEEE Radar Conference (RadarConf21)*. IEEE, 2021, pp. 1–6.

[296] M. Meyer, G. Kuschk, and S. Tomforde, "Graph convolutional networks for 3d object detection on radar data," in *Proceedings of the IEEE/CVF International Conference on Computer Vision*, 2021, pp. 3060–3069.

[297] S. Yun, D. Han, S. J. Oh, S. Chun, J. Choe, and Y. Yoo, “Cutmix: Regularization strategy to train strong classifiers with localizable features,” in *Proceedings of the IEEE/CVF international conference on computer vision*, 2019, pp. 6023–6032.

[298] W. Wang, D. Tran, and M. Feiszli, “What makes training multi-modal classification networks hard?” in *Proceedings of the IEEE/CVF Conference on Computer Vision and Pattern Recognition*, 2020, pp. 12695–12705.

[299] Q. Dou, Q. Liu, P. A. Heng, and B. Glocker, “Unpaired multi-modal segmentation via knowledge distillation,” *IEEE transactions on medical imaging*, vol. 39, no. 7, pp. 2415–2425, 2020.

[300] C. Du, T. Li, Y. Liu, Z. Wen, T. Hua, Y. Wang, and H. Zhao, “Improving multi-modal learning with uni-modal teachers,” *arXiv preprint arXiv:2106.11059*, 2021.

[301] W. Zhang, H. Zhou, S. Sun, Z. Wang, J. Shi, and C. C. Loy, “Robust multi-modality multi-object tracking,” in *Proceedings of the IEEE/CVF International Conference on Computer Vision*, 2019, pp. 2365–2374.

[302] Y. Zhou, L. Liu, H. Zhao, M. López-Benítez, L. Yu, and Y. Yue, “Towards deep radar perception for autonomous driving: Datasets, methods, and challenges,” *Sensors*, vol. 22, no. 11, p. 4208, 2022.

[303] D. J. MacKay, “A practical bayesian framework for backpropagation networks,” *Neural computation*, vol. 4, no. 3, pp. 448–472, 1992.

[304] T. A. Wheeler, M. Holder, H. Winner, and M. J. Kochenderfer, “Deep stochastic radar models,” in *2017 IEEE Intelligent Vehicles Symposium (IV)*. IEEE, 2017, pp. 47–53.

[305] V. Lekic and Z. Babic, “Automotive radar and camera fusion using generative adversarial networks,” *Computer Vision and Image Understanding*, vol. 184, pp. 1–8, 2019.

[306] D. Hall, F. Dayoub, J. Skinner, H. Zhang, D. Miller, P. Corke, G. Carneiro, A. Angelova, and N. Sünderhauf, “Probabilistic object detection: Definition and evaluation,” in *Proceedings of the IEEE/CVF Winter Conference on Applications of Computer Vision*, 2020, pp. 1031–1040.

[307] A. Dhamija, M. Gunther, J. Ventura, and T. Boult, “The overlooked elephant of object detection: Open set,” in *Proceedings of the IEEE/CVF Winter Conference on Applications of Computer Vision*, 2020, pp. 1021–1030.

[308] K. Joseph, S. Khan, F. S. Khan, and V. N. Balasubramanian, “Towards open world object detection,” in *Proceedings of the IEEE/CVF Conference on Computer Vision and Pattern Recognition*, 2021, pp. 5830–5840.

[309] G. Montavon, W. Samek, and K.-R. Müller, “Methods for interpreting and understanding deep neural networks,” *Digital signal processing*, vol. 73, pp. 1–15, 2018.

[310] F. Hohman, M. Kahng, R. Pienta, and D. H. Chau, “Visual analytics in deep learning: An interrogative survey for the next frontiers,” *IEEE transactions on visualization and computer graphics*, vol. 25, no. 8, pp. 2674–2693, 2018.

[311] H. Yu, F. Zhang, P. Huang, C. Wang, and L. Yuanhao, “Autonomous obstacle avoidance for uav based on fusion of radar and monocular camera,” in *2020 IEEE/RSJ International Conference on Intelligent Robots and Systems (IROS)*. IEEE, 2020, pp. 5954–5961.

[312] S. Han, H. Mao, and W. J. Dally, “Deep compression: Compressing deep neural networks with pruning, trained quantization and huffman coding,” *arXiv preprint arXiv:1510.00149*, 2015.

[313] Y. Cheng, D. Wang, P. Zhou, and T. Zhang, “A survey of model compression and acceleration for deep neural networks,” *arXiv preprint arXiv:1710.09282*, 2017.

[314] Z. Liu, H. Tang, A. Amini, X. Yang, H. Mao, D. Rus, and S. Han, “Bevfusion: Multi-task multi-sensor fusion with unified bird’s-eye view representation,” *arXiv preprint arXiv:2205.13542*, 2022.

[315] M. Meyer and G. Kuschk, “Automotive radar dataset for deep learning based 3d object detection,” in *2019 16th european radar conference (EuRAD)*. IEEE, 2019, pp. 129–132.

[316] F. Yu, D. Wang, E. Shelhamer, and T. Darrell, “Deep layer aggregation,” in *Proceedings of the IEEE conference on computer vision and pattern recognition*, 2018, pp. 2403–2412.

[317] Y. Zhou and O. Tuzel, “Voxelpnet: End-to-end learning for point cloud based 3d object detection,” in *Proceedings of the IEEE conference on computer vision and pattern recognition*, 2018, pp. 4490–4499.

[318] F. Drews, D. Feng, F. Faion, L. Rosenbaum, M. Ulrich, and C. Gläser, “Deepfusion: A robust and modular 3d object detector for lidars, cameras and radars,” in *2022 IEEE/RSJ International Conference on Intelligent Robots and Systems (IROS)*. IEEE, 2022, pp. 560–567.

[319] Z. Liu, H. Mao, C.-Y. Wu, C. Feichtenhofer, T. Darrell, and S. Xie, “A convnet for the 2020s,” in *Proceedings of the IEEE/CVF Conference on Computer Vision and Pattern Recognition*, 2022, pp. 11976–11986.



Shanliang Yao (Student Member, IEEE) received the B.E. degree in 2016 from the School of Computer Science and Technology, Soochow University, Suzhou, China, and the M.S. degree in 2021 from the Faculty of Science and Engineering, University of Liverpool, Liverpool, U.K. He is currently a joint Ph.D. student of University of Liverpool, Xi’an Jiaotong-Liverpool University and Institute of Deep Perception Technology, Jiangsu Industrial Technology Research Institute. His current research is centered on multi-modal perception using deep learning approach for autonomous driving. He is also interested in robotics, autonomous vehicles and intelligent transportation systems.



Runwei Guan (Student Member, IEEE) received his M.S. degree in Data Science from University of Southampton, Southampton, United Kingdom, in 2021. He is currently a joint Ph.D. student of University of Liverpool, Xi’an Jiaotong-Liverpool University and Institute of Deep Perception Technology, Jiangsu Industrial Technology Research Institute. His research interests include visual grounding, panoptic perception based on the fusion of radar and camera, lightweight neural network, multi-task learning and statistical machine learning. He serves as the peer reviewer of IEEE TRANSACTIONS ON NEURAL NETWORKS AND LEARNING SYSTEMS, Engineering Applications of Artificial Intelligence, Journal of Supercomputing, IJCNN, etc.



Xiaoyu Huang (Student Member, IEEE) received the B.S. degree in electronic science and technology from Nanjing University of Information Science & Technology in 2019. In 2022, he received the M.S. degree from the University of Liverpool and Xi’an Jiaotong-Liverpool University joint program, where he is currently working toward the Ph.D. degree with the School of Advanced Technology. His research interests include computer vision, pattern recognition, deep learning, and image processing.



Zhuoxiao Li (Student Member, IEEE) received the MSc degree in Information Systems (2020) from the Information School, University of Sheffield, Sheffield, UK. After that, he joined the VR+ Culture Lab of the School of Information Management, Sun Yat-sen University as a research assistant. He is currently a Ph.D student at the Department of Computer Science at the University of Liverpool. His current main research direction is the combination of unmanned surface vehicle and virtual reality/augmented reality. He is also interested in deep learning applications in geographic information systems and remote sensing.



Xiangyu Sha (Student Member, IEEE) is currently working toward the B.S. degree in computer science from University of Liverpool, United Kingdom. She will complete her undergraduate study in 2024. Her research interests include computer vision, virtual reality, extended reality, robotics simulation and sensor fusion in autonomous driving vehicles. She has won full scholarships for two consecutive years and participated the Programme and Poster Competition as a Summer Undergraduate Research Fellow in 2022.



Yong Yue Fellow of Institution of Engineering and Technology (FIET), received the B.Eng. degree in mechanical engineering from Northeastern University, Shenyang, China, in 1982, and the Ph.D. degree in computer aided design from Heriot-Watt University, Edinburgh, U.K., in 1994. He worked in the industry for eight years and followed experience in academia with the University of Nottingham, Cardiff University, and the University of Bedfordshire, U.K. He is currently a Professor and Director with the Virtual Engineering Centre, Xi'an Jiaotong-Liverpool University, Suzhou, China. His current research interests include computer graphics, virtual reality, and robot navigation.



Xiaohui Zhu (Member, IEEE) received his Ph.D. from the University of Liverpool, UK in 2019. He is currently an assistant professor, Ph.D. supervisor and Programme Director with the Department of Computing, School of Advanced Technology, Xi'an Jiaotong-Liverpool University. He focuses on advanced techniques related to autonomous driving, including sensor-fusion perception, fast path planning, autonomous navigation and multi-vehicle collaborative scheduling.



Yutao Yue (Member, IEEE) was born in Qingzhou, Shandong, China, in 1982. He received the B.S. degree in applied physics from the University of Science and Technology of China, in 2004, and the M.S. and Ph.D. degrees in computational physics from Purdue University, USA, in 2006 and 2010, respectively. From 2011 to 2017, he worked as a Senior Scientist with the Shenzhen Kuang-Chi Institute of Advanced Technology and a Team Leader of the Guangdong "Zhujiang Plan" 3rd Introduced Innovation Scientific Research Team. From 2017 to 2018, he was a Research Associate Professor with the Southern University of Science and Technology, China. Since 2018, he has been the Founder and the Director of the Institute of Deep Perception Technology, JITRI, Jiangsu, China. Since 2020, he has been working as an Honorary Recognized Ph.D. Advisor of the University of Liverpool, U.K., and Xi'an Jiaotong-Liverpool University, China. He is the co-inventor of over 300 granted patents of China, USA, and Europe. He is also the author of over 20 journals and conference papers. His research interests include computational modeling, radar vision fusion, perception and cognition cooperation, artificial intelligence theory, and electromagnetic field modulation. Dr. Yue was a recipient of the Wu WenJun Artificial Intelligence Science and Technology Award in 2020.



Eng Gee Lim (Senior Member, IEEE) received the B.Eng. (Hons.) and Ph.D. degrees in Electrical and Electronic Engineering (EEE) from Northumbria University, Newcastle, U.K., in 1998 and 2002, respectively. He worked for Andrew Ltd., Coventry, U.K., a leading communications systems company from 2002 to 2007. Since 2007, he has been with Xi'an Jiaotong-Liverpool University, Suzhou, China, where he was the Head of the EEE Department, and the University Dean of research and graduate studies. He is currently the School Dean of Advanced Technology, the Director of the AI University Research Centre, and a Professor with the Department of EEE. He has authored or coauthored over 100 refereed international journals and conference papers. His research interests are artificial intelligence (AI), robotics, AI+ health care, international standard (ISO/IEC) in robotics, antennas, RF/microwave engineering, EM measurements/simulations, energy harvesting, power/energy transfer, smart-grid communication, and wireless communication networks for smart and green cities. He is a Chartered Engineer and a fellow of The Institution of Engineering and Technology (IET) and Engineers Australia. He is also a Senior Fellow of Higher Education Academy (HEA).



Hyungjoon Seo (Member, IEEE), received the bachelor's degree in civil engineering from Korea University, Seoul, South Korea, in 2007, and the Ph.D. degree in geotechnical engineering from Korea University in 2013. In 2013, he worked as a research professor in Korea University. He served as a visiting scholar at University of Cambridge, Cambridge, UK, and he worked for engineering department in University of Cambridge as a research associate from 2014 to 2016. In August 2016, he got an assistant professor position in the Department of Civil Engineering at the Xi'an Jiaotong Liverpool University (XJTLU), China. He has been an assistant professor at the University of Liverpool, UK, from 2020. His research interests are monitoring using artificial intelligence and SMART monitoring system for infrastructure, soil-structure interaction (tunneling, slope stability, pile), Antarctic survey and freezing ground. Hyungjoon is the director of the CSMI (Centre for SMART Monitoring Infrastructure), CSMI is collaborating with University of Cambridge, University of Oxford, University of Bath, UC Berkeley University, Nanjing University, and Tongji University on SMART monitoring. He presented a keynote speech at the 15th European Conference on Soil Mechanics and Geotechnical Engineering in 2015. He is currently appointed editor of the CivilEng journal and organized two international conferences. He has published more than 50 scientific papers including a book on Geotechnical Engineering and SMART monitoring.



Ka Lok Man (Member, IEEE), received the Dr.Eng. degree in electronic engineering from the Politecnico di Torino, Turin, Italy, in 1998, and the Ph.D. degree in computer science from Technische Universiteit Eindhoven, Eindhoven, The Netherlands, in 2006. He is currently a Professor in Computer Science and Software Engineering with Xi'an Jiaotong-Liverpool University, Suzhou, China. His research interests include formal methods and process algebras, embedded system design and testing, and photovoltaics.

TABLE II: OVERVIEW OF RADAR-CAMERA FUSION DATASETS

Name	Year	Tasks	Annotations	Data Representations	Categories	Size	Link
nuScenes [5]	2019	Object Detection, Object Tracking	3D box-level	Camera: RGB image; Radar: point cloud	23 classes (Vehicle, Pedestrian, Bicycle, Movable Object, Static Object, etc.)	1000 scenes, 1.4M boxes in 40k frames, 5.5 hours	https://www.nuscenes.org/nuscenes
Astyx [315]	2019	Object Detection	3D box-level	Camera: RGB image; Radar: point cloud	7 classes (Bus, Car, Cyclist, Motorcyclist, Person, Trailer, Truck)	500 frames, around 3000 labeled objects	http://www.astyx.net
SeeingThroughFog [31]	2020	Object Detection	2D box-level, 3D box-level	Camera: RGB image, gated image, thermal image; Radar: point cloud	4 classes (Passenger Car, Large Vehicle, Pedestrian, Ridable Vehicle)	12k samples in real-world driving scenes and 1.5k samples in controlled weather conditions within a fog chamber, 100k objects	https://www.uni-ulm.de/en/indriveu/projects/dense-dataset/
CARRADA [131]	2020	Object Detection, Semantic Segmentation, Object Tracking, Scene Understanding	2D box-level, 2D pixel-level	Camera: RGB image; Radar: range-azimuth tensor, range-Doppler tensor	3 classes (Pedestrian, Car, Cyclist)	12,666 frames, 78 instances, 7,139 annotated frames with instances, 23GB synchronized camera and radar views	https://arthrouaknine.github.io/codeanddata/carrada
HawkEye [199]	2020	Semantic Segmentation	3D point-level	Camera: RGB image; Radar: point cloud	9 classes of cars (Sub-compact, Compact, Mid-sized, Full-sized, Sport, SUV, Jeep, Van, Truck)	3k images, 4k scenes, 120 car models	https://jguan.page/HawkEye/
Zendar [186]	2020	Object Detection, Mapping, Localization	2D box-level	Camera: RGB image; Radar: range-Doppler tensor, range-azimuth tensor, point cloud	1 class (Car)	Over 11k moving cars labeled in 27 diverse scenes with over 40k automatically generated labels	http://zendar.io/dataset
RADIATE [187]	2020	Object Detection	2D box-level	Camera: RGB image; Radar: range-azimuth tensor	8 classes (Car, Van, Bus, Truck, Motorbike, Bicycle, Pedestrian, A group of pedestrians)	200k bounding boxes over 44k radar frames	http://pro.hw.ac.uk/radiate/
AIODrive [188]	2020	Object Detection, Semantic Segmentation, Object Tracking, Trajectory Prediction, Depth Estimation	2D box-level, 3D box-level	Camera: RGB image; Radar: point cloud	11 classes (Vehicle, Pedestrian, Vegetation, Building, Road, Sidewalk, Wall, Traffic Sign, Pole and Fence)	500k annotated images for five camera viewpoints, 100k annotated frames for radar sensor	http://www.aiodrive.org/
CRUW [87]	2021	Object Detection	2D box-level	Camera: RGB image; Radar: range-azimuth tensor	3 classes (Pedestrian, Cyclist, Car)	400k frames, 260k objects, 3.5 hours	https://www.cruwdataset.org/
RaDICaL [190]	2021	Object Detection	2D box-level	Camera: RGB image, RGB-D image; Radar: ADC signal	2 classes (Car, Pedestrian)	393k frames	https://publish.illinois.edu/radicldata/
RadarScenes [191]	2021	Semantic Segmentation, Object Tracking	2D pixel-level, 3D point-level	Camera: RGB image; Radar: point cloud	11 classes (Car, Large Vehicle, Truck, Bus, Train, Bicycle, Motorized Two-wheeler, Pedestrian, Pedestrian Group, Animal, Other)	40,208 frames, 158 individual sequences, 118.9M radar points	https://radar-scenes.com/
RADDet [138]	2021	Object Detection	2D box-level, 3D box-level	Camera: RGB image; Radar: range-azimuth-Doppler tensor	6 classes (Person, Bicycle, Car, Motorcycle, Bus, Truck)	10,158 frames	https://github.com/ZhangAoCana/RADDet
FloW [192]	2021	Object Detection	2D box-level	Camera: RGB image; Radar: range-Doppler tensor, point cloud	1 class (Bottle)	4k frames	https://github.com/ORCA-Ubaut/FloW-Dataset

TABLE II: OVERVIEW OF RADAR-CAMERA FUSION DATASETS

Name	Year	Tasks	Annotations	Data Representations	Categories	Size	Link
RADlal [193]	2021	Object Detection, Semantic Segmentation	2D box-level	Camera: RGB image; Radar: ADC signal, range-azimuth-Doppler tensor, range-azimuth tensor, range-Doppler tensor, point cloud	1 class (Vehicle)	8,252 frames are labelled with 9,550 vehicle	https://github.com/valeoai/RADlal
VoD [142]	2022	Object Detection	2D box-level, 3D box-level	Camera: RGB image; Radar: point cloud	13 classes (Car, Pedestrian, Cyclist, Rider, Unused Bicycle, Bicycle Rack, Human Depiction, Moped or Scooter, Motor, Ride Other, Vehicle Other, Truck, Ride Uncertain)	8693 frames, 123,106 annotations of both moving and static objects, including 26,587 pedestrian, 10,800 cyclist and 26,949 car labels	https://tudelft-iv.github.io/vew-of-delft-dataset/
Boreas [194]	2022	Object Detection, Localization, Odometry	2D box-level	Camera: RGB image; Radar: range-azimuth tensor	4 classes (Car, Pedestrian, Cyclist, Misc)	7.1k frames for detection, over 350km of driving data, 326,180 unique 3D box annotations	https://www.boreas.utias.utoronto.ca/
TJ4DRadSet [196]	2022	Object Detection, Object Tracking	3D box-level	Camera: RGB image; Radar: point cloud	8 classes (Car, Pedestrian, Cyclist, Bus, Motorcyclist, Truck, Engineering Vehicle, Tricyclist)	40k frames in total, 7757 frames within 44 consecutive sequences	https://github.com/TJRadarLab/TJ4DRadSet
K-Radar [197]	2022	Object Detection, Object Tracking, SLAM	3D box-level	Camera: RGB image; Radar: range-azimuth-Doppler tensor	5 classes (Pedestrian, Motorbike, Bicycle, Sedan, Bus or Truck)	35k frames of 4D radar tensor	https://github.com/kaist-avelab/k-radar
aiMotive [198]	2022	Object Detection	3D box-level	Camera: RGB image; Radar: point cloud	14 classes (Pedestrian, Car, Bus, Truck, Van, Motorcycle, Pickup, Rider, Bicycle, Trailer, Train, Shopping Cart, Other Object)	26,583 frames, 425k objects	https://github.com/aimotive/aimotive_dataset

TABLE III: SUMMARY OF RADAR-CAMERA FUSION METHODS

Reference	Year	Task	Annotations	Categories	Modalities	Network Architecture	Fusion Level	Fusion Operation	Dataset	Source Code
Chadwick <i>et al.</i> [201]	2019	Object Detection	2D box-level	Vehicle	Camera: RGB image; Radar: point cloud	One-stage network based on ResNet [141]	Feature-level	Addition; Concatenation	Self-recorded	-
RRPN [9]	2019	Object Detection	2D box-level	Car, Truck, Person, Motorcycle, Bicycle, Bus	Camera: RGB image; Radar: point cloud	RRPN [9]	Data-level	Transformation matrix	nuScenes [5]	https://github.com/mrnabati/RRPN
Jha <i>et al.</i> [220]	2019	Object Detection	2D box-level	Pedestrian, Lamp Post	Camera: RGB image; Radar: point cloud	YOLOv3 [55]	Object-level	Transformation matrix	Self-recorded	-
CMGGAN [305]	2019	Semantic Segmentation	2D point-level	Free Space	Camera: RGB image; Radar: grid map	CMGGAN [305]	Feature-level	Addition	Self-recorded	-
Meyer and Kuschk [315]	2019	Object Detection	3D box-level	Car	Camera: RGB image; Radar: point cloud	A 3D region proposal network based on VGG [177]	Data-Level	Transformation matrix	Astyx [315]	-
RVNet [28]	2019	Object Detection	2D box-level	Vehicle, Pedestrian, Two-wheelers, Objects (movable objects and debris)	Camera: RGB image; Radar: point cloud	RVNet [28] based on YOLOv3 [55]	Feature-level	Concatenation	nuScenes [5]	-
FusionNet [217]	2019	Object Detection, Object Classification	2D box-level	Vehicle	Camera: RGB image; Radar: range-azimuth tensor	FusionNet [217] inspired by SSD [61]	Feature-level	Concatenation	nuScenes [5]	-
SO-Net [211]	2020	Object Detection, Semantic Segmentation	2D box-level, 2D pixel-level	Vehicle, Free Space	Camera: RGB image; Radar: point cloud	SO-Net [211] based on the RVNet [28]	Feature-level	Concatenation	nuScenes [5]	-
SAF-FCOS [224]	2020	Object Detection	2D box-level	Bicycle, Car, Motorcycle, Bus, Train, Truck	Camera: RGB image; Radar: point cloud	SAF-FCOS [224] based on FCOS [64]	Feature-level	Addition; Multiplication	nuScenes [5]	https://github.com/Singingkettle/SAF-FCOS
CRF-Net [222]	2019	Object Detection	2D box-level	Car, Bus, Motorcycle, Truck, Trailer, Bicycle, Human	Camera: RGB image; Radar: point cloud	CRF-Net [222] based on RetinaNet [62]	Data-level	Concatenation	nuScenes [5], Self-recorded	https://github.com/TUMFTM/CameraRadarFusionNet
Bijelic <i>et al.</i> [31]	2020	Object Detection	2D box-level	Vehicle	Camera: RGB image; Radar: point cloud	A modified VGG [177] backbone and SSD [61] blocks	Feature-level	Concatenation; Attention	DENSE [31]	https://github.com/princeton-computational-imaging/SeeingThroughFog
BIRANet [205]	2020	Object Detection	2D box-level	Car, Truck, Person, Motorcycle, Bicycle, Bus	Camera: RGB image; Radar: point cloud	RANet and BIRANet [205] based on ResNet [141]	Feature-level	Addition	nuScenes [5]	https://github.com/RituYadav92/Radar-RGB-Attentive-Multimodal-Object-Detection
Nabati and Qi [206]	2020	Object Detection, Depth Estimation	2D box-level	Car, Truck, Person, Motorcycle, Bicycle, Bus	Camera: RGB image; Radar: point cloud	FPN [52] with ResNet [141] as backbone, and RPN in Faster R-CNN [51]	Mixed-level	-	nuScenes [5]	-
YODar [209]	2020	Object Detection	2D box-level	Vehicle	Camera: RGB image; Radar: point cloud	YODar [209] based on YOLOv3 [55]	Feature-level	Concatenation	nuScenes [5]	-
CenterFusion [17]	2020	Object Detection	3D box-level	Car, Truck, Bus, Trailer, Pedestrian, Barrier, Motorcycle, Bicycle, Traffic Cone	Camera: RGB image; Radar: point cloud	CenterNet [204] with the DLA [316] backbone	Feature-level	Concatenation	nuScenes [5]	https://github.com/mrnabati/CenterFusion

TABLE III: SUMMARY OF RADAR-CAMERA FUSION METHODS

Reference	Year	Task	Annotations	Categories	Modalities	Network Architecture	Fusion Level	Fusion Operation	Dataset	Source Code
RODNet [16]	2021	Object Detection	2D box-level	Pedestrian, Cyclist, Car	Camera: RGB image; Radar: range-azimuth tensor	RODNet [16]	Feature-level	-	CRUW [189]	https://github.com/yizhou-wang/RODNet
RAMP-CNN [136]	2021	Object Detection	2D box-level	Pedestrian, Cyclist, Car	Camera: RGB image; Radar: range-azimuth-Doppler tensor	RAMP-CNN [136]	Feature-level	Concatenation	CRUW [189]	-
Li and Xie [208]	2021	Object Detection	3D box-level	Vehicle	Camera: RGB image; Radar: point cloud	A network based on YOLOv3 [55]	Feature-level	Concatenation; Multiplication	nuScenes [5]	-
Kim <i>et al.</i> [221]	2021	Object Detection	3D box-level	Vehicle	Camera: RGB image; Radar: range-azimuth tensor	A network based on VGG [177] and FPN [52]	Feature-level	Concatenation	Self-recorded	-
AssociationNet [212]	2021	Object Detection	2D box-level	Vehicle	Camera: RGB image; Radar: point cloud	AssociationNet [212]	Object-level	Transformation matrix; Concatenation	Self-recorded	-
RVF-Net [250]	2021	Object Detection	3D box-level	Car	Camera: RGB image; Radar: point cloud	RVF-Net [250] based on VoxelNet [317]	Data-level	Concatenation	nuScenes [5]	https://github.com/TUMFTM/RadarVoxelFusionNet
Cui <i>et al.</i> [207]	2021	Object Detection	3D box-level	Car	Camera: RGB image; Radar: point cloud	CNN with SSMA [225] block	Mixed-level	Concatenation	Astyx [315]	-
RISFNet [210]	2021	Object Detection	2D box-level	Bottle	Camera: RGB image; Radar: point cloud	RISFNet [210] based on CSPdarknet53 [56] and VGG [177]	Feature-level	Concatenation; Addition; Multiplication	FloW [192]	-
GRIF Net [252]	2021	Object Detection	3D box-level	Vehicle	Camera: RGB image; Radar: point cloud	GRIF Net [252] based on FPN [52] and SBNet [253]	Feature level	Attention	nuScenes [5]	-
Stäcker <i>et al.</i> [258]	2021	Object Detection	2D box-level	Car, Person, Truck, Bicycle, Motorcycle	Camera: RGB image; Radar: point cloud	A network based on RetinaNet [62] architecture with a ResNet [141] backbone	Feature level	Addition, Concatenation	nuScenes [5]	-
Harley <i>et al.</i> [214]	2021	Semantic Segmentation	2D pixel-level	Vehicle, Background	Camera: RGB image; Radar: point cloud	A network with a ResNet [141] backbone	Feature-level	Concatenation	nuScenes [5]	-
RadSegNet [213]	2022	Object Detection, Semantic Segmentation	2D box-level, 2D pixel-level	Car, Truck	Camera: RGB image; Radar: point cloud, range-azimuth tensor	RadSegNet [213]	Data-level	Concatenation	Astyx [315], RADIATE [187]	-
RCBEV [218]	2022	Object Detection	3D box-level	Car, Truck, Bus, Pedestrian, Barrier, Trailer, Construction Vehicle, Motorcycle, Bicycle, Traffic cone	Camera: RGB image; Radar: point cloud	RCBEV [218] with Swin Transformer [76] as backbone and FPN [52] as neck	Feature-level	Concatenation	nuScenes [5]	-
CRAFT [254]	2022	Object Detection	3D box-level	Car, Truck, Bus, Pedestrian, Barrier, Trailer, Construction Vehicle, Motorcycle, Bicycle, Traffic cone	Camera: RGB image; Radar: point cloud	CRAFT [254] based on DLA [316]	Data-level	Concatenation	nuScenes [5]	-

TABLE III: SUMMARY OF RADAR-CAMERA FUSION METHODS

Reference	Year	Task	Annotations	Categories	Modalities	Network Architecture	Fusion Level	Fusion Operation	Dataset	Source Code
DeepFusion [318]	2022	Object Detection	3D box-level	Car, Truck, Bus, Pedestrian, Barrier, Trailer, Construction Vehicle, Motorcycle, Bicycle, Traffic cone	Camera: RGB image; Radar: point cloud	DeepFusion [318]	Feature-level	Concatenation	Self-recorded, nuScenes [5]	-
CramNet [257]	2022	Object Detection	3D box-level	Car, Van, Truck, Bus, Motorbike, Bicycle	Camera: RGB image; Radar: range-azimuth tensor	CramNet [257]	Feature-level	Attention	RADIATE [187]	-
MVFusion [255]	2023	Object Detection	3D box-level	Car, Truck, Bus, Pedestrian, Barrier, Trailer, Construction Vehicle, Motorcycle, Bicycle, Traffic cone	Camera: RGB image; Radar: point cloud	MVFusion [255]	Feature-level	Addition; Concatenation	nuScenes [5]	-
CRN [256]	2023	Object Detection	3D box-level	Car, Truck, Bus, Pedestrian, Barrier, Trailer, Construction Vehicle, Motorcycle, Bicycle, Traffic cone	Camera: RGB image; Radar: point cloud	CRN [256] based on ResNet [141], ConvNeXt [319] and FPN [52]	Feature-level	Concatenation	nuScenes [5]	-

TABLE IV: SUMMARY OF RADAR-CAMERA FUSION EVALUATION METRICS

Metric	Formula	Definition
Accuracy	$\text{Accuracy} = \frac{\text{TP} + \text{TN}}{\text{TP} + \text{TN} + \text{FP} + \text{FN}}$ (8)	Accuracy is the number of correct predictions over all predictions.
Precision	$\text{Precision} = \frac{\text{TP}}{\text{TP} + \text{FP}}$ (9)	Precision is the fraction of true positive among total predicted positive.
Recall	$\text{Recall} = \frac{\text{TP}}{\text{TP} + \text{FN}}$ (10)	Recall is the fraction of true positive over all actual positive in the dataset.
F1-Score	$\text{F1-Score} = 2 * \frac{\text{Precision} * \text{Recall}}{\text{Precision} + \text{Recall}}$ (11)	F1-Score is the harmonic mean of precision and recall, describing a balance between precision and recall.
Average Precision (AP)	$\text{AP} = \int_0^1 \text{precision}(r)dr$ (12)	AP is the precision averaged over all recall values between 0 and 1 for a single class. It is the area under the Precision-Recall curve. <ul style="list-style-type: none"> r: recall value $\text{precision}(r)$: the precision at recall value of r
Average Recall (AR)	$\text{AR} = 2 \int_{0.5}^1 \text{recall}(o)do$ (13)	AR is the average of all recalls at IoU thresholds from 0.5 to 1.0. It is twice the area under the Recall-IoU curve. <ul style="list-style-type: none"> o: the IoU overlap $\text{recall}(o)$: the recall at IoU value of o
Frame Per Second (FPS)	$\text{FPS} = \frac{m}{s}$ (14)	FPS is a measure of how many images the model processes per second. <ul style="list-style-type: none"> m: the number of images s: total seconds consumed
Mean Average Precision (mAP)	$\text{mAP} = \frac{1}{N} \sum_{i=1}^N \text{AP}_i$ (15)	mAP is the average value of AP, that is, the average of the area under the Precision-Recall curve of each category. <ul style="list-style-type: none"> N: the number of classes AP_i: AP value of the ith class
Mean Intersection over Union (mIoU)	$\text{mIoU} = \frac{1}{N+1} \sum_{i=0}^N \frac{\text{TP}}{\text{FN} + \text{FP} + \text{TP}}$ (16)	IoU is the overlap between the predicted value and the ground truth divided by the area of union. Then, mIoU is the average value of IoU over all classes.
nuScenes Detection Score (NDS)	$\text{NDS} = \frac{1}{10} \left[5\text{mAP} + \sum_{\text{mTP} \in \text{TP}} (1 - \min(1, \text{mTP})) \right]$ (17)	NDS is a weighted sum of mAP and five TP metrics. <ul style="list-style-type: none"> mAP: mean Average Precision over all classes TP: the set of the five mean True Positive metrics, including box location, size, orientation, attributes, and velocity mTP: the mean True Positive over all classes C: the set of classes
Object Location Similarity (OLS)	$\text{OLS} = \exp \left\{ \frac{-d^2}{2(s\kappa_{cls})^2} \right\}$ (19)	OLS describes the correlation between two detections related to distance, classes and scale information. <ul style="list-style-type: none"> d: distance between two points in an RA tensor s: the distance between the object and the radar sensor, indicating object scale information κ_{cls}: a constant value that donates the error tolerance for each class cls, which can be calculated based on the average object size of that class

TABLE IV: SUMMARY OF RADAR-CAMERA FUSION EVALUATION METRICS

Metric	Formula	Definition
Average Heading Similarity (AHS) [7], [182]	$\text{AHS} = \frac{1}{11} \sum_{r \in \{0, 0.1, \dots, 1\}} \max_{\tilde{r}: \tilde{r} \geq r} s(\tilde{r}) \quad (20)$ $s(r) = \frac{1}{ \mathcal{D}(r) } \sum_{i \in \mathcal{D}(r)} \frac{1 + \cos \Delta_{\theta}^{(i)}}{2} - \delta_i \quad (21)$	<p>AHS is the average orientation accuracy in 3D IOU and global orientation angle.</p> <ul style="list-style-type: none"> • r: recall value • $\mathcal{D}(r)$: all object detections at recall rate r • $\Delta_{\theta}^{(i)}$: difference in global orientation of detection i as determined by the estimated and ground truth orientation • δ_i: whether detection i is assigned to a ground truth bounding box

TABLE V: PERFORMANCE OVERVIEW OF RADAR-CAMERA METHODS ON THE NUSCENES DATASET

Method	Metrics				Threshold	Sub-dataset	Hardware
	AP/AR	mAP	Others	Inference Time			
RRPN [9]	AP(NS-F): 0.430 AP ^{.50} (NS-F): 0.649 AP ^{.75} (NS-F): 0.485 AP (NS-FB): 0.355 AP ^{.50} (NS-FB): 0.590 AP ^{.75} (NS-FB): 0.370 AR(NS-F): 0.486 AR(NS-FB): 0.421	-	-	-	IoU={0.5, 0.75}	a) NS-F sub-dataset: from front camera and front radar only, with 23k samples b) NS-FB sub-dataset: from the rear camera and two rear radars, with 45k samples	-
RVNet [28]	AP(Cycle): 0.02 AP(Pedestrian): 0.14 AP(Vehicle): 0.59 AP(Obstacle): 0.26	0.25	-	17ms	IoU={0.5}	Samples from front camera and front radar	One NVIDIA GeForce 1080 GPU
SO-Net [211]	AP(detection): 0.423 AP(segmentation): 0.991	-	-	25ms	IoU={0.5}	Samples under rainy and nighttime conditions (308 pairs for training and 114 pairs for testing)	One NVIDIA GeForce 1080 GPU
SAF-FCOS [224]	AP: 0.724 AP ^{.50} : 0.900 AP ^{.75} : 0.793 AR: 0.790	-	-	-	IoU={0.5, 0.75, 0.5-0.95}	A total of 34,149 radar-camera pairs	Eight NVIDIA GeForce GTX 1080Ti GPUs
CRF-Net [222]	-	0.5523	-	43ms	-	Merge the original 23 object classes into seven classes	One NVIDIA Titan XP GPU
BIRANet [205]	AP: 0.723 AP ^{.50} : 0.889 AP ^{.75} : 0.843 AP ^{.85} : 0.657 AR: 0.753	-	-	-	IoU={0.5, 0.75, 0.85}	Merged relevant classes into six classes	One NVIDIA Titan Pascal GPU
Nabati and Qi [206]	AP: 0.356 AP ^{.50} : 0.6053 AP ^{.75} : 0.3738 AR: 0.421	-	MAE: 2.65	-	IoU={0.5, 0.75}	Samples from front and rear cameras together with all radars	Two NVIDIA Quadro P6000 GPUs
YOdar [209]	AP: 0.431	0.394	-	-	-	Samples from nuScenes (29,853 frames for training, 3,289 frames for validation and 1,006 frames for testing)	One NVIDIA Quadro P6000 GPU
CenterFusion [17]	-	0.326	NDS: 0.449 mATE: 0.631 mASE: 0.261 mAQE: 0.516 mAVE: 0.614 mAAE: 0.115	-	Distance={0.5, 1, 2, 4}	Full nuScenes	Two NVIDIA P5000 GPUs
Li and Xie [208]	AP: 0.243 AP ^{.50} : 0.484 AP ^{.75} : 0.223 AR: 0.337	0.484	-	-	IoU={0.5, 0.75}	Dataset is randomly divided into a training set, a validation set, and a testing set according to the ratio of 6:2:2	One NVIDIA GeForce GTX 1080Ti GPU
RVF-Net [250]	AP: 0.5486	-	-	44ms	Distance={0.5}	Samples under rainy and nighttime conditions	One NVIDIA Titan XP GPU

TABLE V: PERFORMANCE OVERVIEW OF RADAR-CAMERA METHODS ON THE NUSCENES DATASET

Method	Metrics				Threshold	Sub-dataset	Hardware
	AP/AR	mAP	Others	Inference Time			
GRIF Net [252]	AP ^{0.5m} : 0.441 AP ^{1m} : 0.665 AP ^{2m} : 0.719 AP ^{4m} : 0.749	-	-	-	Distance={0.5, 1, 2, 4}	One front camera and 3 front radars	One NVIDIA GeForce GTX 1080Ti GPU
Stäcker <i>et al.</i> [258]	-	0.3678		36.7ms	IoU={0.5}	Sample from front camera and radar	One NVIDIA GeForce RTX 2080 GPU
RCBEV [218]	-	0.406	NDS: 0.456 mATE: 0.484 mASE: 0.257 mAOE: 0.587 mAVE: 0.702 mAAE: 0.140	-	Distance={0.5, 1, 2, 4}	Full nuScenes	Four NVIDIA GeForce GTX 3090 GPUs
CRAFT [254]	-	0.411	NDS: 0.523 mATE: 0.467 mASE: 0.268 mAOE: 0.453 mAVE: 0.519 mAAE: 0.114	4.1 FPS	Distance={0.5, 1, 2, 4}	Full nuScenes	Training: four NVIDIA GeForce RTX 3090 GPUs; Testing: one RTX 3090 GPU
MVFusion [255]	-	0.453	NDS: 0.517 mATE: 0.569 mASE: 0.246 mAOE: 0.379 mAVE: 0.781 mAAE: 0.128	-	Distance={0.5, 1, 2, 4}	Full nuScenes	Eight NVIDIA RTX A6000 GPUs
CRN [256]	-	0.575	NDS: 0.624 mATE: 0.460 mASE: 0.273 mAOE: 0.443 mAVE: 0.352 mAAE: 0.180	7.2 FPS	Distance={0.5, 1, 2, 4}	Full nuScenes	-